
Probabilistic Forecasting with Generative Networks via Scoring Rule Minimization

Lorenzo Pacchiardi

Department of Statistics
University of Oxford
Oxford, UK

lorenzo.pacchiardi@stats.ox.ac.uk

Rilwan A. Adewoyin*

Department of Statistics
University of Warwick
Coventry, UK

Peter Dueben

Earth System Modelling Section
ECMWF
Reading, UK

Ritabrata Dutta

Department of Statistics
University of Warwick
Coventry, UK

Abstract

Generative networks are often trained to minimize a statistical divergence between the reference distribution and the generative one in an adversarial setting. Some works trained instead generative networks to minimize Scoring Rules, functions assessing how well the generative distribution matches each training sample individually. We show how the Scoring Rule formulation easily extends to the so-called prequential (predictive-sequential) score, whose minimization allows performing probabilistic forecasting with generative networks. This objective leads to adversarial-free training, therefore easily avoiding uncertainty underestimation due to mode collapse, which is a common issue in the adversarial setting and undesirable for probabilistic forecasting. We provide consistency guarantees for the minimizer of the prequential score and employ that to perform probabilistic forecasting for two chaotic dynamical models and a benchmark dataset of global weather observations. For this last example, we define scoring rules for spatial data by drawing from the relevant literature, with which we obtain better uncertainty quantification with little hyperparameter tuning compared to adversarial training.

1 Introduction

In many disciplines (for instance econometrics and meteorology), practitioners want to forecast the future state of a phenomenon. Providing prediction uncertainty (ideally by stating a full probability distribution) is often essential. This task is called *probabilistic forecasting* [19] and is commonplace in Numerical Weather Prediction (NWP, 40), where physics-based models are run multiple times to obtain an ensemble of forecasts representing the possible evolution of the weather [31]. To assess the performance of NWP systems, people commonly use Scoring Rules (SRs, 20), functions quantifying the quality of a probabilistic forecast with respect to the observed outcome.

Here, we use *generative networks* to provide probabilistic forecasts. A popular class of generative networks is Generative Adversarial Networks (GANs, 21, 36, 38, 1), which define a min-max game between the generative network and a competitor, termed *critic*. The adversarial training procedure is however unstable: it can lead to *mode collapse*, in which case the generative network fails to model

*Also affiliated with Department of Computer Science and Engineering, Southern University of Science and Technology, Shenzhen, China

the full data distribution [47]. If accurate uncertainty quantification is required, such a behavior is undesirable. Additionally, it is unclear how to extend the GAN training objective to time-dependent data: indeed, most formulations rely on divergences between probability distributions and consider observations as independent and identically distributed samples from one of those distributions.

For these reasons, we recur to framing generative network training as a Scoring Rule minimization problem. For SRs defined as expectations over the generative distribution, Stochastic Gradient Descent without adversarial training is possible, such that mode collapse can be easily avoided. In the independent-data setting, the SR formulation includes previously proposed critic-free approaches as special cases (such as Moment Matching Networks, 33, 17; see also 5, 23, 25). Our contributions are:

- We extend the SR formulation to a *prequential* (predictive-sequential, 10) training objective for time-series, suitable for probabilistic forecasting.
- We show that the minimizers of the empirical and expected prequential objective coincide asymptotically, under stationarity and mixing conditions of the observed time-series.
- Finally, we leverage previous works in meteorology and probabilistic forecasting [20, 52] and design training objectives for high-dimensional spatio-temporal data, which enable good performance with no need to add a learnable data transformation.

We apply our probabilistic forecasting method to two benchmark models of chaotic systems and a spatio-temporal weather dataset. We also compare with GANs approaches applied to the same tasks; with respect to the latter, our method requires less hyperparameter tuning and yields better performance, particularly in terms of uncertainty quantification of the forecast.

The rest of the paper is organized as follows. In Sec. 2, we review the standard setup of generative networks training via divergence minimization, introduce the Scoring Rules formulation and connect to previous works which used it. In Sec. 3, which contains the main contributions of our work, we formalize the training objective for probabilistic forecasting and discuss SRs for time-series and spatial data. We discuss some related works in Sec. 4 and show simulation results in Sec. 5. We conclude in Sec. 6.

Notation We use upper case X, Y and Z to denote random variables, and their lower-case counterpart to denote observed values. Bold symbols denote vectors, and subscripts to bold symbols denote sample index (for instance, \mathbf{y}_t). Instead, subscripts to normal symbols denote component indices (for instance, y_i is the i -th component of \mathbf{y} , and $y_{t,j}$ is the j -th component of \mathbf{y}_t). Finally, we use notation $\mathbf{y}_{j:k} = (\mathbf{y}_j, \mathbf{y}_{j+1}, \dots, \mathbf{y}_{k-1}, \mathbf{y}_k)$, for $j \leq k$.

2 Background

2.1 Generative networks via divergence minimization

A generative network represents distributions on some space \mathcal{Y} via a map $h_\phi : \mathcal{Z} \rightarrow \mathcal{Y}$ transforming samples from a probability distribution Q over the space \mathcal{Z} ; the map is parametrized by a Neural Network (NN) with weights ϕ . Samples from P^ϕ are obtained by generating $\mathbf{z} \sim Q$ and computing $h_\phi(\mathbf{z}) \in \mathcal{Y}$; therefore, expectations $\mathbb{E}_{\mathbf{Y} \sim P^\phi}[g(\mathbf{Y})]$ can be computed by $\mathbb{E}_{\mathbf{z} \sim Q}[g(h_\phi(\mathbf{z}))]$.

Assume now we observe data from a distribution P^* and want to tune ϕ so that P^ϕ is as close as possible to P^* . A divergence $D(P^* || P^\phi)$ is a function of two distributions such that $D(P^* || P^\phi) \geq 0$ and $D(P^* || P^\phi) = 0 \iff P^* = P^\phi$. Therefore, for a given D , we can attempt solving:

$$\arg \min_{\phi} D(P^* || P^\phi). \quad (1)$$

Various proposed approaches differ according to (i) their choice of divergence D and (ii) how they estimate the optimal solution in Eq. (1) using samples from P^* and P^ϕ . A popular strategy is choosing D to be an f -divergence (termed f -GAN, 38), in which case a variational lower bound can be obtained:

$$D_f(P^* || P^\phi) \geq \sup_{c \in \mathcal{C}} (\mathbb{E}_{\mathbf{Y} \sim P^*} c(\mathbf{Y}) - \mathbb{E}_{\mathbf{X} \sim P^\phi} f^*(c(\mathbf{X}))),$$

where f^* is the Fenchel conjugate of the function f (Appendix B.1.1) and \mathcal{C} is any set of functions from \mathcal{Y} to the domain of f^* . By representing the set \mathcal{C} by a neural network c_ψ (termed *critic*) with

parameters $\psi \in \Psi$, the problem in Eq. (1) is:

$$\min_{\phi} \max_{\psi} (\mathbb{E}_{\mathbf{Y} \sim P^*} c_{\psi}(\mathbf{Y}) - \mathbb{E}_{\mathbf{X} \sim P^{\phi}} f^*(c_{\psi}(\mathbf{X}))).$$

The WGAN of Arjovsky et al. [1], which uses the 1-Wasserstein distance, has a similar objective to Eq. (2), differing mainly in taking \mathcal{C} to be the set of 1-Lipschitz functions. Details in Appendix B.1.2.

The problem in Eq. (2) is solved by alternating optimization steps over ψ and ϕ ; the expectations are estimated via samples from both P^* (i.e., a minibatch of observations) and from P^{ϕ} . This approach is termed *adversarial* as P^{ϕ} and c_{ψ} respectively aim to minimize and maximize the same objective.

Adversarial training of generative networks is however unstable and difficult. This is partly due to the fact that learning ψ from data with few steps of an optimization procedure and subsequently using that to obtain the gradient of the objective with respect to ϕ leads to biased gradient estimates [4]. A well-known consequence of unstable adversarial training is mode collapse [47], in which the generative distribution collapses to a single point. To avoid adversarial training altogether and bypass the above issues, Moment Matching Networks [33, 17] are trained by considering D to be the squared Maximum Mean Discrepancy (MMD) induced by a positive definite kernel k :

$$D_k(P^*, P^{\phi}) := \mathbb{E}[k(\mathbf{X}, \mathbf{X}') - 2k(\mathbf{X}, \mathbf{Y}) + k(\mathbf{Y}, \mathbf{Y}')], \quad \mathbf{X}, \mathbf{X}' \sim P^{\phi}, \quad \mathbf{Y}, \mathbf{Y}' \sim P^* \quad (3)$$

From Eq. (3), an empirical unbiased estimate of D_k and its gradients can be obtained without introducing a critic network. However, using a fixed kernel on raw data can yield small discriminative power (as in the case of images, where numerical values have little meaning), leading to poor fit of P^{ϕ} to P^* . Li et al. [32] suggested therefore applying a learnable transformation before computing the kernel, with parameters trained to maximize the MMD. This approach, termed MMD-GAN, leads again to an adversarial setting and to the issues mentioned above. Details in Appendix B.1.3.

Conditional setting To represent a conditional distribution $P^{\phi}(\cdot|\boldsymbol{\theta})$, $\boldsymbol{\theta} \in \Theta$, a map $h_{\phi} : \mathcal{Z} \times \Theta \rightarrow \mathcal{Y}$ can be used; similarly to above, samples from $P^{\phi}(\cdot|\boldsymbol{\theta})$ for fixed $\boldsymbol{\theta}$ can be obtained via $h_{\phi}(\mathbf{z}; \boldsymbol{\theta})$, $\mathbf{z} \sim Q$. In this way, f -GAN, WGAN and MMD-GAN can all be easily extended to the setting in which we have data

$$(\boldsymbol{\theta}_i, \mathbf{y}_i)_{i=1}^n, \text{ where } \boldsymbol{\theta}_i \sim \Pi \text{ and } \mathbf{y}_i \sim P^*(\cdot|\boldsymbol{\theta}_i), \quad (4)$$

and want $P^{\phi}(\cdot|\boldsymbol{\theta}) = P^*(\cdot|\boldsymbol{\theta})$ Π -almost everywhere. For instance, the f -GAN objective in Eq. (2) becomes:

$$\min_{\phi} \max_{\psi} \mathbb{E}_{\boldsymbol{\theta} \sim \Pi} (\mathbb{E}_{\mathbf{Y} \sim P^*(\cdot|\boldsymbol{\theta})} c_{\psi}(\mathbf{Y}; \boldsymbol{\theta}) - \mathbb{E}_{\mathbf{Y} \sim P^{\phi}(\cdot|\boldsymbol{\theta})} f^*(c_{\psi}(\mathbf{Y}; \boldsymbol{\theta}))),$$

where now $c_{\psi} : \mathcal{Y} \times \Theta \rightarrow \text{dom}_{f^*}$. More details can be found in Appendix B.1.

2.2 Generative networks via scoring rules minimization

Here, we review a formulation for training generative networks which, in some cases, is intrinsically adversarial-free, as for Moment Matching Networks. This different perspective is based on Scoring Rules (SR), which we introduce next, and will allow us to design objective functions suitable for probabilistic forecasting of time-series (Sec. 3.1) and for tackling spatial data (Sec. 3.2).

A SR S is a function of a distribution and an observation; specifically, $S(P^{\phi}, \mathbf{y})$ represents the penalty assigned to the distribution P^{ϕ} when \mathbf{y} is observed [20, 12]. If \mathbf{y} is the realization of a random variable $\mathbf{Y} \sim P^*$, the expected SR is: $S(P^{\phi}, P^*) := \mathbb{E}_{\mathbf{Y} \sim P^*} S(P^{\phi}, \mathbf{Y})$. S is said to be *proper* relative to a set of distributions \mathcal{P} if the expected Scoring Rule is minimized in P^{ϕ} when $P^{\phi} = P^*$:

$$S(P^*, P^*) \leq S(P^{\phi}, P^*) \quad \forall P^{\phi}, P^* \in \mathcal{P}.$$

Moreover, S is *strictly proper* relative to \mathcal{P} if $P^{\phi} = P^*$ is the unique minimum. In plain words, P^{ϕ} minimizes an expected proper SR S if it has some features corresponding to those of the data distribution P^* ; if S is strictly proper, P^* and P^{ϕ} coincide.

For a strictly proper SR S , the quantity $D(P^{\phi}||P^*) := S(P^{\phi}, P^*) - S(P^*, P^*)$ is a statistical divergence, as in fact $D(P^{\phi}||P^*) \geq 0$ and $D(P^{\phi}||P^*) = 0 \iff P^{\phi} = P^*$. However, not all divergences can be written in terms of a SR (that is not possible, e.g., for the Wasserstein distance).

SRs have been previously used to train conditional generative networks in [5, 23, 25], where the authors considered:

$$\min_{\phi} \mathbb{E}_{\boldsymbol{\theta} \sim \Pi} \mathbb{E}_{\mathbf{Y} \sim P^*(\cdot|\boldsymbol{\theta})} S(P^{\phi}(\cdot|\boldsymbol{\theta}), \mathbf{Y}); \quad (5)$$

for strictly proper S , the solution is $P^{\phi}(\cdot|\boldsymbol{\theta}) = P^*(\cdot|\boldsymbol{\theta})$ Π -almost everywhere. With data as in Eq. (4), we can replace Eq. (5) with:

$$\min_{\phi} \frac{1}{n} \sum_{i=1}^n S(P^{\phi}(\cdot|\boldsymbol{\theta}_i), \mathbf{y}_i), \quad (6)$$

i.e., we evaluate $P^{\phi}(\cdot|\boldsymbol{\theta}_i)$ according to how well it predicts \mathbf{y}_i . The objective in Eq. (6) is an unbiased estimate of that in Eq. (5); therefore, to train P^{ϕ} via Stochastic Gradient Descent, it is enough to obtain unbiased estimates of $\nabla_{\phi} S(P^{\phi}(\cdot|\boldsymbol{\theta}_i), \mathbf{y}_i)$. That is possible whenever S is defined via an expectation over P^{ϕ} , in which case we can train P^{ϕ} without adversarial setup. More details in Appendix C.

Eq. (5) is equivalent to $\min_{\phi} \mathbb{E}_{\boldsymbol{\theta} \sim \Pi} D(P^{\phi}(\cdot|\boldsymbol{\theta}) || P^*(\cdot|\boldsymbol{\theta}))$, where D is the divergence associated to S . For instance, conditional MMD-GAN corresponds to setting S in Eq. (5) to be the *Kernel Score* [20]:

$$S_k(P^{\phi}, \mathbf{y}) := \mathbb{E}[k(\mathbf{X}, \mathbf{X}')] - 2 \cdot \mathbb{E}[k(\mathbf{X}, \mathbf{y})], \quad \mathbf{X}, \mathbf{X}' \sim P^{\phi} \quad (7)$$

where k is a positive definite kernel. We can obtain unbiased gradient estimates for Eq. (7) by replacing expectations with empirical means over simulations from P^{ϕ} . Under some conditions on P^{ϕ} and for a specific class of kernels, S_k is strictly proper (see Appendix B.2). Additionally, the Energy Score used in [5, 23, 25] can be obtained from S_k by choosing $k(\mathbf{x}, \mathbf{y}) = -\|\mathbf{y} - \mathbf{x}\|^{\beta}$ for $\beta \in (0, 2)$ [20]. See more details in Appendix B.2.

3 Generative networks for spatio-temporal models via SR minimization

We will now extend the SR formulation to a training objective for probabilistic forecasting for time-series (Sec. 3.1). Later (Sec. 3.2), we will exploit the SR formulation to tackle high dimensional spatial data, by relying on scores studied in the probabilistic forecasting and meteorology literature [20, 52]. The resulting objectives can be minimized without recurring to adversarial training.

3.1 Time-series probabilistic forecasting via the prequential SR

Consider a temporal stochastic process $(\mathbf{Y}_1, \mathbf{Y}_2, \dots, \mathbf{Y}_t, \dots) = (\mathbf{Y}_t)_t \sim P^*$, where $\mathbf{Y}_t \in \mathcal{Y}$; in general, \mathbf{Y}_t 's are *not* independent. For a generic distribution P for $(\mathbf{Y}_t)_t$, we denote by P_t the marginal distribution for \mathbf{Y}_t , and by $P_{r:s}$ the marginal distribution for $\mathbf{Y}_{r:s}$; the conditional distribution for $\mathbf{Y}_t | \mathbf{y}_{u:v}$ will be denoted by $P_t(\cdot | \mathbf{y}_{u:v})$ and similar for $\mathbf{Y}_{r:s}$.

Having observed $\mathbf{y}_{1:t}$, we produce a *probabilistic forecast* for \mathbf{Y}_{t+l} for a given lead time l via a generative network conditioned on the last k observations, $P_{t+l}^{\phi}(\cdot | \mathbf{y}_{t-k+1:t})$. By repeating this procedure for all t 's in a recorded window of length T , P^{ϕ} induces a joint distribution over $\mathbf{Y}_{k+l:T}$ given $\mathbf{y}_{1:k+l-1}$, denoted $P_{k+l:T}^{\phi}(\cdot | \mathbf{y}_{1:k+l-1})$ (as in fact the generative network cannot forecast the first elements of the sequence $\mathbf{y}_{1:k+l-1}$). For each t , we evaluate the forecast performance via $S(P_{t+l}^{\phi}(\cdot | \mathbf{y}_{t-k+1:t}), \mathbf{y}_{t+l})$ for a SR S (Fig. 1); summing this for all t 's, we obtain:

$$S_T(P_{k+l:T}^{\phi}(\cdot | \mathbf{y}_{1:k+l-1}), \mathbf{y}_{k+l:T}) := \sum_{t=k}^{T-l} S(P_{t+l}^{\phi}(\cdot | \mathbf{y}_{t-k+1:t}), \mathbf{y}_{t+l}). \quad (8)$$

The above notation only makes sense as the distribution for \mathbf{Y}_{t+l} in $P_{k+l:T}^{\phi}(\cdot | \mathbf{y}_{1:k+l-1})$ depends only on $\mathbf{Y}_{t-k+1:t}$; otherwise, $\mathbf{y}_{1:k+l-1}$ should also appear explicitly in the conditioning of P_{t+l}^{ϕ} . This is formalized by the following property (which recovers the standard k -Markov property for $l = 1$):

Definition 3.1. A probability distribution $P_{1:T}$ is k -Markovian with lag l if, assuming it has density $p_{1:T}$ with respect to some base measure, it can be decomposed as: $p_{1:T}(\mathbf{y}_{1:T}) = p_{1:k+l-1}(\mathbf{y}_{1:k+l-1}) \prod_{t=k}^{T-l} p_{t+l}(\mathbf{y}_{t+l} | \mathbf{y}_{t-k+1:t})$.

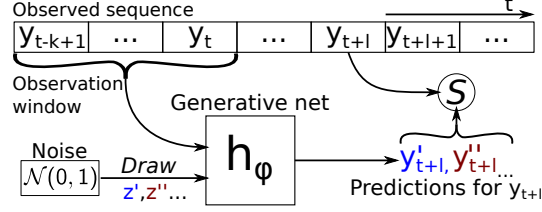


Figure 1: Estimation of the SR evaluating the forecast $P_{t+l}^\phi(\cdot|y_{t-k+1:t})$ for the realization y_{t+l} . The prequential SR is obtained by repeating this procedure for all t 's and summing the scores.

We call S_T in Eq. (8) the *prequential* (or *predictive-sequential*) score [10, 13], as it evaluates sequential predictions. S_T is a SR for distributions over $\mathbf{Y}_{k+l:T}|\mathbf{y}_{1:k+l-1}$ which are k -Markovian with lag l .

We propose therefore to learn ϕ by:

$$\hat{\phi}_T(\mathbf{y}_{1:T}) := \arg \min_{\phi} S_T(P_{k+l:T}^\phi(\cdot|\mathbf{y}_{1:k+l-1}), \mathbf{y}_{k+l:T}), \quad (9)$$

which picks the best ϕ for which the average l -steps ahead forecast in the training data is optimal according to S . Operationally, Eq. (9) can be solved in the same way as Eq. (6), i.e., by simulating from P^ϕ for each observation window $\mathbf{y}_{t-k+1:t}$ in a training batch, unbiasedly estimating the SR S and descending the gradient. However, contrarily to the independent-data setting of Eq. (6), Eq. (9) cannot be motivated as an empirical estimate of an expected SR, as the different \mathbf{y}_t 's are dependent. Still, we show below how the empirical minimizer $\hat{\phi}_T(\mathbf{Y}_{1:T})$ converges, under some stationarity and mixing conditions of $(\mathbf{Y}_t)_t$, to a fixed quantity corresponding to the minimizer of a proper SR. First, Theorem 3.2 below (proven in Appendix A.2.2) establishes propriety properties of S_T :

Theorem 3.2. *If S is (strictly) proper, then S_T is (strictly) proper for distributions over $\mathbf{Y}_{k+l:T}|\mathbf{y}_{1:k+l-1}$ which are k -Markovian with lag l .*

Consider now the following two quantities:

$$\begin{aligned} \tilde{\phi}_T(\mathbf{y}_{1:k+l-1}) &:= \arg \min_{\phi} \mathbb{E}_{\mathbf{Y}_{k+l:T}|\mathbf{y}_{1:k+l-1}} S_T(P_{k+l:T}^\phi(\cdot|\mathbf{y}_{1:k+l-1}), \mathbf{Y}_{k+l:T}), \\ \phi_T^* &:= \arg \min_{\phi} \mathbb{E} S_T(P_{k+l:T}^\phi(\cdot|\mathbf{Y}_{1:k+l-1}), \mathbf{Y}_{k+l:T}). \end{aligned}$$

$\tilde{\phi}_T(\mathbf{y}_{1:k+l-1})$ is the minimizer of the expected prequential SR with respect to $\mathbf{Y}_{k+l:T}|\mathbf{y}_{1:k+l-1}$ which, from Theorem 3.2, is minimized when the true distribution for $\mathbf{Y}_{k+l:T}|\mathbf{y}_{1:k+l-1}$ is recovered. ϕ_T^* instead minimizes the expectation of S_T with respect to the full sequence $\mathbf{Y}_{1:T}$.

Now, each term in the sum defining S_T depends on a finite number of observations; therefore, if $(\mathbf{Y}_t)_t$ satisfies some mixing and stationarity properties, we expect $\tilde{\phi}_T(\mathbf{y}_{1:k+l-1})$ to not depend on $\mathbf{y}_{1:k+l-1}$ for large T ; similarly, we expect the empirical estimator $\hat{\phi}_T(\mathbf{y}_{1:T})$ to converge to a fixed quantity. The following Theorem proves such consistency of $\hat{\phi}_T(\mathbf{y}_{1:T})$ and $\tilde{\phi}_T(\mathbf{y}_{1:k+l-1})$ to ϕ_T^* .

Theorem 3.3. *Assume ϕ_T^* and $\tilde{\phi}_T(\mathbf{y}_{1:k+l-1})$ are unique for each fixed $\mathbf{y}_{1:k+l-1}$, and $(\mathbf{Y}_t)_t$ is asymptotically stationary and satisfies some mixing properties. Then, under some regularity conditions, it exists a metric d such that $d(\phi_T^*, \hat{\phi}_T(\mathbf{Y}_{1:T})) \rightarrow 0$ and $d(\tilde{\phi}_T(\mathbf{Y}_{1:k+l-1}), \hat{\phi}_T(\mathbf{Y}_{1:T})) \rightarrow 0$ when $T \rightarrow \infty$ almost surely with respect to $(\mathbf{Y}_t)_t \sim P^*$. It also follows that $d(\tilde{\phi}_T(\mathbf{Y}_{1:k+l-1}), \phi_T^*) \rightarrow 0$.*

The precise statement of Theorem 3.3 is given and proven in Appendix A.3; our proof holds when P_{t+l}^ϕ depends on t only through the value of the past observations, which is our case of interest as we use the same generative network for all t 's. In plain words, the mixing properties require \mathbf{Y}_{t-m} and \mathbf{Y}_t to become independent as $m \rightarrow \infty$, while asymptotic stationarity means that the average of the marginal distributions over different t converges to a constant distribution.

Under the assumptions of Theorem 3.3, with large enough T , $\hat{\phi}_T(\mathbf{y}_{1:T})$ and $\tilde{\phi}_T(\mathbf{y}_{1:k+l-1})$ will both be independent of the observed sequence $\mathbf{y}_{1:T}$ and will converge to ϕ_T^* . Therefore, minimizing the empirical prequential SR in Eq. (8) asymptotically recovers the minimizer of an expected proper SR, which additionally does not depend on the initial conditions of the sequence $\mathbf{y}_{1:k+l-1}$.

3.2 Scoring rules for spatial data

In contrast to multivariate, spatial data is structured: the relation between different entries depends on their spatial distance. Computing, say, the Kernel SR in Eq. (7) would not capture this structure; we discuss here SRs which instead do, and which we will use for a spatio-temporal dataset (Sec. 5.2).

Variogram Score Say now $\mathcal{Y} \subseteq \mathbb{R}^d$. For any $p > 0$, the Variogram Score [52] is defined as:

$$S_V^{(p)}(P^\phi, \mathbf{y}) := \sum_{i,j=1}^d w_{ij} (|y_i - y_j|^p - \mathbb{E}_{\mathbf{X} \sim P^\phi} |X_i - X_j|^p)^2, \quad (10)$$

where $w_{ij} > 0$ are fixed scalars. Scheuerer and Hamill [52] set w_{ij} to be inversely proportional to the distance of locations i and j to capture the spatial structure. However, $S_V^{(p)}$ is proper but not strictly so: it is invariant to change of sign and shift of all entries of \mathbf{X} by a constant, and only depends on the moments of P^ϕ up to order $2p$ [52]. We will fix $p = 1$ in the rest of our work.

Patched SR To convey the spatial structure of the data, we can compute, say, the Kernel SR on a localized *patch* of the data. In this way, the resulting score only considers correlation between near-by components. We can then shift the patch across the map and cumulate the resulting score (see Fig. 4 in Appendix). However, this SR is not strictly proper as it does not evaluate long-range dependencies. A similar approach was suggested for an adversarial setting in Isola et al. [27], where the critic outputs separate numerical values for different patches of an input image.

Sum of SRs Both SRs introduced above are non-strictly proper: a generative network trained to minimize those may represent some features of the true data distribution, but not all of them (as the sign in the case of the Variogram Score). We can however obtain a strictly proper SR by adding a strictly proper SR to a proper one, as stated by the following (proof in Appendix A.1).

Lemma 3.4. *Consider two proper SRs S_1 and S_2 , and let $\alpha_1, \alpha_2 > 0$; the quantity:*

$$S_+(P, \mathbf{y}) = \alpha_1 \cdot S_1(P, \mathbf{y}) + \alpha_2 \cdot S_2(P, \mathbf{y})$$

is a proper SR. If at least one of S_1 and S_2 is also strictly proper, then S_+ is strictly proper.

Probabilistic forecasting for spatial data Inserting the spatial SRs discussed above in the prequential score in Eq. (8) enables probabilistic forecasting for spatial data using generative networks. For the Variogram Score, unbiased gradient estimates can be computed by simulating from P^ϕ ; same holds for the patched SR if the underlying SR admits unbiased gradient estimates (Appendix C).

4 Related works

In the statistics literature, Dawid et al. [14] studied a SR parameter estimator for independent and identically distributed data; instead, Dawid and Musio [11] used SRs to infer parameters for spatial models, considering the conditional distribution in each location given all the others to be available; finally, Dawid and Musio [13] considered model selection based on SRs and studied a prequential application. Properties of prequential losses for forecasting systems, such as our Eq. (8), were investigated in Skouras [53], which also gave consistency results similar to our Theorem 3.3.

Kwon and Park [30], Koochali et al. [29], Bihlo [3] and Ravuri et al. [46], among others, all used GANs for forecasting. However, they all considered the training samples to be independent in their formulation and did not study theoretically the consequence of using dependent data. Bihlo [3] considered a task similar to ours (which we privileged for ease of reproducibility as it is a standardized dataset) and found the GAN to underestimate uncertainty, so they considered a GANs ensemble increase the uncertainty. Instead, Ravuri et al. [46] exploited GANs for a precipitation *nowcasting* task (i.e., predicting for small lead time), achieving good deterministic and probabilistic performance with large amount of architecture hand-tuning and computing power.

Deterministic forecasting with NNs for the WeatherBench dataset (Sec. 5.2) was studied extensively [16, 49, 50, 54]. Fewer studies tackled probabilistic forecasting: Scher and Messori [51] combined deterministic NNs with ad-hoc strategies, not guaranteed to lead to the correct distribution. Clare et al. [9] binned instead the data, thus mapping the problem to that of estimating a categorical distribution.

5 Simulation study

We first study two low-dimensional time-series model which allow exhaustive hyperparameter tuning and architecture comparison, but still have challenging dynamics due to their chaotic nature. We then move to a high-dimensional spatio-temporal meteorology dataset. For all examples, we train generative models with the Energy and the Kernel Scores (Appendix B.2) and their sum, termed *Energy-Kernel Score* (a strictly proper SR due to Lemma 3.4). Additional SRs, discussed later in Sec. 5.2, are used for the meteorology example. For the Kernel Score, we use the Gaussian kernel (Appendix B.2) with bandwidth γ tuned from the validation set (Appendix E.1). For all SR methods, we use 10 forecasts from the generator for each observation window to estimate SR values during training; however, performance does not degrade when using as few as 3 simulations (Appendix F.3.2), which lowers the computational cost (Appendix F.3.3). We compare with the original GAN [21] and WGAN with gradient penalties (WGAN-GP, 24). The latent variable \mathbf{Z} has independent components with standard normal distribution. To put in context the deterministic performance of the probabilistic methods, we compare with deterministic networks trained to minimize the standard regression loss.

All datasets consist of a long time series, which we split into training, validation and test set. We use the validation set for early stopping and hyperparameter tuning and report final performance on the test set. The adversarial methods do not allow early stopping or hyperparameter selection using the training objective, as the generator loss depends on the critic state. For these methods, therefore, we use other metrics to pick the best hyperparameters (see below).

On the test set, we assess the calibration of the probabilistic forecasts by the *calibration error* (the discrepancy between credible intervals in the forecast distribution and the actual frequencies). We also evaluate how close the means of the forecast distributions are to the observation by the *Normalized Root Mean-Square Error* (NRMSE) and the *coefficient of determination* R^2 ; we detail all these metrics in Appendix D. As all these metrics are for scalar variables, we compute their values independently for each component and report their average (standard deviation in Appendix F).

Our simulations show how the SR methods are easier to train and provide better uncertainty quantification. The adversarial methods require more hyperparameter tuning. We find the original GAN to be unstable and very poor at quantifying uncertainty due to mode collapse; WGAN-GP performs better, but has still inferior performance with respect to the SR approaches. Likely, ad-hoc adversarial training strategies could lead to better performance; however, the possibility of effortlessly training with off-the-shelf methods is an advantage of the SR approaches. Code for reproducing results is available here.

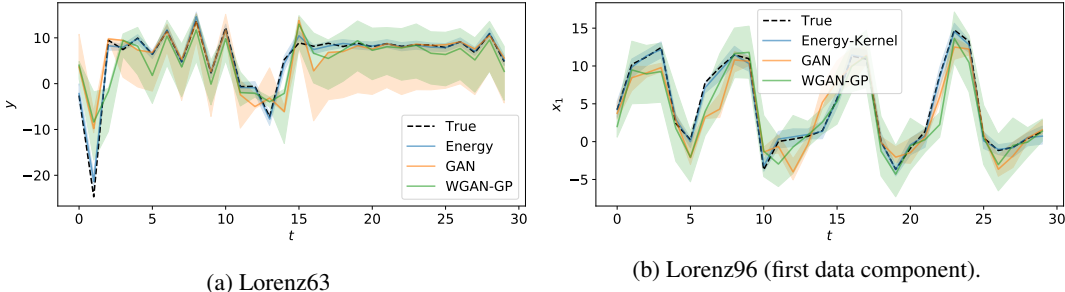


Figure 2: Results for selected methods for Lorenz63 and Lorenz96 (first data component): median forecasts (solid line) and 99% credible area (shaded area) for a part of the test set. For each t , forecasts are obtained using the previous observation window. Credible regions for GAN and WGAN-GP are broader but contain the truth less frequently.

5.1 Time-series models

We consider the Lorenz63 [34] and Lorenz96 [35] chaotic models (Appendices E.2.1 and E.3.1). The former is defined on a 3-dimensional variable, a single component of which we assume to observe. The latter contains two sets of variables; we observe only one of them, which is 8-dimensional. In both cases, we generate an observed trajectory from a long model integration, from which we take the first 60% as training set, the following 20% as validation and the remaining 20% as test.

We train the generative networks to forecast the next time-step ($l = 1$) from an observation window of size $k = 10$. We use recurrent NNs based on Gated Recurrent Units (GRU, [8]; Appendices E.2.2 and E.3.2); we also tested fully connected networks but they had worse performance (see results in Appendix F.1 and F.2). For the SR methods, we select the best learning rate among 6 values according to the validation loss. For the adversarial methods, we consider instead 14 learning rates for both generator and critic; we also try two hidden dimensions for the GRU layers and four numbers of critic training steps for WGAN-GP; overall, we run 392 experiments for GAN and 1568 for WGAN-GP. As the validation loss is not a meaningful metric for adversarial approaches, we report results for 3 different configurations for GAN and WGAN-GP, maximizing either deterministic performance (1) or calibration (2), or striking the best balance between these two (3). More details are in Appendix E.2.3 and E.3.3). These experiments are run on CPU machines and take at most few minutes to complete.

In Table 1, we report performance metrics on the test set. The Kernel Score excels in deterministic forecast, getting close or outperforming the regression loss; however, all SR methods lead to combined great deterministic and probabilistic performance. On the other hand, adversarial methods are capable of good deterministic performance (1) or calibration (2) independently; but either of these two is at the expense of the other; the configuration with the best trade-off (3) is in fact much worse than the SR methods (with WGAN-GP better than GAN). In Fig. 2, we show observation and forecast for a part of the test set, for GAN and WGAN-GP in configuration 3, the Energy Score for Lorenz63 and the Energy-Kernel Score for Lorenz96. For the two SR methods, the median forecast is close to the observation and the credible region contains the true observation for most time-steps. For GAN and WGAN-GP, the match with the observation is worse and credible regions generally contain the truth less frequently albeit being wider. Additional results in Appendices F.1 and F.2.

Table 1: Performance on test set for the different methods, on the Lorenz63 and Lorenz96 models. Results with three hyperparameter configurations are reported for GAN and WGAN-GP, see text. Overall, SR methods perform well on both calibration and deterministic forecast metrics (NMRSE and R^2), while adversarial approaches are incapable of doing so.

	Lorenz63			Lorenz96		
	Cal. error ↓	NRMSE ↓	R^2 ↑	Cal. error ↓	NRMSE ↓	R^2 ↑
Regression	-	0.0079	0.9977	-	0.0198	0.9905
Energy	0.0380	0.0105	0.9960	0.0205	0.0166	0.9933
Kernel	0.0910	0.0083	0.9975	0.2196	0.0164	0.9935
Energy-Kernel	0.1000	0.0114	0.9953	0.0104	0.0173	0.9928
GAN (1)	0.4830	0.0274	0.9729	0.4644	0.0354	0.9696
GAN (2)	0.0860	0.2425	-1.1166	0.2671	0.1500	0.4537
GAN (3)	0.3590	0.0698	0.8245	0.3700	0.0763	0.8590
WGAN-GP (1)	0.4710	0.0398	0.9429	0.4134	0.0330	0.9736
WGAN-GP (2)	0.0270	0.1243	0.4440	0.0565	0.1081	0.7165
WGAN-GP (3)	0.2100	0.0914	0.6996	0.1648	0.0786	0.8502

5.2 Meteorological dataset

The WeatherBench dataset² for data-driven weather forecasting [45] contains hourly values of several atmospheric fields from 1979 to 2018 at different resolutions; we choose here a resolution of 5.625° over both longitude and latitude, corresponding to a 32×64 grid. We consider a single observation per day (12:00 UTC) and the 500 hPa geopotential (Z500) variable. We forecast with a lead of 3 days ($l = 3$) from a single observation ($k = 1$). We use the years from 1979 to 2006 as training set, 2007 to 2016 as validation test and 2017 to 2018 as test set.

In addition to the Energy, Kernel and Energy-Kernel Scores, we test the spatial SRs introduced in Sec 3.2. Specifically, we consider the Variogram Score with weights w inversely proportional to the distance on the globe (Appendix E.4.1) and sum it to the Energy (*Energy-Variogram*) or to the Kernel (*Kernel-Variogram*) Scores. We also consider the Patched Energy Score with patch size 8

²Released under MIT license, see here.

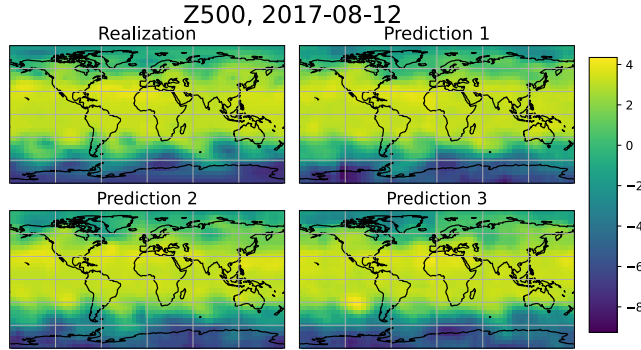


Figure 3: Realization and example of predictions obtained with the patched Energy Score (patch size 16) for a specific date in the test set for the WeatherBench dataset. The predictions capture the main features but are slightly different from each other.

Table 2: Performance on WeatherBench test set for different methods. Results with three hyperparameter configurations are reported for GAN, see text. SR methods perform well on both calibration and deterministic forecast metrics (NRMSE and R^2). WGAN-GP is worse and GAN is drastically worse.

	Cal. error ↓	NRMSE ↓	R^2 ↑
Regression	-	0.1162	0.5300
Patched Regression, 8	-	0.1147	0.5459
Patched Regression, 16	-	0.1144	0.5509
Energy	0.0863	0.1208	0.4968
Kernel	0.0797	0.1200	0.5097
Energy-Kernel	0.0794	0.1194	0.5150
Energy-Variogram	0.0899	0.1192	0.5177
Kernel-Variogram	0.1704	0.1203	0.5050
Patched Energy, 8	0.0550	0.1189	0.5217
Patched Energy, 16	0.0690	0.1186	0.5248
GAN (1)	0.4845	0.1573	0.1418
GAN (2)	0.3130	0.2487	-2.7970
GAN (3)	0.3625	0.1693	-0.0117
WGAN-GP	0.1009	0.1302	0.4340

and 16; to ensure the score is strictly proper, we add the overall Energy Score (summation weights in Appendix E.4.2). We also consider patched regression loss.

We employ a U-NET architecture [39] for the generative network and a PatchGAN discriminator [27] for the critic (Appendix E.4.3). For the SR methods, we select the best learning rate among 6 values according to the validation loss; for the adversarial ones, we consider instead 7 values for both generator and critic, resulting in 49 experiments. We then pick the setups optimizing deterministic or calibration performance. For WGAN-GP, a single configuration optimizes both; for GAN, that did not happen. As for the time-series models, we report therefore results for setups maximizing either deterministic performance (1) or calibration (2), or striking the best balance between these two (3). All trainings are run on a single Tesla V100 GPU; computing times are reported in Appendix F.3.3.

Table 2 contains performance metrics on the test set. The Patched Energy Scores yield the best performance, with deterministic skill only slightly worse than the regression loss. Energy-Variogram and Kernel-Variogram are worse than the standard Energy and Kernel ones; moreover, as the Variogram Score requires quadratic memory in data size, a smaller batch size was needed for training (Appendix E.4.4). All GAN configurations have bad performance, while WGAN-GP is acceptable, but still worse than the SR methods. In Fig. 3 we show observation and three different predictions obtained with the Patched Energy Score for a date in the test set. More results in Appendix F.3.

6 Conclusions

We gave an overview of a formulation for generative networks training based on Scoring Rules and compared it to the standard one based on divergences, to which the former is complementary. The advantages of the Scoring Rule formulation are: (i) it provides a principled objective for probabilistic forecasting; (ii) it yields adversarial-free training, with which better uncertainty quantification is possible, as we show empirically; (iii) it enables leveraging the literature on SRs to define objectives for spatio-temporal datasets. The resulting training method is easier to use and requires less hyperparameter tuning compared to adversarial methods.

We highlight the following limitations of our work: first, our Theorem 3.3 relies on assumptions which are hard to verify; however, we believe similar consistency properties hold provided the temporal process satisfies some generic stationarity and memory-less properties. Secondly, we do not experiment forecasting multiple time-steps at once as we preferred focusing on single time-step forecast tasks for the matter of analytical simplicity while developing our framework. Doing so would be however a useful extension of our work; in practice, SRs assessing temporal coherence analogous to what done with temporal discriminators in [46] in the adversarial setting could be developed.

Acknowledgments and Disclosure of Funding

LP is supported by the EPSRC and MRC through the OxWaSP CDT programme (EP/L016710/1), which also funds the computational resources used to perform this work. RD is funded by EPSRC (grant nos. EP/V025899/1, EP/T017112/1) and NERC (grant no. NE/T00973X/1). PD gratefully acknowledges funding from the Royal Society for his University Research Fellowship, as well as from the ESiWACE Horizon 2020 project (#823988) and the MAELSTROM EuroHPC Joint Undertaking project (#955513). We thank Geoff Nicholls, Christian Robert, Peter Watson, Matthew Chantry, Mihai Alexe and Eugenio Clerico for valuable feedback and suggestions.

References

- [1] M. Arjovsky, S. Chintala, and L. Bottou. Wasserstein generative adversarial networks. In *International conference on machine learning*, pages 214–223. PMLR, 2017.
- [2] M. G. Bellemare, I. Danihelka, W. Dabney, S. Mohamed, B. Lakshminarayanan, S. Hoyer, and R. Munos. The Cramer distance as a solution to biased Wasserstein gradients. *arXiv preprint arXiv:1705.10743*, 2017.
- [3] A. Bihlo. A generative adversarial network approach to (ensemble) weather prediction. *Neural Networks*, 139:1–16, 2021.
- [4] M. Bińkowski, D. J. Sutherland, M. Arbel, and A. Gretton. Demystifying MMD GANs. In *International Conference on Learning Representations*, 2018.
- [5] D. Bouchacourt, P. K. Mudigonda, and S. Nowozin. DISCO nets: DISsimilarity COefficient networks. *Advances in Neural Information Processing Systems*, 29:352–360, 2016.
- [6] R. C. Bradley. Basic properties of strong mixing conditions. a survey and some open questions. *Probability surveys*, 2:107–144, 2005.
- [7] B.-E. Chérif-Abdellatif and P. Alquier. MMD-Bayes: Robust Bayesian estimation via maximum mean discrepancy. In *Symposium on Advances in Approximate Bayesian Inference*, pages 1–21. PMLR, 2020.
- [8] K. Cho, B. van Merriënboer, D. Bahdanau, and Y. Bengio. On the properties of neural machine translation: Encoder–decoder approaches. In *Proceedings of SSST-8, Eighth Workshop on Syntax, Semantics and Structure in Statistical Translation*, pages 103–111, Doha, Qatar, Oct. 2014. Association for Computational Linguistics. doi: 10.3115/v1/W14-4012. URL <https://aclanthology.org/W14-4012>.
- [9] M. C. Clare, O. Jamil, and C. J. Morcrette. Combining distribution-based neural networks to predict weather forecast probabilities. *Quarterly Journal of the Royal Meteorological Society*, 147(741):4337–4357, 2021.

- [10] A. P. Dawid. Present position and potential developments: Some personal views statistical theory the prequential approach. *Journal of the Royal Statistical Society: Series A (General)*, 147(2):278–290, 1984.
- [11] A. P. Dawid and M. Musio. Estimation of spatial processes using local scoring rules. *ASta Advances in Statistical Analysis*, 97(2):173–179, 2013.
- [12] A. P. Dawid and M. Musio. Theory and applications of proper scoring rules. *Metron*, 72(2): 169–183, 2014.
- [13] A. P. Dawid and M. Musio. Bayesian model selection based on proper scoring rules. *Bayesian analysis*, 10(2):479–499, 2015.
- [14] A. P. Dawid, M. Musio, and L. Ventura. Minimum scoring rule inference. *Scandinavian Journal of Statistics*, 43(1):123–138, 2016.
- [15] I. Domowitz and H. White. Misspecified models with dependent observations. *Journal of Econometrics*, 20(1):35–58, 1982. ISSN 0304-4076. doi: [https://doi.org/10.1016/0304-4076\(82\)90102-6](https://doi.org/10.1016/0304-4076(82)90102-6). URL <https://www.sciencedirect.com/science/article/pii/0304407682901026>.
- [16] P. D. Dueben and P. Bauer. Challenges and design choices for global weather and climate models based on machine learning. *Geoscientific Model Development*, 11(10):3999–4009, 2018.
- [17] G. K. Dziugaite, D. M. Roy, and Z. Ghahramani. Training generative neural networks via maximum mean discrepancy optimization. *arXiv preprint arXiv:1505.03906*, 2015.
- [18] D. J. Gagne, H. M. Christensen, A. C. Subramanian, and A. H. Monahan. Machine learning for stochastic parameterization: Generative adversarial networks in the Lorenz’96 model. *Journal of Advances in Modeling Earth Systems*, 12(3):e2019MS001896, 2020.
- [19] T. Gneiting and M. Katzfuss. Probabilistic forecasting. *Annual Review of Statistics and Its Application*, 1:125–151, 2014.
- [20] T. Gneiting and A. E. Raftery. Strictly proper scoring rules, prediction, and estimation. *Journal of the American statistical Association*, 102(477):359–378, 2007.
- [21] I. Goodfellow, J. Pouget-Abadie, M. Mirza, B. Xu, D. Warde-Farley, S. Ozair, A. Courville, and Y. Bengio. Generative adversarial nets. *Advances in neural information processing systems*, 27, 2014.
- [22] A. Gretton, K. M. Borgwardt, M. J. Rasch, B. Schölkopf, and A. Smola. A kernel two-sample test. *The Journal of Machine Learning Research*, 13(1):723–773, 2012.
- [23] A. A. Gritsenko, T. Salimans, R. v. d. Berg, J. Snoek, and N. Kalchbrenner. A spectral energy distance for parallel speech synthesis. *arXiv preprint arXiv:2008.01160*, 2020.
- [24] I. Gulrajani, F. Ahmed, M. Arjovsky, V. Dumoulin, and A. Courville. Improved training of Wasserstein GANs. In *Proceedings of the 31st International Conference on Neural Information Processing Systems*, pages 5769–5779, 2017.
- [25] A. Harakeh and S. L. Waslander. Estimating and evaluating regression predictive uncertainty in deep object detectors. In *International Conference on Learning Representations*, 2021. URL <https://openreview.net/forum?id=YLewtnvKgR7>.
- [26] H. Hersbach. Decomposition of the continuous ranked probability score for ensemble prediction systems. *Weather and Forecasting*, 15(5):559–570, 2000.
- [27] P. Isola, J.-Y. Zhu, T. Zhou, and A. A. Efros. Image-to-image translation with conditional adversarial networks. In *Proceedings of the IEEE conference on computer vision and pattern recognition*, pages 1125–1134, 2017.
- [28] D. P. Kingma and M. Welling. Auto-encoding variational Bayes. *arXiv preprint arXiv:1312.6114*, 2013.

- [29] A. Koochali, A. Dengel, and S. Ahmed. If you like it, GAN it—probabilistic multivariate times series forecast with GAN. *Engineering Proceedings*, 5(1):40, Jul 2021. ISSN 2673-4591. doi: 10.3390/engproc2021005040. URL <http://dx.doi.org/10.3390/engproc2021005040>.
- [30] Y.-H. Kwon and M.-G. Park. Predicting future frames using retrospective cycle gan. In *Proceedings of the IEEE/CVF Conference on Computer Vision and Pattern Recognition*, pages 1811–1820, 2019.
- [31] M. Leutbecher and T. N. Palmer. Ensemble forecasting. *Journal of computational physics*, 227(7):3515–3539, 2008.
- [32] C.-L. Li, W.-C. Chang, Y. Cheng, Y. Yang, and B. Póczos. MMD GAN: Towards deeper understanding of moment matching network. In *NIPS*, 2017.
- [33] Y. Li, K. Swersky, and R. Zemel. Generative moment matching networks. In *International Conference on Machine Learning*, pages 1718–1727. PMLR, 2015.
- [34] E. N. Lorenz. Deterministic nonperiodic flow. *Journal of atmospheric sciences*, 20(2):130–141, 1963.
- [35] E. N. Lorenz. Predictability: A problem partly solved. In *Proc. Seminar on predictability*, volume 1, 1996.
- [36] M. Mirza and S. Osindero. Conditional generative adversarial nets. *arXiv preprint arXiv:1411.1784*, 2014.
- [37] H. D. Nguyen, J. Arbel, H. Lü, and F. Forbes. Approximate Bayesian computation via the energy statistic. *IEEE Access*, 8:131683–131698, 2020.
- [38] S. Nowozin, B. Cseke, and R. Tomioka. f-GAN: Training generative neural samplers using variational divergence minimization. In *Proceedings of the 30th International Conference on Neural Information Processing Systems*, pages 271–279, 2016.
- [39] R. Olaf, F. Philipp, and B. Thomas. U-Net: Convolutional networks for biomedical image segmentation, 2015.
- [40] T. Palmer. Towards the probabilistic Earth-system simulator: a vision for the future of climate and weather prediction. *Quarterly Journal of the Royal Meteorological Society*, 138(665): 841–861, 2012.
- [41] M. Park, W. Jitkrittum, and D. Sejdinovic. K2-ABC: Approximate Bayesian computation with kernel embeddings. In *Artificial Intelligence and Statistics*, 2016.
- [42] A. Paszke, S. Gross, F. Massa, A. Lerer, J. Bradbury, G. Chanan, T. Killeen, Z. Lin, N. Gimelshein, L. Antiga, A. Desmaison, A. Kopf, E. Yang, Z. DeVito, M. Raison, A. Tejani, S. Chilamkurthy, B. Steiner, L. Fang, J. Bai, and S. Chintala. PyTorch: An imperative style, high-performance deep learning library. In H. Wallach, H. Larochelle, A. Beygelzimer, F. d’Alché Buc, E. Fox, and R. Garnett, editors, *Advances in Neural Information Processing Systems 32*, pages 8024–8035. Curran Associates, Inc., 2019.
- [43] B. M. Pötscher and I. R. Prucha. A uniform law of large numbers for dependent and heterogeneous data processes. *Econometrica: Journal of the Econometric Society*, pages 675–683, 1989.
- [44] S. T. Radev, U. K. Mertens, A. Voss, L. Ardizzone, and U. Köthe. BayesFlow: Learning complex stochastic models with invertible neural networks. *IEEE Transactions on Neural Networks and Learning Systems*, 2020.
- [45] S. Rasp, P. D. Dueben, S. Scher, J. A. Weyn, S. Mouatadid, and N. Thuerey. WeatherBench: a benchmark data set for data-driven weather forecasting. *Journal of Advances in Modeling Earth Systems*, 12(11):e2020MS002203, 2020.
- [46] S. Ravuri, K. Lenc, M. Willson, D. Kangin, R. Lam, P. Mirowski, M. Fitzsimons, M. Athanasiadou, S. Kashem, S. Madge, et al. Skillful precipitation nowcasting using deep generative models of radar. *arXiv preprint arXiv:2104.00954*, 2021.

- [47] E. Richardson and Y. Weiss. On GANs and GMMs. In *Proceedings of the 32nd International Conference on Neural Information Processing Systems*, pages 5852–5863, 2018.
- [48] M. L. Rizzo and G. J. Székely. Energy distance. *Wiley interdisciplinary reviews: Computational statistics*, 8(1):27–38, 2016.
- [49] S. Scher. Toward data-driven weather and climate forecasting: Approximating a simple general circulation model with deep learning. *Geophysical Research Letters*, 45(22):12–616, 2018.
- [50] S. Scher and G. Messori. Weather and climate forecasting with neural networks: using general circulation models (GCMs) with different complexity as a study ground. *Geoscientific Model Development*, 12(7):2797–2809, 2019.
- [51] S. Scher and G. Messori. Ensemble methods for neural network-based weather forecasts. *Journal of Advances in Modeling Earth Systems*, 13(2), 2021.
- [52] M. Scheuerer and T. M. Hamill. Variogram-based proper scoring rules for probabilistic forecasts of multivariate quantities. *Monthly Weather Review*, 143(4):1321–1334, 2015.
- [53] K. Skouras. *On the optimal performance of forecasting systems: The prequential approach*. University of London, University College London (United Kingdom), 1998.
- [54] J. A. Weyn, D. R. Durran, and R. Caruana. Can machines learn to predict weather? Using deep learning to predict gridded 500-hPa geopotential height from historical weather data. *Journal of Advances in Modeling Earth Systems*, 11(8):2680–2693, 2019.

Appendix

A Proofs of theoretical results

A.1 Proof of Lemma 3.4

Proof. By the definition of proper SR, we have that:

$$\alpha_1 \cdot S_1(Q, Q) \leq \alpha_1 \cdot S_1(P, Q) \forall P, Q \in \mathcal{P},$$

and similar for S_2 . By adding the two inequalities, we have therefore that:

$$\alpha_1 \cdot S_1(Q, Q) + \alpha_2 \cdot S_2(Q, Q) \leq \alpha_1 \cdot S_1(P, Q) + \alpha_2 \cdot S_2(P, Q) \forall P, Q \in \mathcal{P},$$

which implies that S_+ is a proper SR.

Assume now additionally that S_1 , without loss of generality, is strictly proper, i.e.:

$$\alpha_1 \cdot S_1(Q, Q) < \alpha_1 \cdot S_1(P, Q) \forall P, Q \in \mathcal{P};$$

then, summing the above with the corresponding inequality for S_2 gives that:

$$\alpha_1 \cdot S_1(Q, Q) + \alpha_2 \cdot S_2(Q, Q) < \alpha_1 \cdot S_1(P, Q) + \alpha_2 \cdot S_2(P, Q) \forall P, Q \in \mathcal{P},$$

which implies that S_+ is a strictly proper SR. \square

A.2 Propriety of the prequential SR

In this Section, let P^* denote the data generating distribution for $(\mathbf{Y}_1, \mathbf{Y}_2, \dots, \mathbf{Y}_t, \dots) = (\mathbf{Y}_t)_t$, and let P denote a generic distribution assigned to $(\mathbf{Y}_t)_t$. From the distribution on the full sequence P , conditional and marginals can be obtained, and denoted as follows: $P_{t+1}(\cdot|\mathbf{y}_{1:t})$ denotes the conditional distribution for \mathbf{Y}_{t+1} given $\mathbf{y}_{1:t}$, and $P_{1:t}$ the (marginal) distribution for $(\mathbf{Y}_1, \mathbf{Y}_2, \dots, \mathbf{Y}_t)$. Similar notation will be used for the conditional and marginals induced by P^* .

A.2.1 Generic 1-step ahead prequential SR

We first consider a simplified case in which we can access the marginal for \mathbf{Y}_1 and all subsequent conditionals from P . Given $\mathbf{y}_{1:t}$, we use the distribution P to construct a forecast distribution for \mathbf{Y}_{t+1} , namely $P_{t+1}(\cdot|\mathbf{y}_{1:t})$; we penalize the forecast, against the verifying observation \mathbf{y}_{t+1} , via a SR S :

$$S(P_{t+1}(\cdot|\mathbf{y}_{1:t}), \mathbf{y}_{t+1}).$$

From the above, we construct the *prequential* SR for the forecast $P_{1:T}$ as follows:

$$S_T(P_{1:T}, \mathbf{y}_{1:T}) = \frac{1}{T} \left[\sum_{t=1}^{T-1} S(P_{t+1}(\cdot|\mathbf{y}_{1:t}), \mathbf{y}_{t+1}) + S(P_1, \mathbf{y}_1) \right]; \quad (11)$$

the above assumes that at each time instant we obtain a probabilistic forecast $P_{t+1}(\cdot|\mathbf{y}_{1:t})$ from the distribution P and we verify it against the next observed element of the sequence \mathbf{y}_{t+1} . Additionally, at the first time step, we have not yet received any observation, so our forecast P_1 is unconditional. Also, let us define the expected prequential score as:

$$S_T(P_{1:T}, P_{1:T}^*) := \mathbb{E}_{\mathbf{Y}_{1:T} \sim P_{1:T}^*} S_T(P_{1:T}, \mathbf{Y}_{1:T}),$$

Theorem A.1. *If the scoring rule S is proper, then the prequential score S_T in Eq. (11) is proper for distributions over \mathcal{Y}^T , i.e.:*

$$S_T(P_{1:T}^*, P_{1:T}^*) \leq S_T(P_{1:T}, P_{1:T}^*).$$

Similarly, if S is strictly proper, the prequential score S_T is strictly proper, i.e. the equality only holds if $P_{1:T} = P_{1:T}^$.*

Proof. First, notice that $P_{1:T}$ is fully determined by the marginal P_1 and by the conditionals $P_{t+1}(\cdot|\mathbf{y}_{1:t})$, $1 \leq t \leq T-1$. In fact, if $P_{1:T}$ has densities, you can write: $p_{1:T}(\mathbf{y}_{1:T}) = p_1(\mathbf{y}_1)p_2(\mathbf{y}_2|\mathbf{y}_1)p_3(\mathbf{y}_3|\mathbf{y}_{1:2}) \dots p_{T-1}(\mathbf{y}_{T-1}|\mathbf{y}_{1:T-2})p_T(\mathbf{y}_T|\mathbf{y}_{1:T-1})$.

By definition of proper SR, we have that:

$$\mathbb{E}_{\mathbf{Y}_{t+1} \sim P_{t+1}^*(\cdot|\mathbf{y}_{1:t})} S(P_{t+1}^*(\cdot|\mathbf{y}_{1:t}), \mathbf{Y}_{t+1}) \leq \mathbb{E}_{\mathbf{Y}_{t+1} \sim P_{t+1}(\cdot|\mathbf{y}_{1:t})} S(P_{t+1}(\cdot|\mathbf{y}_{1:t}), \mathbf{Y}_{t+1})$$

for any conditional distribution $P_{t+1}(\cdot|\mathbf{y}_{1:t})$ and for any values $\mathbf{y}_{1:t}$.

Similarly, it holds:

$$\mathbb{E}_{\mathbf{Y}_1 \sim P_1^*} S(P_1^*, \mathbf{Y}_1) \leq \mathbb{E}_{\mathbf{Y}_1 \sim P_1} S(P_1, \mathbf{Y}_1), \quad (12)$$

for any distribution P_1 .

For the expected prequential SR, it holds that:

$$\begin{aligned} S_T(P_{1:T}, P_{1:T}^*) &= \mathbb{E}_{\mathbf{Y}_{1:T} \sim P_{1:T}^*} S_T(P_{1:T}, \mathbf{Y}_{1:T}) \\ &= \frac{1}{T} \left[\sum_{t=1}^{T-1} \mathbb{E}_{\mathbf{Y}_{1:T} \sim P_{1:T}^*} S(P_{t+1}(\cdot|\mathbf{Y}_{1:t}), \mathbf{Y}_{t+1}) + \mathbb{E}_{\mathbf{Y}_{1:T} \sim P_{1:T}^*} S(P_1, \mathbf{Y}_1) \right] \\ &= \frac{1}{T} \left[\sum_{t=1}^{T-1} \mathbb{E}_{\mathbf{Y}_{1:t+1} \sim P_{1:t+1}^*} S(P_{t+1}(\cdot|\mathbf{Y}_{1:t}), \mathbf{Y}_{t+1}) + \mathbb{E}_{\mathbf{Y}_1 \sim P_1^*} S(P_1, \mathbf{Y}_1) \right]; \end{aligned}$$

but now:

$$\begin{aligned} \mathbb{E}_{\mathbf{Y}_{1:t+1} \sim P_{1:t+1}^*} S(P_{t+1}(\cdot|\mathbf{Y}_{1:t}), \mathbf{Y}_{t+1}) &= \mathbb{E}_{\mathbf{Y}_{1:t} \sim P_{1:t}^*} \left[\mathbb{E}_{\mathbf{Y}_{t+1} \sim P_{t+1}^*(\cdot|\mathbf{Y}_{1:t})} S(P_{t+1}(\cdot|\mathbf{Y}_{1:t}), \mathbf{Y}_{t+1}) \right] \\ &\geq \mathbb{E}_{\mathbf{Y}_{1:t} \sim P_{1:t}^*} \left[\mathbb{E}_{\mathbf{Y}_{t+1} \sim P_{t+1}(\cdot|\mathbf{Y}_{1:t})} S(P_{t+1}^*(\cdot|\mathbf{Y}_{1:t}), \mathbf{Y}_{t+1}) \right], \end{aligned} \quad (13)$$

so that:

$$\begin{aligned} S_T(P_{1:T}, P_{1:T}^*) &\geq \frac{1}{T} \left[\sum_{t=1}^{T-1} \mathbb{E}_{\mathbf{Y}_{1:t+1} \sim P_{1:t+1}^*} S(P_{t+1}^*(\cdot|\mathbf{Y}_{1:t}), \mathbf{Y}_{t+1}) + \mathbb{E}_{\mathbf{Y}_1 \sim P_1^*} S(P_1^*, \mathbf{Y}_1) \right] \\ &= \frac{1}{T} \left[\sum_{t=1}^{T-1} \mathbb{E}_{\mathbf{Y}_{1:T} \sim P_{1:T}^*} S(P_{t+1}^*(\cdot|\mathbf{Y}_{1:t}), \mathbf{Y}_{t+1}) + \mathbb{E}_{\mathbf{Y}_{1:T} \sim P_{1:T}^*} S(P_1^*, \mathbf{Y}_1) \right] \\ &= S_T(P_{1:T}^*, P_{1:T}^*), \end{aligned} \quad (14)$$

which proves that S_T is proper.

To show that S_T is strictly proper if S is, notice that the equality in Eq. (14) holds if and only if the equalities in Eq. (12) and (13) are verified for all $1 \leq t \leq T$; if S is strictly proper, however, that requires that $P_1 = P_1^*$ and $P_{t+1}(\cdot|\mathbf{y}_{1:t}) = P_{t+1}^*(\cdot|\mathbf{y}_{1:t})$ for $1 \leq t \leq T-1$, which implies that $P_{1:T} = P_{1:T}^*$ due to distributions on $\mathbf{Y}_{1:T}$ being determined by the marginal for \mathbf{Y}_1 and the conditional on $\mathbf{Y}_{t+1}|\mathbf{Y}_{1:t}$. \square

A.2.2 l -steps ahead prequential SR (Theorem 3.2)

We now go back to the specific setting considered in the main body of the paper. By discarding the model parameter ϕ in the notation for simplicity, the generative network induces conditional distributions $P_{t+l}(\cdot|\mathbf{y}_{1:t})$ for \mathbf{Y}_{t+l} which only depend on the last k observations, i.e. $P_{t+l}(\cdot|\mathbf{y}_{1:t}) = P_{t+l}(\cdot|\mathbf{y}_{t-k+1:t})$. Therefore, the joint distribution for $\mathbf{Y}_{k+l:T}$ induced by the generative network satisfies the following property:

Definition A.2. A probability distribution $P_{1:T}$ is k -Markovian with lag l if it can be decomposed as follows, assuming it has density $p_{1:T}$ with respect to some base measure:

$$p_{1:T}(\mathbf{y}_{1:T}) = p_{1:k+l-1}(\mathbf{y}_{1:k+l-1}) \prod_{t=k}^{T-l} p_{t+l}(\mathbf{y}_{t+l}|\mathbf{y}_{t-k+1:t}).$$

Setting $l = 1$ recovers the standard definition of k -Markovian models.

Notice also that the set of distributions which are k -Markovian with lag l is a subset of $(k + l - 1)$ -Markovian distributions, for which in fact:

$$\begin{aligned} p_{1:T}(\mathbf{y}_{1:T}) &= p_{1:k+l-1}(\mathbf{y}_{1:k+l-1}) \prod_{t=k+l}^T p_t(\mathbf{y}_t | \mathbf{y}_{t-k-l+1:t-1}) \\ &= p_{1:k+l-1}(\mathbf{y}_{1:k+l-1}) \prod_{t=k}^{T-l} p_{t+l}(\mathbf{y}_{t+l} | \mathbf{y}_{t-k+1:t+l-1}); \end{aligned}$$

the additional assumption in Definition A.2 with respect to $(k+l-1)$ -Markovian is that the conditional distribution for \mathbf{Y}_t is *not* influenced by the last $l-1$ elements.

In our setting, we can only access $P_{t+l}(\cdot | \mathbf{y}_{t-k+1:t})$ for $k \leq t \leq T-l$; the marginals $P_{1:k+l-1}$ are not available. Therefore, we consider the following quantity:

$$S_T^{k,l}(P_{k+l:T}(\cdot | \mathbf{y}_{1:k+l-1}), \mathbf{y}_{k+l:T}) := \frac{1}{T-l-k+1} \sum_{t=k}^{T-l} S(P_{t+l}(\cdot | \mathbf{y}_{t-k+1:t}), \mathbf{y}_{t+l}); \quad (15)$$

in contrast to Eq. (8) in the main text, we explicit the dependence on k and l in the notation for $S_T^{k,l}$ and introduce a scaling constant for simplicity, which however does not impact the following arguments. The notation in Eq. (15) only makes sense if P is a $(k+l-1)$ -Markovian distribution, as otherwise $\mathbf{y}_{1:k+l-1}$ would also appear explicitly in the conditioning of P_{t+l} on the right hand-side. The notation therefore makes sense for P obtained from the generative network, as that is k -Markovian with lag l which, as mentioned above, is a specific case of $(k+l-1)$ -Markovian.

As mentioned in the main text, $S_T^{k,l}$ is the prequential score and is a SR for distributions over $\mathbf{Y}_{k+l:T} | \mathbf{y}_{1:k+l-1}$ which are $(k+l-1)$ -Markovian.

From Eq. (15), we can define the expected SR as:

$$\begin{aligned} S_T^{k,l}(P_{k+l:T}(\cdot | \mathbf{y}_{1:k+l-1}), P_{k+l:T}^*(\cdot | \mathbf{y}_{1:k+l-1})) &:= \\ \mathbb{E}_{\mathbf{Y}_{k+l:T} \sim P_{k+l:T}^*(\cdot | \mathbf{y}_{1:k+l-1})} S_T^{k,l}(P_{k+l:T}(\cdot | \mathbf{y}_{1:k+l-1}), \mathbf{Y}_{k+l:T}). \end{aligned}$$

For the scoring rule defined in Eq. (15), the following Theorem, which we state in more generality with respect to Theorem 3.2 in the main text:

Theorem A.3. *If the scoring rule S is proper, then, for all choices of $\mathbf{y}_{1:k+l-1}$, the prequential score $S_T^{k,l}$ in Eq. (15) is proper for distributions on $\mathbf{Y}_{k+l:T} | \mathbf{y}_{1:k+l-1}$ which are $(k+l-1)$ -Markov; namely, the following inequality holds:*

$$S_T^{k,l}(P_{k+l:T}^*(\cdot | \mathbf{y}_{1:k+l-1}), P_{k+l:T}^*(\cdot | \mathbf{y}_{1:k+l-1})) \leq S_T^{k,l}(P_{k+l:T}(\cdot | \mathbf{y}_{1:k+l-1}), P_{k+l:T}^*(\cdot | \mathbf{y}_{1:k+l-1})), \quad (16)$$

where $P_{1:T}$ and $P_{1:T}^*$ are $(k+l-1)$ -Markovian.

If additionally S is strictly proper, then, for all choices of $\mathbf{y}_{1:k+l-1}$, $S_T^{k,l}$ is proper for distributions on $\mathbf{Y}_{k+l:T} | \mathbf{y}_{1:k+l-1}$ which are k -Markovian with lag l , i.e. the equality in Eq. (16) only holds if $P_{k+l:T}(\cdot | \mathbf{y}_{1:k+l-1}) = P_{k+l:T}^(\cdot | \mathbf{y}_{1:k+l-1})$, where $P_{1:T}$ and $P_{1:T}^*$ are k -Markovian with lag l .*

The prequential score S_T^{k+l} is non-strictly proper for distributions that are $(k+l-1)$ -Markovian but not k -Markovian with lag l . In fact, it builds forecasts from $P_{k+l:T}^*(\cdot | \mathbf{y}_{1:k+l-1})$ with lead of l timesteps, meaning that the information included in observations $\mathbf{y}_{t+1:t+l-1}$ is not used in formulating the forecast for \mathbf{Y}_{t+l} . It is therefore unable to distinguish between different distributions for $\mathbf{Y}_{k+l:T} | \mathbf{y}_{1:k+l-1}$ which have the same conditionals at lead l , but for which the conditionals change if one takes into account $\mathbf{y}_{t+1:t+l-1}$ in forecasting \mathbf{Y}_{t+l} . Therefore, you need to restrict the class of distributions to those in which the value $\mathbf{y}_{t+1:t+l-1}$ does not impact the distribution for \mathbf{Y}_{t+l} in order to get strict propriety.

We now prove the Theorem.

Proof. The proof steps follow those of Theorem A.1.

By definition of proper SR, we have that, for all $t \geq k$:

$$\mathbb{E}_{\mathbf{Y}_{t+l} \sim P_{t+l}^*(\cdot | \mathbf{y}_{t-k+1:t})} S(P_{t+l}^*(\cdot | \mathbf{y}_{t-k+1:t}), \mathbf{Y}_{t+l}) \leq \mathbb{E}_{\mathbf{Y}_{t+l} \sim P_{t+l}^*(\cdot | \mathbf{y}_{t-k+1:t})} S(P_{t+l}(\cdot | \mathbf{y}_{t-k+1:t}), \mathbf{Y}_{t+l}) \quad (17)$$

for any conditional distribution $P_{t+l}(\cdot | \mathbf{y}_{t-k+1:t})$ and for any values $\mathbf{y}_{t-k+1:t}$.

For the expected prequential SR, it holds that:

$$\begin{aligned} & S_T^{k,l}(P_{k+l:T}^*(\cdot | \mathbf{y}_{1:k+l-1}), P_{k+l:T}^*(\cdot | \mathbf{y}_{1:k+l-1})) \\ &= \mathbb{E}_{\mathbf{Y}_{k+l:T} \sim P_{k+l:T}^*(\cdot | \mathbf{y}_{1:k+l-1})} S_T^{k,l}(P_{k+l:T}^*(\cdot | \mathbf{y}_{1:k+l-1}), \mathbf{Y}_{k+l:T}) \\ &= \mathbb{E}_{\mathbf{Y}_{1:T} \sim P_{1:T}^*(\cdot | \mathbf{y}_{1:k+l-1})} S_T^{k,l}(P_{k+l:T}^*(\cdot | \mathbf{Y}_{1:k+l-1}), \mathbf{Y}_{k+l:T}) \\ &= \frac{1}{T-l-k+1} \sum_{t=k}^{T-l} \mathbb{E}_{\mathbf{Y}_{1:T} \sim P_{1:T}^*(\cdot | \mathbf{y}_{1:k+l-1})} S(P_{t+l}^*(\cdot | \mathbf{Y}_{t-k+1:t}), \mathbf{Y}_{t+l}) \\ &= \frac{1}{T-l-k+1} \sum_{t=k}^{T-l} \mathbb{E}_{\mathbf{Y}_{1:t+l} \sim P_{1:t+l}^*(\cdot | \mathbf{y}_{1:k+l-1})} S(P_{t+l}^*(\cdot | \mathbf{Y}_{t-k+1:t}), \mathbf{Y}_{t+l}); \end{aligned}$$

the second equality in the Equation above is trivial but we use it to simplify notation in the following. Now:

$$\begin{aligned} & \mathbb{E}_{\mathbf{Y}_{1:t+l} \sim P_{1:t+l}^*(\cdot | \mathbf{y}_{1:k+l-1})} S(P_{t+l}^*(\cdot | \mathbf{Y}_{t-k+1:t}), \mathbf{Y}_{t+l}) \\ &= \mathbb{E}_{\mathbf{Y}_{t-k+1:t} \sim P_{t-k+1:t}^*(\cdot | \mathbf{y}_{1:k+l-1})} \left[\mathbb{E}_{\mathbf{Y}_{t+l} \sim P_{t+l}^*(\cdot | \mathbf{Y}_{t-k+1:t}, \mathbf{y}_{1:k+l-1})} S(P_{t+l}^*(\cdot | \mathbf{Y}_{t-k+1:t}), \mathbf{Y}_{t+l}) \right] \\ &= \mathbb{E}_{\mathbf{Y}_{t-k+1:t} \sim P_{t-k+1:t}^*(\cdot | \mathbf{y}_{1:k+l-1})} \left[\mathbb{E}_{\mathbf{Y}_{t+l} \sim P_{t+l}^*(\cdot | \mathbf{Y}_{t-k+1:t})} S(P_{t+l}^*(\cdot | \mathbf{Y}_{t-k+1:t}), \mathbf{Y}_{t+l}) \right] \\ &\leq \mathbb{E}_{\mathbf{Y}_{t-k+1:t} \sim P_{t-k+1:t}^*(\cdot | \mathbf{y}_{1:k+l-1})} \left[\mathbb{E}_{\mathbf{Y}_{t+l} \sim P_{t+l}^*(\cdot | \mathbf{Y}_{t-k+1:t})} S(P_{t+l}(\cdot | \mathbf{Y}_{t-k+1:t}), \mathbf{Y}_{t+l}) \right] \\ &= \mathbb{E}_{\mathbf{Y}_{1:t+l} \sim P_{1:t+l}^*(\cdot | \mathbf{y}_{1:k+l-1})} S(P_{t+l}(\cdot | \mathbf{Y}_{t-k+1:t}), \mathbf{Y}_{t+l}); \end{aligned} \quad (18)$$

in the first equality above, we have marginalized over all components of $\mathbf{Y}_{1:t+l}$ which do not appear in the expected quantity and we have used the definition of conditional probability together with the tower property of expectations. In the second equality, we have exploited the $(k+l-1)$ -Markov property³ of P^* which ensures that the distribution for \mathbf{Y}_{t+l} does not depend on $\mathbf{Y}_{1:t-k}$. The inequality holds for any conditional distribution $P_{t+l}(\cdot | \mathbf{y}_{t-k+1:t})$ and for any values $\mathbf{y}_{t-k+1:t}$ thanks to Eq. (17). Finally, the last equality is obtained via the reverse of the argument used for the first one.

Now, we can write:

$$\begin{aligned} & S_T^{k,l}(P_{k+l:T}^*(\cdot | \mathbf{y}_{1:k+l-1}), P_{k+l:T}^*(\cdot | \mathbf{y}_{1:k+l-1})) \\ &\leq \frac{1}{T-l-k+1} \sum_{t=k}^{T-l} \mathbb{E}_{\mathbf{Y}_{1:t+l} \sim P_{1:t+l}^*(\cdot | \mathbf{y}_{1:k+l-1})} S(P_{t+l}(\cdot | \mathbf{Y}_{t-k+1:t}), \mathbf{Y}_{t+l}) \\ &= \frac{1}{T-l-k+1} \sum_{t=k}^{T-l} \mathbb{E}_{\mathbf{Y}_{1:T} \sim P_{1:T}^*(\cdot | \mathbf{y}_{1:k+l-1})} S(P_{t+l}(\cdot | \mathbf{Y}_{t-k+1:t}), \mathbf{Y}_{t+l}) \quad (19) \\ &= \frac{1}{T-l-k+1} \sum_{t=k}^{T-l} \mathbb{E}_{\mathbf{Y}_{k+l:T} \sim P_{k+l:T}^*(\cdot | \mathbf{y}_{1:k+l-1})} S(P_{t+l}(\cdot | \mathbf{Y}_{t-k+1:t}), \mathbf{Y}_{t+l}) \\ &= S_T^{k,l}(P_{k+l:T}(\cdot | \mathbf{y}_{1:k+l-1}), P_{k+l:T}^*(\cdot | \mathbf{y}_{1:k+l-1})), \end{aligned}$$

which proves that $S_T^{k,l}$ is proper for distributions over $\mathbf{Y}_{k+l:T} | \mathbf{y}_{1:k+l-1}$ which are $(k+l)$ -Markov.

Now, consider $P_{1:T}$ and $P_{1:T}^*$ to be k -Markovian with lag l . The equality in Eq. (19) holds if and only if the equality in Eq. (18) is verified for all $k \leq t \leq T-l$; if S is strictly proper, however, that requires that $P_{t+l}(\cdot | \mathbf{y}_{t-k+1:t}) = P_{t+l}^*(\cdot | \mathbf{y}_{t-k+1:t})$ for $k \leq t \leq T-l$, which implies that $P_{k+l:T}(\cdot | \mathbf{y}_{1:k+l-1}) = P_{k+l:T}^*(\cdot | \mathbf{y}_{1:k+l-1})$ due to the k -Markov with lag l property. \square

³Technically, you can relax the $(k+l-1)$ -Markov assumption for the full sequence to assuming $(k+l-1)$ -Markovianity for $\mathbf{Y}_{1:2k+l-1}$ and independence of $\mathbf{Y}_{2k+l:T}$ on $\mathbf{Y}_{1:k+l-1}$; this is however quite artificial.

A.3 Proof and precise statement of the consistency result (Theorem 3.3)

We follow here the notation introduced at the start of Appendix A.2. Specifically, P^* denotes the data generating distribution for $(\mathbf{Y}_1, \mathbf{Y}_2, \dots, \mathbf{Y}_t, \dots) = (\mathbf{Y}_t)_t$.

We consider a model class parametrized by a set of parameters ϕ . For such models, we assume the conditional distributions $P_{t+l}^\phi(\cdot | \mathbf{y}_{1:t})$ for \mathbf{Y}_{t+l} only depends on the last k observations, i.e. $P_{t+l}^\phi(\cdot | \mathbf{y}_{1:t}) = P_{t+l}^\phi(\cdot | \mathbf{y}_{t-k+1:t})$. Additionally, we assume that the conditional distribution does not depend explicitly on t , such that $P_{t+l}^\phi(\cdot | \mathbf{y}_{t-k+1:t}) = P_{(l)}^\phi(\cdot | \mathbf{y}_{t-k+1:t})$, where the bracketed subscript denotes that the forecast is for l steps ahead. This is the setting considered in the main manuscript.

In this specific case, therefore, the scoring rule used to penalize the forecast $P_{(l)}^\phi(\cdot | \mathbf{y}_{t-k+1:t})$ against the verification \mathbf{y}_{t+1} (Eq. (15)) becomes:

$$S_{(l)}(P_{(l)}^\phi(\cdot | \mathbf{y}_{t-k+1:t}), \mathbf{y}_{t+1}).$$

Therefore, the prequential score defined in Eq. (15) becomes:

$$S_T^{k,l}(P_{k+l:T}^\phi(\cdot | \mathbf{y}_{1:k+l-1}), \mathbf{y}_{k+l:T}) = \frac{1}{T-l-k+1} \sum_{t=k}^{T-l} S(P_{(l)}^\phi(\cdot | \mathbf{y}_{t-k+1:t}), \mathbf{y}_{t+l}); \quad (20)$$

notice that we introduce here a scaling constant for simplicity; that however does not impact any of the following arguments. Recall also the definition of the expected prequential score:

$$\begin{aligned} S_T^{k,l}(P_{k+l:T}^\phi(\cdot | \mathbf{y}_{1:k+l-1}), P_{k+l:T}^*(\cdot | \mathbf{y}_{1:k+l-1})) \\ := \mathbb{E}_{\mathbf{Y}_{k+l:T} \sim P_{k+l:T}^*(\cdot | \mathbf{y}_{1:k+l-1})} S_T^{k,l}(P_{k+l:T}^\phi(\cdot | \mathbf{y}_{1:k+l-1}), \mathbf{y}_{k+l:T}), \end{aligned} \quad (21)$$

for which we will use the following notation for brevity:

$$\tilde{S}_T^{k,l}(P_{k+l:T}^\phi(\cdot | \mathbf{y}_{1:k+l-1})) := S_T^{k,l}(P_{k+l:T}^\phi(\cdot | \mathbf{y}_{1:k+l-1}), P_{k+l:T}^*(\cdot | \mathbf{y}_{1:k+l-1}))$$

As discussed in Appendix A.2.2 and shown in Theorem A.3, provided that S is strictly proper, $S_T^{k,l}$ is a strictly proper SR for k -Markovian with lag l distributions over $\mathbf{Y}_{k+l:T} | \mathbf{y}_{1:k+l-1}$, for all values of $\mathbf{y}_{1:k+l-1}$.

We will also consider the minimizer of the expectation of the expected prequential SR in Eq. (21) with respect to the initial data $\mathbf{y}_{1:k+l-1}$, i.e.:

$$\begin{aligned} S_T^{k,l*}(P_{k+l:T}^\phi) &:= \mathbb{E}_{\mathbf{Y}_{1:k+l-1} \sim P_{1:k+l-1}} S_T^{k,l}(P_{k+l:T}^\phi(\cdot | \mathbf{Y}_{1:k+l-1}), P_{k+l:T}^*(\cdot | \mathbf{Y}_{1:k+l-1})) \\ &= \mathbb{E}_{\mathbf{Y}_{1:T} \sim P_{1:T}^*} S_T^{k,l}(P_{k+l:T}^\phi(\cdot | \mathbf{Y}_{1:k+l-1}), \mathbf{Y}_{k+l:T}). \end{aligned} \quad (22)$$

Theorem 3.3 in the main text states that the minimizer of the empirical prequential SR (Eq. (20)) converges to both the minimizer of the expected (with respect to $\mathbf{Y}_{k+l:T} | \mathbf{y}_{1:k+l-1}$ for fixed $\mathbf{y}_{1:k+l-1}$) SR in Eq. (21) and to the minimizer of the expected (with respect to $\mathbf{Y}_{k+l:T}$) SR in Eq. (22). We will split the original result in two separate statements, which hold under similar Assumptions.

We now set notation and introduce the relevant quantities. From now onwards, we will drop k and l for brevity in the definition of S_T ; all following results hold for each fixed value of k and l . We write therefore $S_T(P_{k+l:T}^\phi(\cdot | \mathbf{y}_{1:k+l-1}), \mathbf{y}_{k+l:T}) = S_T^{k,l}(P_{k+l:T}^\phi(\cdot | \mathbf{y}_{1:k+l-1}), \mathbf{y}_{k+l:T})$, $\tilde{S}_T(P_{k+l:T}^\phi(\cdot | \mathbf{y}_{1:k+l-1})) = \tilde{S}_T^{k,l}(P_{k+l:T}^\phi(\cdot | \mathbf{y}_{1:k+l-1}))$ and $S_T^*(P_{k+l:T}^\phi) = S_T^{k,l*}(P_{k+l:T}^\phi)$. Next, we define the minimizers of the empirical and expected prequential scores:

$$\begin{aligned} \hat{\phi}_T(\mathbf{y}_{1:T}) &: S_T(P_{k+l:T}^{\hat{\phi}_T(\mathbf{y}_{1:T})}(\cdot | \mathbf{y}_{1:k+l-1}), \mathbf{y}_{k+l:T}) = \min_{\phi \in \Phi} S_T(P_{k+l:T}^\phi(\cdot | \mathbf{y}_{1:k+l-1}), \mathbf{y}_{k+l:T}) \\ \tilde{\phi}_T(\mathbf{y}_{1:k+l-1}) &: \tilde{S}_T(P_{k+l:T}^{\tilde{\phi}_T(\mathbf{y}_{1:k+l-1})}(\cdot | \mathbf{y}_{1:k+l-1})) = \min_{\phi \in \Phi} \tilde{S}_T(P_{k+l:T}^\phi(\cdot | \mathbf{y}_{1:k+l-1})). \\ \phi_T^* &: S_T^*(P_{k+l:T}^{\phi_T^*}) = \min_{\phi \in \Phi} S_T^*(P_{k+l:T}^\phi). \end{aligned}$$

Convergence of $\hat{\phi}_T$ to ϕ_T^* We first introduce Assumptions and give the statement linking $\hat{\phi}_T(\mathbf{y}_{1:T})$ to ϕ_T^* (Theorem A.4). We require the sequence $(\mathbf{Y}_t)_t$ to be stationary and to satisfy some mixing properties. Specifically, the following Assumptions are required. The precise definition of the mixing properties is postponed to later in Appendix A.3.2.

A1 Φ is compact.

A2 ϕ_T^* is unique; additionally, there exist a metric d on Φ such that, for all $\epsilon > 0$:

$$\liminf_{T \rightarrow +\infty} \left\{ \min_{\phi: d(\phi, \phi_T^*) \geq \epsilon} S_T^*(P_{k+l:T}^\phi) - S_T^*(P_{k+l:T}^{\phi_T^*}) \right\} > 0$$

A3 (Asymptotic stationarity) Let G_t be the marginal distribution of $\mathbf{Y}_{t-k+1:t+l}$ for $t \geq k$; then, $(T-l-k+1)^{-1} \sum_{t=k}^{T-l} G_t$ converges weakly to some probability measure on \mathcal{Y}^{k+l} as $T \rightarrow \infty$.

A4 Both conditions below are satisfied:

(a) (Mixing) Either one of the following holds:

- i. $(\mathbf{Y}_t)_t$ is α -mixing with mixing coefficient of size $r/(2r-1)$, with $r \geq 1$, or
- ii. $(\mathbf{Y}_t)_t$ is φ -mixing with mixing coefficient of size $r/(r-1)$ with $r > 1$.

(b) (Moment boundedness) Define $H(\mathbf{y}_{t-k+1:t+l}) = \sup_{\phi \in \Phi} |S(P^\phi(\cdot|\mathbf{y}_{t-k+1:t}), \mathbf{y}_{t+l})|$; then, $\sup_{t \geq k} \mathbb{E} [H(\mathbf{Y}_{t-k+1:t+l})^{r+\delta}] < \infty$ for some $\delta > 0$, for the value of r corresponding to the condition above which is satisfied.

S being strictly proper and $P_{k+l:T}^\phi(\cdot|\mathbf{y}_{1:k+l-1})$ being a well specified model for $\mathbf{Y}_{k+l:T}|\mathbf{y}_{1:k+l-1}$ is a sufficient (but not necessary) condition for the uniqueness of ϕ_T^* in Assumption **A2** (see Lemma A.8 in Appendix A.3.1), provided that the parameters ϕ are identifiable. Notice that neural networks do not have identifiable parameters; we require however this assumption to prove the Theorem. In case the parameters are not identifiable, we believe it is possible to show asymptotic convergence of the distributions minimizing the empirical and expected prequential SR, instead of convergence of the parameters. Extending the proof to this setting is technically challenging, as the distance in Assumption **A1** needs to be replaced by a divergence between probability distributions. We leave this extension for future work.

The rest of Assumption **A2** is a standard condition ensuring that the function which we are minimizing does not get flatter and flatter around the optimal value as $T \rightarrow \infty$. The asymptotic stationarity condition in Assumption **A3** is implied by the stronger condition of the marginals G_t being the same for each t . Assumption **A4(a)** is a mixing condition, ensuring that the dependence between two different $\mathbf{Y}_t, \mathbf{Y}_{t'}$ decreases as $t - t' \rightarrow \infty$ (defined precisely in Appendix A.3.2). Finally, Assumption **A4(b)** is a boundedness condition; for the specific case of the Kernel and Energy SR, that can be verified by simpler conditions as discussed in Lemma A.9 in Appendix A.3.1.

We will now state our first result.

Theorem A.4. *If Assumptions **A1**, **A2**, **A3** and **A4** hold, and if $(\mathbf{y}_{t-k+1:t+l}, \phi) \rightarrow S(P^\phi(\cdot|\mathbf{y}_{t-k+1:t}), \mathbf{y}_{t+l})$ is continuous on $\mathcal{Y}^{k+l} \times \Phi$, then $d(\hat{\phi}_T(\mathbf{Y}_{1:T}), \phi_T^*) \rightarrow 0$ with probability 1 with respect to $(\mathbf{Y}_t)_t \sim P^*$.*

The Theorem above relies on a generic consistency result (discussed in Appendix A.3.3) for which a uniform law of large numbers is required. Such a uniform law of large numbers can be obtained under stationarity and mixing conditions; we report in Appendix A.3.4 a result ensuring this. We prove Theorem A.4 by combining the above two elements in Appendix A.3.5.

Convergence of $\tilde{\phi}_T$ to ϕ_T^* We now give the statement linking $\hat{\phi}_T(\mathbf{y}_{1:T})$ to $\tilde{\phi}_T(\mathbf{y}_{1:t})$ (Theorem A.6). We will require similar Assumptions to what considered above, but holding for fixed values of $\mathbf{y}_{1:k+l-1}$:

B1 $\tilde{\phi}_T(\mathbf{y}_{1:k+l-1})$ is unique; additionally, there exist a metric d on Φ such that, for all $\epsilon > 0$:

$$\liminf_{T \rightarrow +\infty} \left\{ \min_{\phi: d(\phi, \tilde{\phi}_T(\mathbf{y}_{1:k+l-1})) \geq \epsilon} \tilde{S}_T(P_{k+l:T}^\phi(\cdot|\mathbf{y}_{1:k+l-1})) - \tilde{S}_T(P_{k+l:T}^{\tilde{\phi}_T(\mathbf{y}_{1:k+l-1})}(\cdot|\mathbf{y}_{1:k+l-1})) \right\} > 0$$

B2 (Asymptotic stationarity) Let \tilde{G}_t be the marginal distribution of $\mathbf{Y}_{t-k+1:t+l} | \mathbf{y}_{1:k+l-1}$ for $t \geq k$; then,

$$(T-l-k+1)^{-1} \sum_{t=k}^{T-l} \tilde{G}_t$$

converges weakly to some probability measure on \mathcal{Y}^{k+l} as $T \rightarrow \infty$.

B3 Both conditions below are satisfied:

- (a) (Mixing) Let $(\mathbf{X}_t)_t \sim P^*(\cdot | \mathbf{y}_{1:k+l-1})$; then, either one of the following holds:
 - i. $(\mathbf{X}_t)_t$ is α -mixing with mixing coefficient of size $r/(2r-1)$, with $r \geq 1$, or
 - ii. $(\mathbf{X}_t)_t$ is φ -mixing with mixing coefficient of size $r/(r-1)$ with $r > 1$.
- (b) (Moment boundedness) Define $H(\mathbf{y}_{t-k+1:t+l}) = \sup_{\phi \in \Phi} |S(P^\phi(\cdot | \mathbf{y}_{t-k+1:t}), \mathbf{y}_{t+l})|$; then, $\sup_{t \geq k} \mathbb{E}_{\mathbf{Y}_{t-k+1:t+l} | \mathbf{y}_{1:k+l-1}} [H(\mathbf{Y}_{t-k+1:t+l})^{r+\delta}] < \infty$ for some $\delta > 0$, for the value of r corresponding to the condition above which is satisfied.

We can therefore state the following:

Theorem A.5. *If Assumptions A1, B1, B2 and B3 hold, and if $(\mathbf{y}_{t-k+1:t+l}, \phi) \rightarrow S(P^\phi(\cdot | \mathbf{y}_{t-k+1:t}), \mathbf{y}_{t+l})$ is continuous on $\mathcal{Y}^{k+l} \times \Phi$, then $d(\hat{\phi}_T(\mathbf{y}_{1:k+l-1}, \mathbf{Y}_{k+l:T}), \tilde{\phi}_T(\mathbf{y}_{1:k+l-1})) \rightarrow 0$ with probability 1 with respect to $(\mathbf{Y}_t)_t \sim P^*(\cdot | \mathbf{y}_{1:k+l-1})$.*

Notice how now in $\hat{\phi}_T$ we split the dependence with respect to the fixed $\mathbf{y}_{1:k+l-1}$ and the random $\mathbf{Y}_{k+l:T}$.

Proof. Theorem A.5 is proven following the same steps as Theorem A.4 (given in Appendix A.3.5). Specifically, Corollary A.16 can be used to obtain a uniform Law of Large Numbers such as in Assumption A5. Then, an equivalent to Theorem A.13 can be shown following the exact same steps. That implies the result of Theorem A.5. \square

The above result is saying that, for the sequence $(\mathbf{Y}_t)_t$ conditioned on $\mathbf{y}_{1:k+l-1}$, if stationarity and mixing conditions holds for a fixed $\mathbf{y}_{1:k+l-1}$, then the empirical minimizer $\hat{\phi}_T$ converges to the minimizer $\tilde{\phi}$, both with fixed $\mathbf{y}_{1:k+l-1}$.

Clearly, if the above Assumptions hold for all values of $\mathbf{y}_{1:k+l-1}$, the statement also does. This is made precise by the following Corollary:

Corollary A.6. *If Assumptions A1, B1, B2 and B3 hold almost surely for $\mathbf{Y}_{1:k+l-1} \sim P_{1:k+l-1}^*$, and if $(\mathbf{y}_{t-k+1:t+l}, \phi) \rightarrow S(P^\phi(\cdot | \mathbf{y}_{t-k+1:t}), \mathbf{y}_{t+l})$ is continuous on $\mathcal{Y}^{k+l} \times \Phi$, then $d(\hat{\phi}_T(\mathbf{Y}_{1:k+l-1}, \mathbf{Y}_{k+l:T}), \tilde{\phi}_T(\mathbf{Y}_{1:k+l-1})) \rightarrow 0$ with probability 1 with respect to $(\mathbf{Y}_t)_t \sim P^*$.*

Proof. If Assumptions A1, B1, B2 and B3 hold almost surely for $\mathbf{Y}_{1:k+l-1} \sim P_{1:k+l-1}^*$, and under the continuity condition, the following statement holds with probability 1 with respect to $\mathbf{Y}_{1:k+l-1} \sim P_{1:k+l-1}^*$: “ $d(\hat{\phi}_T(\mathbf{Y}_{1:k+l-1}, \mathbf{Y}_{k+l:T}), \tilde{\phi}_T(\mathbf{Y}_{1:k+l-1})) \rightarrow 0$ with probability 1 with respect to $(\mathbf{Y}_t)_t \sim P^*(\cdot | \mathbf{Y}_{1:k+l-1})$,” from which the result follows by considering that a statement holding with probability 1 with respect to $(\mathbf{Y}_t)_t \sim P^*(\cdot | \mathbf{Y}_{1:k+l-1})$, for each value $\mathbf{Y}_{1:k+l-1}$ takes, and with probability 1 with respect to $\mathbf{Y}_{1:k+l-1} \sim P_{1:k+l-1}^*$ holds almost surely with respect to $(\mathbf{Y}_t)_t \sim P^*$. \square

Putting the two results together Finally, we also have the following, which is a precise version of Theorem 3.3 in the main text:

Corollary A.7. *If Assumptions A1, A2, A3 and A4 hold, and if Assumptions B1, B2 and B3 hold almost surely for $\mathbf{Y}_{1:k+l-1} \sim P_{1:k+l-1}^*$, and if $(\mathbf{y}_{t-k+1:t+l}, \phi) \rightarrow S(P^\phi(\cdot | \mathbf{y}_{t-k+1:t}), \mathbf{y}_{t+l})$ is continuous on $\mathcal{Y}^{k+l} \times \Phi$, then*

1. $d(\hat{\phi}_T(\mathbf{Y}_{1:T}), \phi_T^*) \rightarrow 0$ with probability 1 with respect to $(\mathbf{Y}_t)_t \sim P^*$;
2. $d(\hat{\phi}_T(\mathbf{Y}_{1:T}), \tilde{\phi}_T(\mathbf{Y}_{1:k+l-1})) \rightarrow 0$ with probability 1 with respect to $(\mathbf{Y}_t)_t \sim P^*$;

3. $d(\phi_T^*, \tilde{\phi}_T(\mathbf{Y}_{1:k+l-1})) \rightarrow 0$ with probability 1 with respect to $\mathbf{Y}_{1:k+l-1} \sim P_{1:k+l-1}^*$.

Proof. Under the Assumptions, both Theorem A.4 and Corollary A.6 hold, from which the first two statements follow. For the last statement, applying the triangle inequality yields:

$$d(\phi_T^*, \tilde{\phi}_T(\mathbf{Y}_{1:k+l-1})) \leq d(\hat{\phi}_T(\mathbf{Y}_{1:T}), \tilde{\phi}_T(\mathbf{Y}_{1:k+l-1})) + d(\hat{\phi}_T(\mathbf{Y}_{1:T}), \phi_T^*) \rightarrow 0.$$

As the left-hand side above depends only on $\mathbf{Y}_{1:k+l-1}$, the result holds almost surely with respect to $\mathbf{Y}_{1:k+l-1} \sim P_{1:k+l-1}^*$. \square

In case in which all the Assumption hold, therefore, the minimizer of the expected prequential SR over $\mathbf{Y}_{k+l:T} | \mathbf{Y}_{1:k+l-1}$ converges to the minimizer of the expected prequential SR over $\mathbf{Y}_{1:T}$, which is a deterministic quantity. Therefore, this result is saying that for large T , $\tilde{\phi}_T$ does not depend on the initial conditions, as it is intuitive under mixing and stationarity of $(\mathbf{Y}_t)_t$. Indeed, the same holds for the empirical minimizer $\hat{\phi}_T$, in which no expectation at all is computed.

In the next Subsections, we will discuss how to verify the Assumptions in some specific cases, and then move to introducing preliminary results for proving Theorem A.4, which we do in Appendix A.3.5. As mentioned above, the proof of Theorem A.5 follows the same steps as the one for Theorem A.4, but with the corresponding set of Assumptions. For this reason, we do not give that in details.

A.3.1 Verifying the Assumptions in specific cases

Before delving into proving Theorem A.4, we here show sufficient conditions under which ϕ_T^* and $\tilde{\phi}_T(\mathbf{y}_{1:k+l-1})$ are unique and under which Assumption A4(b) holds. Specifically, for the former (Lemma A.8), we consider the model $P_{k+l:T}^\phi(\cdot | \mathbf{y}_{1:k+l-1})$ to be a well specified model and the scoring rule S to be strictly proper; for the latter, we consider instead the Kernel and Energy SR satisfy and obtain more precise conditions, which are easily satisfied.

First, consider uniqueness of ϕ_T^* :

Lemma A.8. *If S is strictly proper and $P_{k+l:T}^\phi(\cdot | \mathbf{y}_{1:k+l-1})$ is a well specified model for $\mathbf{Y}_{k+l:T} | \mathbf{y}_{1:k+l-1}$, for all values of T , then ϕ_T^* and $\tilde{\phi}_T(\mathbf{y}_{1:k+l-1})$ are unique for all values of T and $\mathbf{y}_{1:k+l-1}$.*

Proof. If P^ϕ is well specified, there exists a ϕ^* such that $P_{k+l:T}^*(\cdot | \mathbf{y}_{1:k+l-1}) = P_{k+l:T}^{\phi^*}(\cdot | \mathbf{y}_{1:k+l-1}) \forall T, \forall \mathbf{y}_{1:k+l-1}$. Notice that this implies that P^* is k -Markovian with lag l . If S is strictly proper, we have by Theorem A.3 that:

$$\phi^* = \arg \min_{\phi \in \Phi} S_T(P_{k+l:T}^\phi(\cdot | \mathbf{y}_{1:k+l-1}), P_{k+l:T}^*(\cdot | \mathbf{y}_{1:k+l-1}))$$

is unique, for all $\mathbf{y}_{1:k+l-1}$. Therefore, $\tilde{\phi}_T(\mathbf{y}_{1:k+l-1}) = \phi^*$ for all values of $\mathbf{y}_{1:k+l-1}$. Recalling now the definition of $S_T^*(P_{k+l:T}^\phi)$ in Eq. (22), notice that the quantity inside the expectation $\mathbb{E}_{\mathbf{Y}_{1:k+l-1} \sim P_{1:k+l-1}^*}$ is minimized uniquely by $\phi = \phi^*$, so that $S_T^*(P_{k+l:T}^\phi)$ is also uniquely minimized by $\phi = \phi^*$. \square

We now consider Assumption A4(b):

Lemma A.9. *Assumption A4(b) is verified in the following cases:*

- **Kernel SR** When $S = S_k$ for a kernel k which satisfies either of the following:
 1. with probability 1 with respect to $(\mathbf{Y}_t)_t \sim P^{*4}$, for all $t \geq k$ and ϕ , $\mathbb{E}_{\mathbf{X}, \mathbf{X}' \sim P_{(t)}^\phi(\cdot | \mathbf{Y}_{t-k+1:t})} |k(\mathbf{X}, \mathbf{X}')| < \infty$ and $\mathbb{E}_{\mathbf{X} \sim P_{(t)}^\phi(\cdot | \mathbf{Y}_{t-k+1:t})} |k(\mathbf{X}, \mathbf{Y}_{t+l})| < \infty$;
 2. k is bounded, i.e. $|k(\mathbf{y}, \mathbf{x})| < +\infty \forall \mathbf{y}, \mathbf{x} \in \mathcal{Y}$ (this implies the above condition).
- **Energy SR** When $S = S_E^{(\beta)}$ and either of the following holds:

⁴Put simply, this condition means that the following has to be true for all observed sequences $(\mathbf{y}_t)_t$ which can be generated by the distribution P^* .

1. with probability 1 with respect to $(\mathbf{Y}_t)_t \sim P^*$, for all $t \geq k$ and ϕ , $\mathbb{E}_{\mathbf{X}, \mathbf{X}' \sim P_{(l)}^\phi(\cdot | \mathbf{Y}_{t-k+1:t})} \|\mathbf{X} - \mathbf{X}'\| < \infty$ and $\mathbb{E}_{\mathbf{X} \sim P_{(l)}^\phi(\cdot | \mathbf{Y}_{t-k+1:t})} \|\mathbf{X} - \mathbf{Y}_{t+l}\| < \infty$;
2. the space \mathcal{Y} is bounded, such that $\|\mathbf{y}\| \leq B < \infty \forall \mathbf{y} \in \mathcal{Y}$ (this implies the first condition);
3. $\beta \geq 1$, $\mathbb{E} \|\mathbf{Y}_{t+l}\|^{\beta(r+\delta)} < \infty$ for all t and, with probability 1 with respect to $(\mathbf{Y}_t)_t \sim P^*$, for all t and ϕ , $\mathbb{E}_{\mathbf{X} \sim P_{(l)}^\phi(\cdot | \mathbf{Y}_{t-k+1:t})} \|\mathbf{X}\|^\beta \leq B < \infty$.

Proof. First, notice that $\sup_{t \geq k} \mathbb{E} [H(\mathbf{Y}_{t-k+1:t+l})^{r+\delta}] < \infty \iff \mathbb{E} [H(\mathbf{Y}_{t-k+1:t+l})^{r+\delta}] < \infty \forall t \geq k$.

Kernel SR Consider the kernel SR $S = S_k$:

$$\begin{aligned} |S_k(P_{(l)}^\phi(\cdot | \mathbf{y}_{t-k+1:t}), \mathbf{y}_{t+l})| &= |\mathbb{E}_{\mathbf{X}, \mathbf{X}' \sim P_{(l)}^\phi(\cdot | \mathbf{y}_{t-k+1:t})} [k(\mathbf{X}, \mathbf{X}') - 2k(\mathbf{X}, \mathbf{y}_{t+l})]| \\ &\leq \mathbb{E}_{\mathbf{X}, \mathbf{X}' \sim P_{(l)}^\phi(\cdot | \mathbf{y}_{t-k+1:t})} |k(\mathbf{X}, \mathbf{X}') - 2k(\mathbf{X}, \mathbf{y}_{t+l})| \\ &\leq \mathbb{E}_{\mathbf{X}, \mathbf{X}' \sim P_{(l)}^\phi(\cdot | \mathbf{y}_{t-k+1:t})} [|k(\mathbf{X}, \mathbf{X}')| + 2|k(\mathbf{X}, \mathbf{y}_{t+l})|]. \end{aligned} \quad (23)$$

We first show why condition 1 yields the result. If, with probability 1 with respect to $(\mathbf{Y}_t)_t \sim P^*$, for all $t \geq k$ and ϕ :

$$\mathbb{E}_{\mathbf{X}, \mathbf{X}' \sim P_{(l)}^\phi(\cdot | \mathbf{Y}_{t-k+1:t})} |k(\mathbf{X}, \mathbf{X}')| \leq \kappa_1 < \infty \quad \text{and} \quad \mathbb{E}_{\mathbf{X} \sim P_{(l)}^\phi(\cdot | \mathbf{Y}_{t-k+1:t})} |k(\mathbf{X}, \mathbf{Y}_{t+l})| \leq \kappa_2 < \infty,$$

we have that:

$$|S_k(P_{(l)}^\phi(\cdot | \mathbf{Y}_{t-k+1:t}), \mathbf{Y}_{t+l})| \leq \kappa_1 + 2\kappa_2 < \infty,$$

from which:

$$\begin{aligned} \mathbb{E} [H(\mathbf{Y}_{t-k+1:t+l})^{r+\delta}] &= \mathbb{E} \left[\left(\sup_{\phi \in \Phi} |S_k(P_{(l)}^\phi(\cdot | \mathbf{Y}_{t-k+1:t}), \mathbf{Y}_{t+l})| \right)^{r+\delta} \right] \\ &\leq \mathbb{E} \left[\left(\sup_{\phi \in \Phi} \kappa_1 + 2\kappa_2 \right)^{r+\delta} \right] = (\kappa_1 + 2\kappa_2)^{r+\delta} < \infty. \end{aligned}$$

Now, condition 2 implies condition 1. Therefore, condition 1 yields the result.

Energy SR Notice how the kernel SR recovers the Energy SR when $k(\mathbf{y}, \mathbf{x}) = -\|\mathbf{y} - \mathbf{x}\|^\beta$; condition 1 for the kernel SR corresponds therefore to condition 1 for the Energy SR; therefore, the result holds under condition 1.

For condition 2 for the Energy SR, notice that

$$|k(\mathbf{y}, \mathbf{x})| = \|\mathbf{y} - \mathbf{x}\|^\beta \leq (\|\mathbf{y}\| + \|\mathbf{x}\|)^\beta \leq (2B)^\beta,$$

where the first inequality comes from applying the triangle inequality and the second comes from condition 2 for the Energy SR. Therefore, condition 2 for the Energy SR implies condition 2 for the corresponding Kernel SR, from which the result follows.

Finally, an alternative route leads to condition 3. Specifically, for the Energy SR, Equation (23) becomes:

$$\begin{aligned} |S_E^{(\beta)}(P_{(l)}^\phi(\cdot | \mathbf{y}_{t-k+1:t}), \mathbf{y}_{t+l})| &\leq \mathbb{E}_{\mathbf{X}, \mathbf{X}' \sim P_{(l)}^\phi(\cdot | \mathbf{y}_{t-k+1:t})} [|\|\mathbf{X} - \mathbf{X}'\|^\beta + 2\|\mathbf{X} - \mathbf{y}_{t+l}\|^\beta|] \\ &\leq \mathbb{E}_{\mathbf{X}, \mathbf{X}' \sim P_{(l)}^\phi(\cdot | \mathbf{y}_{t-k+1:t})} [(\|\mathbf{X}\| + \|\mathbf{X}'\|)^\beta + 2(\|\mathbf{X}\| + \|\mathbf{y}_{t+l}\|)^\beta] \end{aligned}$$

by triangle inequality. Now, for any $\beta > 1$, $a, b > 0$, $(a + b)^\beta \leq 2^{\beta-1}(a^\beta + b^\beta)$;⁵ therefore,

$$|S_E^{(\beta)}(P_{(l)}^\phi(\cdot | \mathbf{y}_{t-k+1:t}), \mathbf{y}_{t+l})| \leq \mathbb{E}_{\mathbf{X}, \mathbf{X}' \sim P_{(l)}^\phi(\cdot | \mathbf{y}_{t-k+1:t})} [2^{\beta-1}(\|\mathbf{X}\|^\beta + \|\mathbf{X}'\|^\beta) + 2^\beta(\|\mathbf{X}\|^\beta + \|\mathbf{y}_{t+l}\|^\beta)].$$

⁵This inequality is well-known and can be shown by convexity.

From the above, we have that:

$$\begin{aligned} \mathbb{E} [H(\mathbf{Y}_{t-k+1:t+l})^{r+\delta}] &= \mathbb{E} \left[\left(\sup_{\phi \in \Phi} |S_E^{(\beta)}(P_{(l)}^\phi(\cdot | \mathbf{Y}_{t-k+1:t}), \mathbf{Y}_{t+l})| \right)^{r+\delta} \right] \\ &\leq \mathbb{E} \left[\left(\sup_{\phi \in \Phi} \mathbb{E}_{\mathbf{X}, \mathbf{X}' \sim P_{(l)}^\phi(\cdot | \mathbf{Y}_{t-k+1:t})} [2^{\beta-1}(\|\mathbf{X}\|^\beta + \|\mathbf{X}'\|^\beta) + 2^\beta(\|\mathbf{X}\|^\beta + \|\mathbf{Y}_{t+l}\|^\beta)] \right)^{r+\delta} \right]. \end{aligned}$$

If, with probability 1 with respect to $(\mathbf{Y}_t)_t \sim P^*$, for all $t \geq k$ and ϕ , $\mathbb{E}_{\mathbf{X} \sim P_{(l)}^\phi(\cdot | \mathbf{Y}_{t-k+1:t})} \|\mathbf{X}\|^\beta \leq B < \infty$, we have therefore:

$$\begin{aligned} \mathbb{E} [H(\mathbf{Y}_{t-k+1:t+l})^{r+\delta}] &\leq \mathbb{E} \left[(2^{\beta-1}(B+B) + 2^\beta(B + \|\mathbf{Y}_{t+l}\|^\beta))^{r+\delta} \right] \\ &= \mathbb{E} \left[(2^{\beta+1}B + 2^\beta\|\mathbf{Y}_{t+l}\|^\beta)^{r+\delta} \right]. \end{aligned}$$

Now, denote $\delta' = r + \delta$; $\delta' > 1$ by assumption. It holds therefore, as above, $(a+b)^{\delta'} \leq 2^{\delta'-1}(a^{\delta'} + b^{\delta'})$ for $a, b > 0$; we have therefore that:

$$\mathbb{E} [H(\mathbf{Y}_{t-k+1:t+l})^{\delta'}] \leq 2^{-1} (2^{\beta+2}B)^{\delta'} + 2^{\delta'(\beta+1)-1} \mathbb{E} \|\mathbf{Y}_{t+l}\|^{\beta\delta'};$$

the above expression is therefore bounded whenever $\mathbb{E} \|\mathbf{Y}_{t+l}\|^{\beta(r+\delta)} < \infty$. \square

A.3.2 Mixing

Here, we give the precise definitions for the mixing conditions stated in Assumption **A4(a)**. More background on the following definitions can be found, for instance, in 6.

Definition A.10 (Measures of dependence). Consider a probability space (Ω, \mathcal{F}, P) ; for any two sigma algebras $\mathcal{A} \subseteq \mathcal{F}$ and $\mathcal{B} \subseteq \mathcal{F}$, define:

$$\begin{aligned} \alpha_P(\mathcal{A}, \mathcal{B}) &:= \sup_{A \in \mathcal{A}, B \in \mathcal{B}} |P(A \cap B) - P(A)P(B)|, \\ \varphi_P(\mathcal{A}, \mathcal{B}) &:= \sup_{A \in \mathcal{A}, B \in \mathcal{B}: P(B) > 0} |P(B|A) - P(B)|. \end{aligned}$$

For $1 \leq r \leq s \leq \infty$, define the Borel σ -algebra of events generated from $(\mathbf{Y}_r, \mathbf{Y}_{r+1}, \dots, \mathbf{Y}_{s-1}, \mathbf{Y}_s)$ as \mathcal{G}_r^s . Then, we define:

$$\alpha^{\mathbf{Y}}(m) = \sup_{r \geq 1} \alpha_{P^*}(\mathcal{G}_1^r, \mathcal{G}_{r+m}^{+\infty}), \quad \varphi^{\mathbf{Y}}(m) = \sup_{r \geq 1} \varphi_{P^*}(\mathcal{G}_1^r, \mathcal{G}_{r+m}^{+\infty}).$$

Definition A.11. The random sequence $(\mathbf{Y}_t)_t$ is said α -mixing if $\alpha^{\mathbf{Y}}(m) \rightarrow 0$ as $m \rightarrow \infty$ and φ -mixing if $\varphi^{\mathbf{Y}}(m) \rightarrow 0$ as $m \rightarrow \infty$. It can be seen that φ -mixing implies α -mixing [15].

Definition A.12. We say that the mixing coefficients $\varphi^{\mathbf{Y}}(m)$ are of size s [15] if $\varphi^{\mathbf{Y}}(m) = \mathcal{O}(m^{-\lambda})$ for $\lambda > s$; similar definition can be given for the coefficients $\alpha^{\mathbf{Y}}(m)$.

In [6], the definitions for the quantities above consider a sequence $(\mathbf{X}_t)_{t \in \mathbb{Z}}$, and defined:

$$\alpha^{\mathbf{X}}(m) = \sup_{r \in \mathbb{Z}} \alpha_P(\mathcal{G}_{-\infty}^r, \mathcal{G}_{r+m}^{+\infty}),$$

for some distribution P , and similar for $\varphi^{\mathbf{X}}(m)$. Our definition can be cast in this way by defining $\mathbf{X}_t = \mathbf{Y}_t \forall t \geq 1$ and $\mathbf{X}_t = 0 \forall t \leq 0$.

A.3.3 Generic consistency result

We consider here the following Assumption:

A5 (Uniform Law of Large Numbers.) The following holds with probability 1 with respect to $(\mathbf{Y}_t)_t \sim P^*$:

$$\sup_{\phi \in \Phi} \left| S_T(P_{k+l:T}^\phi(\cdot | \mathbf{Y}_{1:k+l-1}), \mathbf{Y}_{k+l:T}) - S_T^*(P_{k+l:T}^\phi) \right| \rightarrow 0.$$

We give here a consistency result more general than Theorem A.4, as in fact Assumption **A5** is more general than the stationarity and mixing conditions in Assumption **A3** and **A4**.

Theorem A.13 (Theorem 5.1 in 53). *If Assumptions **A2** and **A5** hold, then $d(\hat{\phi}_T(\mathbf{Y}_{1:T}), \phi_T^*) \rightarrow 0$ with probability 1 with respect to $(\mathbf{Y}_t)_t \sim P^*$.*

We report here a proof for ease of reference.

Proof. By the definition of \liminf , for a fixed $\epsilon > 0$, Assumption **A2** implies that there exists $T_1(\epsilon)$ such that:

$$\delta(\epsilon) := \left\{ \inf_{T > T_1(\epsilon)} \min_{\phi: d(\phi, \phi_T^*) \geq \epsilon} S_T^*(P_{k+l:T}^\phi) - S_T^*(P_{k+l:T}^{\phi_T^*}) \right\} > 0. \quad (24)$$

Due to Assumption **A5**, with probability 1 with respect to $(\mathbf{Y}_t)_t \sim P^*$, there exists $T_2((\mathbf{Y}_t)_t, \delta(\epsilon))$ such that, for all $T > T_2((\mathbf{Y}_t)_t, \delta(\epsilon))$:

$$\left| S_T(P_{k+l:T}^{\phi_T^*}(\cdot | \mathbf{Y}_{1:k+l-1}), \mathbf{Y}_{k+l:T}) - S_T^*(P_{k+l:T}^{\phi_T^*}) \right| < \delta(\epsilon)/2,$$

which implies:

$$S_T^*(P_{k+l:T}^{\phi_T^*}) > S_T(P_{k+l:T}^{\phi_T^*}(\cdot | \mathbf{Y}_{1:k+l-1}), \mathbf{Y}_{k+l:T}) - \delta(\epsilon)/2 \geq S_T(P_{k+l:T}^{\hat{\phi}_T(\mathbf{Y}_{1:T})}(\cdot | \mathbf{Y}_{1:k+l-1}), \mathbf{Y}_{k+l:T}) - \delta(\epsilon)/2, \quad (25)$$

where the second inequality is valid thanks to the definition of $\hat{\phi}_T(\mathbf{Y}_{1:T})$.

Similarly, by exploiting Assumption **A5** again, with probability 1 with respect to $(\mathbf{Y}_t)_t \sim P^*$, there exists $T_3((\mathbf{Y}_t)_t, \delta(\epsilon))$ such that, for all $T > T_3((\mathbf{Y}_t)_t, \delta(\epsilon))$:

$$\left| S_T^*(P_{k+l:T}^{\hat{\phi}_T(\mathbf{Y}_{1:T})}) - S_T(P_{k+l:T}^{\hat{\phi}_T(\mathbf{Y}_{1:T})}(\cdot | \mathbf{Y}_{1:k+l-1}), \mathbf{Y}_{k+l:T}) \right| < \delta(\epsilon)/2. \quad (26)$$

Then, with probability 1 with respect to $(\mathbf{Y}_t)_t \sim P^*$, for all $T > \max\{T_2((\mathbf{Y}_t)_t, \delta(\epsilon)), T_3((\mathbf{Y}_t)_t, \delta(\epsilon))\}$:

$$\begin{aligned} S_T^*(P_{k+l:T}^{\hat{\phi}_T(\mathbf{Y}_{1:T})}) - S_T^*(P_{k+l:T}^{\phi_T^*}) &\leq S_T^*(P_{k+l:T}^{\hat{\phi}_T(\mathbf{Y}_{1:T})}) - S_T(P_{k+l:T}^{\hat{\phi}_T(\mathbf{Y}_{1:T})}(\cdot | \mathbf{Y}_{1:k+l-1}), \mathbf{Y}_{k+l:T}) + \delta(\epsilon)/2 \\ &< \delta(\epsilon)/2 + \delta(\epsilon)/2 = \delta(\epsilon), \end{aligned} \quad (27)$$

where the first inequality is thanks to Eq. (25) and the second is thanks to Eq (26).

Now, Eq. (24) and Eq. (27) both hold with probability 1 with respect to $(\mathbf{Y}_t)_t \sim P^*$ for all $T > \max\{T_1(\delta(\epsilon)), T_2((\mathbf{Y}_t)_t, \delta(\epsilon)), T_3((\mathbf{Y}_t)_t, \delta(\epsilon))\}$. Notice that Eq. (27) ensures that the distance considered in Eq. (24) is smaller than $\delta(\epsilon)$ for $\phi = \hat{\phi}_T(\mathbf{Y}_{1:T})$; However, Eq. (24) states that the same distance is larger or equal than $\delta(\epsilon)$ for all $\phi : d(\phi, \phi_T^*) \geq \epsilon$, from which it follows that $d(\hat{\phi}_T(\mathbf{Y}_{1:T}), \phi_T^*) < \epsilon$ with probability 1 with respect to $(\mathbf{Y}_t)_t \sim P^*$. As ϵ is however arbitrary, it follows that, with probability 1 with respect to $(\mathbf{Y}_t)_t \sim P^*$:

$$d(\hat{\phi}_T(\mathbf{Y}_{1:T}), \phi_T^*) \rightarrow 0.$$

□

A.3.4 Uniform law of large numbers

We will here show how the Uniform Law of Large Numbers in Assumption **A5** can be obtained from the stationarity and mixing conditions in **A3** and **A4**. To this aim, we exploit a result in 43.

We consider now a generic sequence of random variables $\mathbf{Z}_t \in \mathcal{Z}$, and a function $q : \mathcal{Z} \times \Phi \rightarrow \mathbb{R}$. Let us denote now by \mathcal{F} the Borel σ -algebra generated by the sequence $(\mathbf{Z}_t)_t$, $\Omega_{\mathbf{Z}}$ the space of realizations of $(\mathbf{Z}_t)_t$ and Q^* the probability distribution for it.

Consider the following Assumptions:

C1 (Dominance condition) For $D(\mathbf{z}) = \sup_{\phi \in \Phi} |q(\mathbf{z}, \phi)|$, there is some $\delta > 0$ such that

$$\sup_t \frac{1}{N} \sum_{t=1}^N \mathbb{E} [D(\mathbf{Z}_t)^{1+\delta}] < \infty.$$

C2 (Asymptotic stationarity) Let Q_t^* be the marginal distribution of \mathbf{Z}_t ; then, $N^{-1} \sum_{t=1}^N Q_t^*$ converges weakly to some probability measure F on \mathcal{Z} .

C3 (Pointwise law of large numbers) For some metric ρ on Φ , let:

$$\bar{q}(\mathbf{z}, \phi, \tau) := \sup_{\phi': \rho(\phi, \phi') < \tau} q(\mathbf{z}, \phi'), \quad \underline{q}(\mathbf{z}, \phi, \tau) := \inf_{\phi': \rho(\phi, \phi') < \tau} q(\mathbf{z}, \phi').$$

For all $\phi \in \Phi$, there exists a sequence of positive numbers $\tau_i(\phi)$ such that $\tau_i(\phi) \rightarrow 0$ as $i \rightarrow \infty$, and such that for each τ_i the random variables $\bar{q}(\mathbf{Z}_t, \phi, \tau_i)$ and $\underline{q}(\mathbf{Z}_t, \phi, \tau_i)$ satisfy a strong law of large numbers, i.e., as $N \rightarrow \infty$:

$$\begin{aligned} \frac{1}{N} \sum_{t=1}^N \{\bar{q}(\mathbf{Z}_t, \phi, \tau_i) - \mathbb{E}[\bar{q}(\mathbf{Z}_t, \phi, \tau_i)]\} &\rightarrow 0 \\ \frac{1}{N} \sum_{t=1}^N \{\underline{q}(\mathbf{Z}_t, \phi, \tau_i) - \mathbb{E}[\underline{q}(\mathbf{Z}_t, \phi, \tau_i)]\} &\rightarrow 0, \end{aligned}$$

where the two above equations hold with probability 1 with respect to $(\mathbf{Z}_t)_t \sim Q^*$.

Theorem A.14 (Theorem 2 in 43). *If Assumptions A1, C1, C2 and C3 hold and if $q(\mathbf{z}, \phi)$ is continuous on $\mathcal{Z} \times \Phi$, then:*

(i) *with probability 1 with respect to $(\mathbf{Z}_t)_t \sim Q^*$,*

$$\limsup_{t \rightarrow \infty} \sup_{\phi \in \Phi} \left| \frac{1}{N} \sum_{t=1}^N \{q(\mathbf{Z}_t, \phi) - \mathbb{E}[q(\mathbf{Z}_t, \phi)]\} \right| = 0;$$

(ii) *$\int q(\mathbf{z}, \phi) dF(\mathbf{z})$ exists and is finite, continuous on Φ and, with probability 1 with respect to $(\mathbf{Z}_t)_t \sim Q^*$,*

$$\limsup_{t \rightarrow \infty} \sup_{\phi \in \Phi} \left| \frac{1}{N} \sum_{t=1}^N q(\mathbf{Z}_t, \phi) - \int q(\mathbf{z}, \phi) dF(\mathbf{z}) \right| = 0;$$

We now give sufficient conditions for Assumption **C3** to hold. In fact, sequences for which the dependence of \mathbf{Z}_t on a past observation \mathbf{Z}_{t-m} decreases to 0 quickly enough as $m \rightarrow \infty$ satisfy Assumption **C3**. This can be made more rigorous considering the definitions of α - and φ -mixing sequences given in Appendix A.3.2.

Given the sequence $(\mathbf{Z}_t)_t$, for $1 \leq r \leq s \leq \infty$, define the Borel σ -algebra of events generated from $(\mathbf{Z}_r, \mathbf{Z}_{r+1}, \dots, \mathbf{Z}_{s-1}, \mathbf{Z}_s)$ as \mathcal{F}_r^s . Then, we define the mixing coefficients for $(\mathbf{Z}_t)_t$ as:

$$\alpha^{\mathbf{Z}}(m) = \sup_{r \geq 1} \alpha_{Q^*}(\mathcal{F}_1^r, \mathcal{F}_{r+m}^{+\infty}), \quad \varphi^{\mathbf{Z}}(m) = \sup_{r \geq 1} \varphi_{Q^*}(\mathcal{F}_1^r, \mathcal{F}_{r+m}^{+\infty}).$$

Similarly to before, the random sequence $(\mathbf{Z}_t)_{t \in \mathbb{Z}}$ is said α -mixing if $\alpha^{\mathbf{Z}}(m) \rightarrow 0$ as $m \rightarrow \infty$ and φ -mixing if $\varphi^{\mathbf{Z}}(m) \rightarrow 0$ as $m \rightarrow \infty$. Additionally, we say that the mixing coefficients $\varphi^{\mathbf{Z}}(m)$ are of size s [15] if $\varphi^{\mathbf{Z}}(m) = \mathcal{O}(m^{-\lambda})$ for $\lambda > s$; similar definition can be given for the coefficients $\alpha^{\mathbf{Z}}(m)$.

Let us define now the following additional assumption:

C4 Both conditions below hold:

(a) (Mixing) Either one of the following holds:

- i. $(\mathbf{Z}_t)_t$ is α -mixing with mixing coefficient of size $r/(2r-1)$, with $r \geq 1$, or
- ii. $(\mathbf{Z}_t)_t$ is φ -mixing with mixing coefficient of size $r/(r-1)$ with $r > 1$.

(b) (Moment boundedness) $\sup_t \mathbb{E}[D(\mathbf{Z}_t)^{r+\delta}] < \infty$ for some $\delta > 0$, for the value of r corresponding to the condition above which is satisfied.

We give the following Lemma, which is contained in Corollary 1 in 43.

Lemma A.15 (Corollary 1 in 43). *Assumption C4 implies Assumptions C1 and C3.*

We can therefore state the following.

Corollary A.16. *If Assumptions A1, C2 and C4 hold and if $q(\mathbf{z}, \phi)$ is continuous on $\mathcal{Z} \times \Phi$, then the conclusions of Theorem A.14 are satisfied.*

A.3.5 Proving Theorem A.4

Here, we finally prove Theorem A.4 by combining the generic consistency result in Appendix A.3.3 with the uniform law of large number result reported in Appendix A.3.4.

Notice that, in stating Theorem A.14 and Corollary A.16, we have considered a generic sequence $(\mathbf{Z}_t)_t$. In the setting of our interest, however, we want to study the prequential scoring rule defined in Eq. (20), and use Corollary A.16 to state conditions under which Assumption **A5**, and therefore Theorem A.13, hold.

To this aim, we identify now $N = T - k - l + 1$, $\mathbf{Z}_t = \mathbf{Y}_{t:t+k+l-1}$ and $q(\mathbf{Z}_t, \phi) = S(P_{(l)}^\phi(\cdot | \mathbf{Y}_{t:t+k-1}), \mathbf{Y}_{t+k+l-1})$; which leads to:

$$\begin{aligned} \frac{1}{N} \sum_{t=1}^N q(\mathbf{Z}_t, \phi) &= \frac{1}{T - k - l + 1} \sum_{t=1}^{T-k-l+1} S(P_{(l)}^\phi(\cdot | \mathbf{Y}_{t:t+k-1}), \mathbf{Y}_{t+k+l-1}) \\ &= \frac{1}{T - k - l + 1} \sum_{t=k}^{T-l} S(P_{(l)}^\phi(\cdot | \mathbf{Y}_{t-k+1:t}), \mathbf{Y}_{t+l}) \\ &= S_T(P_{k+l:T}^\phi(\cdot | \mathbf{Y}_{1:k+l-1}), \mathbf{Y}_{k+l:T}). \end{aligned}$$

The distribution Q^* on $(\mathbf{Z}_t)_t$ considered in the previous section is induced therefore by P^* over $(\mathbf{Y}_t)_t$.

We want now to relate $\alpha^{\mathbf{Y}}(m)$ and $\varphi^{\mathbf{Y}}(m)$ to $\alpha^{\mathbf{Z}}(m)$ and $\varphi^{\mathbf{Z}}(m)$; in order to do so, notice that, as $\mathbf{Z}_t = \mathbf{Y}_{t:t+k+l-1}$, $\mathcal{F}_r^{\mathbf{Z}} = \mathcal{G}_r^{s+k+l-1}$. Therefore,

$$\begin{aligned} \alpha^{\mathbf{Z}}(m) &= \sup_{r \geq 1} \alpha^{\mathbf{Z}}(\mathcal{F}_1^r, \mathcal{F}_{r+m}^{+\infty}) = \sup_{r \geq 1} \alpha^{\mathbf{Y}}(\mathcal{G}_1^{r+k+l-1}, \mathcal{G}_{r+m}^{+\infty}) \\ &= \sup_{r \geq k+l} \alpha^{\mathbf{Y}}(\mathcal{G}_1^r, \mathcal{G}_{r+m-k-l+1}^{+\infty}) \leq \sup_{r \geq 1} \alpha^{\mathbf{Y}}(\mathcal{G}_1^r, \mathcal{G}_{r+m-k-l+1}^{+\infty}) = \alpha^{\mathbf{Y}}(m - k - l + 1), \end{aligned}$$

and, similarly, $\varphi^{\mathbf{Z}}(m) \leq \varphi^{\mathbf{Y}}(m - k - l + 1)$. As k is fixed, $\varphi^{\mathbf{Y}}(m) \rightarrow 0 \implies \varphi^{\mathbf{Z}}(m) \rightarrow 0$ as $m \rightarrow \infty$, which is to say, $(\mathbf{Y}_t)_t$ being φ -mixing implies $(\mathbf{Z}_t)_t$ is φ -mixing as well, and similar for α -mixing. Additionally, if the mixing coefficients for $(\mathbf{Z}_t)_t$ have a given size s , then the mixing coefficients for $(\mathbf{Y}_t)_t$ will have the same size, and viceversa. In fact, $\varphi^{\mathbf{Z}}(m) \leq \varphi^{\mathbf{Y}}(m - k - l + 1) = \mathcal{O}(m^{-\lambda})$ implies either $\varphi^{\mathbf{Y}}(m) = \mathcal{O}(m^{-\lambda})$ or $\varphi^{\mathbf{Y}}(m) = o(m^{-\lambda})$, and similar for α -mixing.

We are now ready to prove Theorem A.4.

Proof of Theorem A.4. Notice that, by identifying $\mathbf{Z}_t = \mathbf{Y}_{t:t+k+l-1}$ and $q(\mathbf{Z}_t, \phi) = S(P_{(l)}^\phi(\cdot | \mathbf{y}_{t:t+k-1}), \mathbf{y}_{t+k+l-1})$, Assumption **A3** corresponds to Assumption **C2**, and Assumption **A4** implies Assumption **C4**, due to the conservation of size of the mixing coefficients discussed above.

Together with Assumption **A1** and the continuity condition, therefore, Corollary A.16 holds, from which you have that, with probability 1 with respect to $(\mathbf{Y}_t)_t \sim P^*$,

$$\lim_{T \rightarrow \infty} \sup_{\phi \in \Phi} \left| \frac{1}{T - k - l + 1} \sum_{t=k}^{T-l} \left\{ S(P_{(l)}^\phi(\cdot | \mathbf{Y}_{t-k+1:t}), \mathbf{Y}_{t+l}) - \mathbb{E} \left[S(P_{(l)}^\phi(\cdot | \mathbf{Y}_{t-k+1:t}), \mathbf{Y}_{t+l}) \right] \right\} \right| = 0;$$

which, recalling the definition of $S_T(P_{k+l:T}^\phi(\cdot | \mathbf{Y}_{1:k+l-1}), \mathbf{Y}_{k+l:T})$ and $S_T^*(P_{k+l:T}^\phi)$ in Eqs. (20) and (21), is the same as Assumption **A5**. Thanks to this and Assumption **A2**, therefore, Theorem A.13 holds, from which the result follows. \square

B More details on the different methods

B.1 Training generative networks via divergence minimization

B.1.1 f -GAN

The f -GAN approach is defined by considering an f -divergence in place of D in Eq. (1) in the main text:

$$D_f(P^* || P^\phi) = \int_{\mathcal{Y}} p^\phi(\mathbf{y}) f\left(\frac{p^*(\mathbf{y})}{p^\phi(\mathbf{y})}\right) d\mu(\mathbf{y}),$$

where $f : \mathbb{R}_+ \rightarrow \mathbb{R}$ is a convex, lower-semicontinuous function for which $f(1) = 0$, and where p^ϕ and p^* are densities of P^ϕ and P^* with respect to a base measure μ . Let now dom_f denote the domain of f . By exploiting the Fenchel conjugate $f^*(t) = \sup_{u \in \text{dom}_f} \{ut - f(u)\}$, 38 obtain the following variational lower bound:

$$D_f(P^* || P^\phi) \geq \sup_{c \in \mathcal{C}} (\mathbb{E}_{\mathbf{Y} \sim P^*} c(\mathbf{Y}) - \mathbb{E}_{\mathbf{X} \sim P^\phi} f^*(c(\mathbf{X}))),$$

which holds for any set of functions \mathcal{C} from \mathcal{Y} to dom_{f^*} . By considering a parametric set of functions $\mathcal{C} = \{c_\psi : \mathcal{Y} \rightarrow \text{dom}_{f^*}, \psi \in \Psi\}$, a surrogate to the problem in Eq. (1) in the main text becomes:

$$\min_{\phi} \max_{\psi} (\mathbb{E}_{\mathbf{Y} \sim P^*} c_\psi(\mathbf{Y}) - \mathbb{E}_{\mathbf{X} \sim P^\phi} f^*(c_\psi(\mathbf{X}))).$$

In the conditional setting discussed in Section 2.1 in the main text, the above generalizes to:

$$\min_{\phi} \max_{\psi} \mathbb{E}_{\theta \sim \Pi} (\mathbb{E}_{\mathbf{Y} \sim P^*(\cdot | \theta)} c_\psi(\mathbf{Y}; \theta) - \mathbb{E}_{\mathbf{X} \sim P^\phi(\cdot | \theta)} f^*(c_\psi(\mathbf{X}; \theta))), \quad (29)$$

By denoting as $P_{\theta, \mathbf{Y}}^*$ and $P_{\theta, \mathbf{X}}^\phi$ the joint distributions over $\Theta \times \mathcal{Y}$, Eq. (29) corresponds to the relaxation of $D_f(P_{\theta, \mathbf{Y}}^* || P_{\theta, \mathbf{X}}^\phi)$ under the constraint that the marginal of $P_{\theta, \mathbf{Y}}^*$ for θ is equal to Π .

In order to solve the problem in Eq. (29), alternating optimization over ϕ and ψ can be performed; in Algorithm 1, we show a single epoch (i.e., a loop on the full training dataset) of conditional f -GAN training; for simplicity, we consider here using a single pair (θ_i, \mathbf{y}_i) to estimate the expectations in Eq. (29) (i.e., the batch size is 1), but using a larger number of samples is indeed possible. Notice how in Algorithm 1 we update the critic once every generator update; however, multiple critic updates can be done.

Algorithm 1 Single epoch conditional f -GAN training.

Require: Parametric map h_ϕ , critic network c_ψ , learning rates ϵ, γ .
for each training pair (θ_i, \mathbf{y}_i) **do**
 Sample $\mathbf{z} \sim Q$
 Obtain $\hat{\mathbf{x}}_i^\phi = h_\phi(\mathbf{z}, \theta_i)$
 Set $\psi \leftarrow \psi + \gamma \cdot \nabla_{\psi} [c_\psi(\mathbf{y}_i, \theta_i) - f^*(c_\psi(\hat{\mathbf{x}}_i^\phi, \theta_i))]$
 Set $\phi \leftarrow \phi - \epsilon \cdot \nabla_{\phi} [-f^*(c_\psi(\hat{\mathbf{x}}_i^\phi, \theta_i))]$
end for

B.1.2 Wasserstein-GAN (WGAN)

I exploited the following expression for the 1-Wasserstein distance:

$$W(P^*, P^\phi) = \sup_{c: \|c\|_L \leq 1} \mathbb{E}_{\mathbf{Y} \sim P^*} [c(\mathbf{Y})] - \mathbb{E}_{\mathbf{X} \sim P^\phi} [c(\mathbf{X})], \quad (30)$$

where $\|c\|_L$ denotes the Lipschitz constant of the function c . The different notation here highlights how W is a symmetric function. Plugging Eq. (30) into Eq. (1) in the main text leads again to an adversarial setting; here, the Lipschitz constraint can be enforced by clipping the weights of the neural network to a given range [1]. Alternatively, this hard constraint can be relaxed to a soft one via gradient penalization [24].

B.1.3 MMD-GAN

A specific case of the MMD (Eq. 3 in the main text) is the Energy Distance:

$$\mathcal{E}(P^*, P^\phi) = \mathbb{E} \left[2\|\mathbf{X} - \mathbf{Y}\|_2^\beta - \|\mathbf{X} - \mathbf{X}'\|_2^\beta - \|\mathbf{Y} - \mathbf{Y}'\|_2^\beta \right], \quad (31)$$

where $\beta \in (0, 2)$ and $\|\cdot\|_2$ denotes the ℓ_2 norm. In 2, the above is used to define an algorithm to train generative networks, termed Cramer-GAN.

In [32], the authors proposed to compute the kernel k in Eq. (3) in the main text on learnable transformation c_ψ , whose weights are trained to maximize the discrepancy. Specifically, that leads to a new discrepancy measure:

$$\max_{\psi} \mathbb{E} \left[k(c_\psi(\mathbf{X}), c_\psi(\mathbf{X}')) - 2k(c_\psi(\mathbf{X}), c_\psi(\mathbf{Y})) + k(c_\psi(\mathbf{Y}), c_\psi(\mathbf{Y}')) \right],$$

which is a meaningful divergence between probability distributions [32]. In this setting, again people recur to alternating maximization steps over ψ with minimization over ϕ . This, as mentioned in the main text, leads to biased estimates of gradients. However, for MMD-GANs, training is made easier by applying the gradient regularization techniques described in 24, as shown in 4.

Notice that, in minimizing Equations (3) in the main text with respect to ϕ , one could ignore the term involving \mathbf{Y}, \mathbf{Y}' ; however, when introducing c_ψ , this cannot be done as that term depends on ψ as well.

In the conditional setting, a natural approach for MMD-GAN is minimizing $\mathbb{E}_{\theta \sim \Pi} [\text{MMD}^2(P^*(\cdot|\theta), P^\phi(\cdot|\theta))]$, as $\text{MMD}^2(P_{\theta, \mathbf{Y}}^*, P_{\theta, \mathbf{Y}}^\phi)$ would require computing kernel over $\Theta \times \mathcal{Y}$.

Notice however how, in estimating $\text{MMD}^2(P^*(\cdot|\theta), P^\phi(\cdot|\theta))$, multiple samples $\mathbf{Y}, \mathbf{Y}' \sim P^*(\cdot|\theta)$ are used (see Eq. 3 in the main text), but those are unavailable (empirical samples are of the form in Eq. 4 in the main text); as discussed before, however, $k(\mathbf{Y}, \mathbf{Y}')$ does not depend on ϕ , so that it can be discarded in the minimization process. However, if the data is transformed via c_ψ , $k(c_\psi(\mathbf{Y}), c_\psi(\mathbf{Y}'))$ cannot be dropped anymore, which makes the problem intractable. In 2, this problem is solved by replacing $k(c_\psi(\mathbf{Y}), c_\psi(\mathbf{Y}'))$ with some other tractable terms; however, that approach leads to an ill-defined statistical divergence, as it can be minimized by two distributions which are not the same [4].

B.2 Scoring Rules

We now introduce some common SRs; let $\mathbf{X}, \mathbf{X}' \sim P^\phi$ be independent samples for the forecast distribution P^ϕ .

Energy Score For $\beta \in (0, 2)$, the energy score is:

$$S_E^{(\beta)}(P^\phi, \mathbf{y}) = 2 \cdot \mathbb{E} \|\mathbf{X} - \mathbf{y}\|_2^\beta - \mathbb{E} \|\mathbf{X} - \mathbf{X}'\|_2^\beta. \quad (32)$$

The probabilistic forecasting literature [20] use a different convention of the energy score and the subsequent kernel score, which amounts to multiplying our definitions by 1/2. We follow here the convention used in the statistical inference literature [48, 7, 37]

The Energy Score is strictly proper for the class of probability measures P^ϕ such that $\mathbb{E}_{\mathbf{X} \sim P^\phi} \|\mathbf{X}\|^\beta < \infty$ [20]. The Energy Score is related to the Energy distance (Eq. (31)), which is a metric between probability distributions [48]. We will fix $\beta = 1$ in the rest of this work. Additionally, for a univariate distribution and $\beta = 1$, the Energy Score recovers the Continuous Ranked Probability Score (CRPS), widely used in meteorology (e.g, see 26).

Kernel Score For a positive definite kernel $k(\cdot, \cdot)$, the kernel Scoring Rule can be defined as [20]:

$$S_k(P^\phi, \mathbf{y}) = \mathbb{E}[k(\mathbf{X}, \mathbf{X}')] - 2 \cdot \mathbb{E}[k(\mathbf{X}, \mathbf{y})].$$

The Kernel Score is connected to the squared Maximum Mean Discrepancy (MMD, 22) relative to the kernel k , see Eq. (3) in the main text. S_k is proper for the class of probability distributions for which $\mathbb{E}[k(\mathbf{X}, \mathbf{X}')] is finite (by Theorem 4 in 20). Additionally, it is strictly proper under conditions on k ensuring that the MMD is a metric for probability distributions on \mathcal{Y} [22]. These conditions are satisfied, among others, by the Gaussian kernel (which we will use in this work):$

$$k(\mathbf{x}, \mathbf{y}) = \exp\left(-\frac{\|\mathbf{x} - \mathbf{y}\|_2^2}{2\gamma^2}\right), \quad (33)$$

in which γ is a scalar bandwidth.

Patched Score For the Patched Score, we consider different overlapping patches of the input data; denote as \mathcal{P} the set of patches and as $p \in \mathcal{P}$ an individual patch; the patches are of a given size and spaced by a given spacing.

Then, we compute a SR S for multivariate distributions on each patch separately, and then add the results:

$$S_p(P^\phi, \mathbf{y}) = \sum_{p \in \mathcal{P}} S(P^\phi|_p, \mathbf{y}|_p), \quad (34)$$

where $\mathbf{y}|_p$ denotes the components of \mathbf{y} in the patch p and $P^\phi|_p$ denotes the marginal distribution induced by P^ϕ for components in the patch p . See Figure 4 for a representation. As mentioned in the main body (Sec. 3.2 in the main text), the resulting SR is not strictly proper, as far away correlations are discarded. Notice how the topology of data for our global weather dataset is periodic along the longitudinal direction (i.e., horizontally in Figure 4). The patches we define follow this.

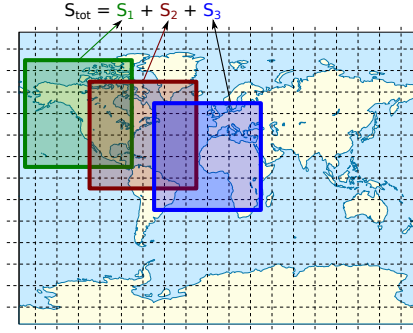


Figure 4: Patched SR: a SR for multivariate data is computed on localized patches, and the resulting values are summed.

C Stochastic Gradient Descent for generative-SR networks

We discuss here how we can get unbiased gradient estimates for the prequential SR in Eq. (8) in the main text with respect to the parameters of the generative network ϕ .

In order to do that, we first discuss how to obtain unbiased estimates of the SRs we use across this work. Then, we show how those allow to obtain unbiased gradient estimates.

C.1 Unbiased scoring rule estimates

Consider we have draws $\mathbf{x}_j \sim P, j = 1, \dots, m$.

Energy Score An unbiased estimate of the energy score can be obtained by unbiasedly estimating the expectations in $S_E^{(\beta)}(P, \mathbf{y})$ in Eq. (32):

$$\hat{S}_E^{(\beta)}(\{\mathbf{x}_j\}_{j=1}^m, \mathbf{y}) = \frac{2}{m} \sum_{j=1}^m \|\mathbf{x}_j - \mathbf{y}\|_2^\beta - \frac{1}{m(m-1)} \sum_{\substack{j,k=1 \\ k \neq j}}^m \|\mathbf{x}_j - \mathbf{x}_k\|_2^\beta.$$

Kernel Score Similarly to the energy score, we obtain an unbiased estimate of $S_k(P, y)$ by:

$$\hat{S}_k(\{\mathbf{x}_j\}_{j=1}^m, \mathbf{y}) = \frac{1}{m(m-1)} \sum_{\substack{j,k=1 \\ k \neq j}}^m k(\mathbf{x}_j, \mathbf{x}_k) - \frac{2}{m} \sum_{j=1}^m k(\mathbf{x}_j, \mathbf{y}).$$

Variogram Score It is immediate to obtain an unbiased estimate of $S_v^{(p)}(P, \mathbf{y})$ in Eq. (10) in the main text by:

$$\hat{S}_v^{(p)}(\{\mathbf{x}_j\}_{j=1}^m, \mathbf{y}) = \sum_{i,j=1}^d w_{ij} \left(|y_i - y_j|^p - \frac{1}{m} \sum_{k=1}^m |x_{k,i} - x_{k,j}|^p \right)^2.$$

Patched SR Assume the patched SR in Eq. (34) is built from a SR S which admits an unbiased empirical estimate $\hat{S}(\{\mathbf{x}_j\}_{j=1}^m, \mathbf{y})$. Therefore, an unbiased estimate of the patched SR can be obtained as:

$$\hat{S}_p(\{\mathbf{x}_j\}_{j=1}^m, \mathbf{y}) = \sum_{p \in \mathcal{P}} S(\{\mathbf{x}_j|_p\}_{j=1}^m, \mathbf{y}|_p),$$

as in fact the components of samples \mathbf{x}_j in the patch p are samples from the marginal distribution over the patch $P|_p$.

Sum of SRs When adding multiple SRs, an unbiased estimate of the sum can be obtained by adding unbiased estimates of the two addends.

C.2 Unbiased estimate for S_T

Recall now we want to solve:

$$\hat{\phi}_T(\mathbf{y}_{1:T}) := \arg \min_{\phi} S_T(P_{k+l:T}^{\phi}(\cdot | \mathbf{y}_{1:k+l-1}), \mathbf{y}_{k+l:T}),$$

where, for simplicity, we re-define S_T in Eq. (8) in the main text with an additional scaling constant:

$$S_T(P_{k+l:T}^{\phi}(\cdot | \mathbf{y}_{1:k+l-1}), \mathbf{y}_{k+l:T}) := \frac{1}{T-l-k+1} \sum_{t=k}^{T-l} S(P_{t+l}^{\phi}(\cdot | \mathbf{y}_{t-k+1:t}), \mathbf{y}_{t+l}). \quad (35)$$

In order to do this, we exploit Stochastic Gradient Descent (SGD), which requires unbiased estimates of $S_T(P_{k+l:T}^{\phi}(\cdot | \mathbf{y}_{1:k+l-1}), \mathbf{y}_{k+l:T})$ (notice we are not talking here of unbiased estimates with respect to the observed sequence $\mathbf{y}_{1:T}$).

Notice how, for all the Scoring Rules used across this work, as well as any weighted sum of those, we can write: $S(P, \mathbf{y}) = \mathbb{E}_{\mathbf{Y}, \mathbf{Y}' \sim P} [g(\mathbf{Y}, \mathbf{Y}', \mathbf{y})]$ for some function g ; namely, the SR is defined through an expectation over (possibly multiple) samples from P . That is the form exploited in Appendix C.1 to obtain unbiased SR estimates.

Now, we will use this fact to obtain unbiased estimates for the objective in Eq. (35). For brevity, let us now denote $J(\phi) = S_T(P_{k+l:T}^{\phi}(\cdot | \mathbf{y}_{1:k+l-1}), \mathbf{y}_{k+l:T})$, which we can rewrite as (letting $N = T-l-k+1$ for brevity):

$$\begin{aligned} J(\phi) &= \frac{1}{N} \sum_{t=k}^{T-l} \mathbb{E}_{\mathbf{Y}, \mathbf{Y}' \sim P^{\phi}(\cdot | \mathbf{y}_{t-k+1:t})} [g(\mathbf{Y}, \mathbf{Y}', \mathbf{y}_{t+l})] \\ &= \frac{1}{N} \sum_{t=k}^{T-l} \mathbb{E}_{\mathbf{Z}, \mathbf{Z}' \sim Q} [g(h_{\phi}(\mathbf{Z}; \mathbf{y}_{t-k+1:t}), h_{\phi}(\mathbf{Z}'; \mathbf{y}_{t-k+1:t}), \mathbf{y}_{t+l})], \end{aligned}$$

where we used the fact that P^{ϕ} is the distribution induced by a generative network with transformation h_{ϕ} ; this is called the reparametrization trick [28]. Now:

$$\begin{aligned} \nabla_{\phi} J(\phi) &= \nabla_{\phi} \frac{1}{N} \sum_{t=k}^{T-l} \mathbb{E}_{\mathbf{Z}, \mathbf{Z}' \sim Q} [g(h_{\phi}(\mathbf{Z}; \mathbf{y}_{t-k+1:t}), h_{\phi}(\mathbf{Z}'; \mathbf{y}_{t-k+1:t}), \mathbf{y}_{t+l})] \\ &= \frac{1}{N} \sum_{t=k}^{T-l} \mathbb{E}_{\mathbf{Z}, \mathbf{Z}' \sim Q} [\nabla_{\phi} g(h_{\phi}(\mathbf{Z}; \mathbf{y}_{t-k+1:t}), h_{\phi}(\mathbf{Z}'; \mathbf{y}_{t-k+1:t}), \mathbf{y}_{t+l})]. \end{aligned}$$

In the latter equality, the exchange between expectation and gradient is not a trivial step, due to the non-differentiability of functions (such as ReLU) used in h_{ϕ} . Luckily, Theorem 5 in [4] proved the

above step to be valid almost surely with respect to a measure on Φ , under mild conditions on the NN architecture.

We can now easily obtain an unbiased estimate of the above. Additionally, Stochastic Gradient Descent usually consider a small batch of training samples, obtained by considering a random subset $\mathcal{T} \subseteq \{k, k+1, \dots, n-l-1, n-l\}$. Therefore, the following unbiased estimator of $\nabla_{\phi} J(\phi)$ can be obtained, with samples $\mathbf{z}_{t,j} \sim Q, j = 1, \dots, m$:

$$\widehat{\nabla_{\phi} J(\phi)} = \frac{1}{|\mathcal{T}|} \sum_{t \in \mathcal{T}} \frac{1}{m(m-1)} \sum_{\substack{i,j=1 \\ i \neq j}}^m \nabla_{\phi} g(h_{\phi}(\mathbf{z}_{t,i}; \mathbf{y}_{t-k+1:t}), h_{\phi}(\mathbf{z}_{t,j}; \mathbf{y}_{t-k+1:t}), \mathbf{y}_{t+l}).$$

In practice, we then use autodifferentiation libraries (see for instance 42) to compute the gradients in the above quantity.

In Algorithm 2, we train a generative network for a single epoch using a scoring rule S for which unbiased estimators can be obtained by using more than one sample from P^{ϕ} . As in Algorithm 1, we use a single pair $(\boldsymbol{\theta}_i, \mathbf{y}_i)$ to estimate the gradient.

Algorithm 2 Single epoch generative-SR training.

Require: Parametric map h_{ϕ} , SR S , learning rate ϵ .

for each training pair $(\boldsymbol{\theta}_i, \mathbf{y}_i)$ **do**

 Sample **multiple** $\mathbf{z}_1, \dots, \mathbf{z}_m$

 Obtain $\hat{\mathbf{x}}_{i,j}^{\phi} = h_{\phi}(\mathbf{z}_j, \boldsymbol{\theta}_i)$

 Obtain unbiased estimate $\hat{S}(P^{\phi}(\cdot|\boldsymbol{\theta}_i), \mathbf{y}_i)$ from $\hat{\mathbf{x}}_{i,j}^{\phi}$

 Set $\phi \leftarrow \phi - \epsilon \cdot \nabla_{\phi} \hat{S}(P^{\phi}(\cdot|\boldsymbol{\theta}_i), \mathbf{y}_i)$

end for

D Performance measures for probabilistic forecast

D.1 Deterministic performance measures

We discuss two measures of performance of a deterministic forecast \hat{y}_{t+l} for a realization y_{t+l} ; across our work, we take \hat{y}_{t+l} to be the mean of the probability distribution $P^{\phi}(\cdot|\mathbf{y}_{t-k+1:t})$.

D.1.1 Normalized RMSE

We first introduce the Root Mean-Square Error (RMSE) as:

$$\text{RMSE} = \sqrt{\frac{1}{N} \sum_{t=1}^N (\hat{y}_{t+l} - y_{t+l})^2},$$

where we consider here for simplicity $t = 1, \dots, N$. From the above, we obtain the Normalized RMSE (NRMSE) as:

$$\text{NRMSE} = \frac{\text{RMSE}}{\max_t \{y_{t+l}\} - \min_t \{y_{t+l}\}}.$$

NRMSE = 0 means that $\hat{y}_{t+l} = y_{t+l}$ for all t 's.

D.1.2 Coefficient of determination

The coefficient of determination R^2 measures how much of the variance in $\{y_{t+l}\}_{t=1}^N$ is explained by $\{\hat{y}_{t+l}\}_{t=1}^N$. Specifically, it is given by:

$$R^2 = 1 - \frac{\sum_{t=1}^N (y_{t+l} - \hat{y}_{t+l})^2}{\sum_{t=1}^N (y_{t+l} - \bar{y})^2},$$

where $\bar{y} = \frac{1}{N} \sum_{t=1}^N y_{t+l}$. When $R^2 = 1$, $\hat{y}_{t+l} = y_{t+l}$ for all t 's.

D.2 Calibration error

We review here a measure of calibration of a probabilistic forecast; this measure considers the univariate marginals of the probabilistic forecast distribution $P^\phi(\cdot|\mathbf{y}_{t-k+1:t})$; for component i , let us denote that by $P_{\phi,i}(\cdot|\mathbf{y}_{t-k+1:t})$.

The calibration error [44] quantifies how well the credible intervals of the probabilistic forecast $P_{\phi,i}(\cdot|\mathbf{y}_{t-k+1:t})$ match the distribution of the verification $Y_{t+l,i}$. Specifically, let $\alpha^*(i)$ be the proportion of times the verification $y_{t+l,i}$ falls into an α -credible interval of $P_{\phi,i}(\cdot|\mathbf{y}_{t-k+1:t})$, computed over all values of t . If the marginal forecast distribution is perfectly calibrated for component i , $\alpha^*(i) = \alpha$ for all values of $\alpha \in (0, 1)$.

We define therefore the calibration error as the median of $|\alpha^*(i) - \alpha|$ over 100 equally spaced values of $\alpha \in (0, 1)$. Therefore, the calibration error is a value between 0 and 1, where 0 denotes perfect calibration.

In practice, the credible intervals of the predictive are estimated using a set of samples from $P^\phi(\cdot|\mathbf{y}_{t-k+1:t})$.

E Additional experimental details

E.1 Tuning γ in the Gaussian kernel

Similar to what was suggested for instance in 41, we set γ in the Gaussian kernel in Eq. (33) to be the median of the pairwise distances $\|\mathbf{y}_i - \mathbf{y}_j\|$ over all pairs of observations $\mathbf{y}_i, \mathbf{y}_j, i \neq j$ in the validation window.

E.2 Lorenz63 model

E.2.1 Model definition

The Lorenz63 model [34] is defined by the following differential equations:

$$\begin{aligned}\frac{dx}{dt} &= \sigma(y - x), \\ \frac{dy}{dt} &= x(\rho - z) - y, \\ \frac{dz}{dt} &= xy - \beta z.\end{aligned}$$

To generate our dataset, we consider $\sigma = 10$, $\rho = 28$, $\beta = 2.667$ and integrate the model using Euler scheme with $dt = 0.01$ starting from $x = 0$, $y = 1$, $z = 1.05$. We discard the first 10 time units and integrate the model for additional 9000 time units, during which we record the value of y every $\Delta t = 0.3$ and discard the values of x and z .

E.2.2 Neural Networks architecture

We experiment with a Fully Connected Neural Network (FCNN) and a Recurrent Neural Network (RNN). The latter performs better as it is more suitable to capture the temporal structure in the data; we therefore report results for that in the main text, while results with FCNN are reported in Appendix F.1.2.

FCNN The generative network is a Fully Connected NN with 5 hidden layers which takes as input the concatenation of the values in the observation window and a latent variable \mathbf{Z} with size 1, and outputs a forecast for the next timestep. For the deterministic setting trained with the regression loss, the architecture is analogous, the only difference being that no latent variable \mathbf{Z} is concatenated to the input.

In the adversarial settings, the critic is a fully connected NN again, which takes as input the concatenation of the values in the observation window and the observation/forecast. In the GAN case,

the critic outputs a value between 0 and 1 indicating how confident the critic believes that is a fake sample. In the WGAN-GP case, the critic output is a real number.

RNN For the generative network, the observation window is passed through a Gated Recurrent Units (GRU, [8]) layer with depth 1 and hidden size 8 or 16 (that is a tuning hyperparameter, the choice of which we discuss below). The output of the GRU layer is then concatenated to the latent variable \mathbf{Z} with size 1 and passed through 3 fully connected layers, which output a forecast for the next timestep. For the deterministic setting trained with the regression loss, the architecture is analogous, the only difference being that no latent variable \mathbf{Z} is concatenated to the output of the GRU layer.

In the adversarial settings, the critic has a GRU layer with depth 1 that, analogously to the generative net, processes the information in the past observation window. As above, we try hidden sizes 8 and 16. Then, the output of the GRU layer and the observation/forecast are concatenated and transformed by 3 fully connected layers. In the GAN case, the critic outputs a value between 0 and 1 indicating how confident the critic believes that is a fake sample. In the WGAN-GP case, the critic output is a real number.

E.2.3 Training hyperparameters

For the experiments on Lorenz63, we considered the batch size to be 1000. For the SR and deterministic approaches, we used Adam optimizer and tested the following learning rate values: 10^{-i} for $i = 1, \dots, 6$ for the SR methods and 10^{-i-1} and $3 \cdot 10^{-i-1}$ for $i = 1, \dots, 3$ for regression. For the RNN setting, we fix the GRU hidden size to 8. We report then the performance achieved with the learning rate yielding lower loss on the validation set, which is indicated in Table 3.

Table 3: Optimal learning rate values for SR and regression (deterministic) approaches for Lorenz63.

	Energy	Kernel	Energy-Kernel	Regression
FCNN	0.01	0.01	0.01	0.003
RNN	0.01	0.001	0.01	0.001

For the GAN and WGAN-GP approach, we used Adam optimizer and we tested the following learning rate values for both critic and generative network: 10^{-i} and $3 \cdot 10^{-i}$ for $i = 1, \dots, 7$. In total, those are 14 learning rate values. For the FCNN case, we fixed additionally the number of critic training steps each generator training steps to 1 for GAN and 5 for WGAN-GP. Overall, therefore, we run $14^2 = 196$ experiments for GAN and WGAN-GP respectively. For the RNN, we hidden size 8 and 16; further, we experiment with 4 number of critic training steps for WGAN-GP (1, 3, 5, 10), in order to have the best possible results to compare with our SR methods, while we left the number of critic training steps to 1 for GAN. Overall, therefore, we had $2 \cdot 14^2 = 392$ experiments for GAN and $2 \cdot 4 \cdot 14^2 = 1568$ for WGAN-GP; notice the extremely larger number number of experiments for the adversarial approaches with respect to SR ones, which highlights an advantage of our approach. We stress that such a number of trials could be possible only for the low-dimensional setting of the Lorenz63 and Lorenz96 models, in which training is cheap, but not in real-life applications.

Additionally, the adversarial approaches do not allow to select hyperparameters according to loss on a validation set, as the generator loss depends on the current state of the discriminator (i.e., there is no absolute loss scale). Therefore, we report results for 3 different configurations for GAN and WGAN-GP, maximizing either deterministic performance (1) or calibration (2), or striking the best balance between these two (3). The resulting learning rates are in Table 4 below.

E.3 Lorenz96 model

E.3.1 Model definition

The Lorenz96 model [35] is a toy representation of atmospheric behavior containing slow (\mathbf{x}) and fast (\mathbf{y}) evolving variables.

Table 4: Optimal hyperparameter values for adversarial approaches for Lorenz63 model.

		GAN (1)	GAN (2)	GAN (3)	WGAN-GP (1)	WGAN-GP (2)	WGAN-GP (3)
FCNN	Generator l.r.	0.03	0.00003	0.0001	0.0003	0.0003	0.003
	Critic l.r.	0.01	0.03	0.0003	0.01	0.003	0.01
RNN	Generator l.r.	0.0003	0.001	0.0001	0.003	0.0003	0.0003
	Critic l.r.	0.03	0.01	0.001	0.001	0.1	0.03
	GRU hidden size	16	8	8	8	8	8
	Critic training steps	1	1	1	5	5	5

Specifically, the evolution of the variables is determined by the following differential equations:

$$\frac{dx_k}{dt} = -x_{k-1}(x_{k-2} - x_{k+1}) - x_k + F - \frac{hc}{b} \sum_{j=J(k-1)+1}^{kJ} y_j;$$

$$\frac{dy_j}{dt} = -cby_{j+1}(y_{j+2} - y_{j-1}) - cy_j + \frac{hc}{b} X_{\text{int}[(j-1)/J]+1}.$$

where $k = 1, \dots, K$, and $j = 1, \dots, JK$, and cyclic boundary conditions are assumed, so that index $k = K + 1$ corresponds to $k = 1$ and similarly for j . The above equations connect the fast and slow variables in a cyclic way. Additionally, x_k reciprocally depends on J fast variables.

Following 18, we take $K = 8$, $J = 32$, $h = 1$, $b = 10$, $c = 10$ and $F = 20$. We then integrate the above equations with RK4 scheme with $dt = 0.001$, starting from $x_k = y_j = 0$ for $k = 2, \dots, K$ and $j = 2, \dots, JK$ and $x_1 = y_1 = 1$. We discard the first 2 time units and record the values of \mathbf{x} every $\Delta t = 0.2$ (which corresponding to roughly one atmospheric day with respect to predictability, 18). We do this for additional 4000 time units, and split the resulting dataset in training, validation and test according to the proportions 60%, 20% and 20%.

E.3.2 Neural Networks architecture

We experiment with a Fully Connected Neural Network (FCNN) and a Recurrent Neural Network (RNN). The latter performs better as it is more suitable to capture the temporal structure in the data; we therefore report results for that in the main text, while results with FCNN are reported in Appendix F.2.2.

FCNN The generative network is a Fully Connected NN with 5 hidden layers which takes as input the concatenation of the values in the observation window (flattened to an $8 \cdot 10 = 80$ dimensional vector) and a latent variable \mathbf{Z} with size 8, and outputs a forecast for the next timestep. For the deterministic setting trained with the regression loss, the architecture is analogous, the only difference being that no latent variable \mathbf{Z} is concatenated to the input.

In the adversarial settings, the critic is a fully connected NN again, which takes as input the concatenation of the flattened values in the observation window and the observation/forecast. In the GAN case, the critic outputs a value between 0 and 1 indicating how confident the critic believes that is a fake sample. In the WGAN-GP case, the critic output is a real number.

RNN For the generative network, the observation window is passed through a Gated Recurrent Units (GRU, [8]) layer with depth 1 and hidden size 32 or 64 (that is a tuning hyperparameter, the choice of which we discuss below). The output of the GRU layer is then concatenated to the latent variable \mathbf{Z} with size 1 and passed through 3 fully connected layers, which output a forecast for the next timestep. For the deterministic setting trained with the regression loss, the architecture is analogous, the only difference being that no latent variable \mathbf{Z} is concatenated to the output of the GRU layer.

In the adversarial settings, the critic has a GRU layer with depth 1 that, analogously to the generative net, processes the information in the past observation window. As above, we try hidden sizes 8 and 16. Then, the output of the GRU layer and the observation/forecast are concatenated and transformed by 3 fully connected layers. In the GAN case, the critic outputs a value between 0 and 1 indicating how confident the critic believes that is a fake sample. In the WGAN-GP case, the critic output is a real number.

E.3.3 Training hyperparameters

For the experiments on Lorenz96, we considered the batch size to be 1000. For the SR and deterministic approaches, we used Adam optimizer and tested the following learning rate values: 10^{-i} for $i = 1, \dots, 6$ for the SR methods and 10^{-i-1} and $3 \cdot 10^{-i-1}$ for $i = 1, \dots, 3$ for regression. For the RNN setting, we fix the GRU hidden size to 32. We report then the performance achieved with the learning rate yielding lower loss on the validation set, which is indicated in Table 5.

Table 5: Optimal learning rate values for SR and regression (deterministic) approaches for Lorenz96.

	Energy	Kernel	Energy-Kernel	Regression
FCNN	0.001	0.001	0.001	0.0003
RNN	0.01	0.001	0.001	0.003

For the GAN and WGAN-GP approach, we used Adam optimizer and we tested the following learning rate values for both critic and generative network: 10^{-i} and $3 \cdot 10^{-i}$ for $i = 1, \dots, 7$. In total, those are 14 learning rate values. For the FCNN case, we fixed additionally the number of critic training steps each generator training steps to 1 for GAN and 5 for WGAN-GP. Overall, therefore, we run $14^2 = 196$ experiments for GAN and WGAN-GP respectively. For the RNN, we hidden size 8 and 16; further, we experiment with 4 number of critic training steps for WGAN-GP (1, 3, 5, 10), in order to have the best possible results to compare with our SR methods, while we left the number of critic training steps to 1 for GAN. Overall, therefore, we had $2 \cdot 14^2 = 392$ experiments for GAN and $2 \cdot 4 \cdot 14^2 = 1568$ for WGAN-GP; notice the extremely larger number number of experiments for the adversarial approaches with respect to SR ones, which highlights an advantage of our approach. We stress that such a number of trials could be possible only for the low-dimensional setting of the Lorenz63 and Lorenz96 models, in which training is cheap, but not in real-life applications.

Additionally, the adversarial approaches do not allow to select hyperparameters according to loss on a validation set, as the generator loss depends on the current state of the discriminator (i.e., there is no absolute loss scale). Therefore, we report results for 3 different configurations for GAN and WGAN-GP, maximizing either deterministic performance (1) or calibration (2), or striking the best balance between these two (3). The resulting learning rates are in Table 6 below. Notice that, for GAN, there was no configuration leading to intermediate performance between (1) and (2), so that the column for (3) is left empty.

Table 6: Optimal hyperparameter values for adversarial approaches for Lorenz96 model.

		GAN (1)	GAN (2)	GAN (3)	WGAN-GP (1)	WGAN-GP (2)	WGAN-GP (3)
FCNN	Generator l.r.	0.01	0.0001	-	0.0001	0.0001	0.0001
	Critic l.r.	0.001	0.001	-	0.003	0.03	0.01
RNN	Generator l.r.	0.01	0.0001	0.0001	0.001	0.00003	0.0001
	Critic l.r.	0.001	0.003	0.001	0.001	0.1	0.01
	GRU hidden size	64	32	64	64	64	64
	Critic training steps	1	1	1	10	1	5

E.4 WeatherBench dataset

E.4.1 Variogram Score

For the Variogram Score, we use a weight matrix which is inversely proportional to the Haversine distance, which measures the angular distance between two points on the surface of a sphere. Specifically, by denoting the longitude and latitude (in radians) of component i of \mathbf{y} as $\text{lon}_i, \text{lat}_i$, the Haversine distance is defined as:

$$d_{ij} = 2 \arcsin \left[\sqrt{\sin^2((\text{lat}_i - \text{lat}_j)/2) + \cos(\text{lat}_i) \cos(\text{lat}_j) \sin^2((\text{lon}_i - \text{lon}_j)/2)} \right]$$

The physical distance along the sphere can be computed by multiplying the above by Earth’s radius (approximately 6371 km). However, that is just a scaling constant, therefore we ignore it in defining the variogram, which we take to be $w_{ij} = 1/d_{ij}$.

E.4.2 Choice of weights for summed scores

In the summed Scores (Energy-Variogram, Kernel-Variogram, Energy-Kernel and Patched Energy Score), we need to select the weights for the two addends. Notice that, in the Patched Energy Score, we consider the Energy Score computed on the full data to be the first addend, and the sum of the Energy Scores computed on each patch to be the second addend.

We fix the weights such that the two addends have roughly the same magnitude. This results, for the Energy-Variogram, Kernel-Variogram, Energy-Kernel, in the choices reported in the following Table:

Table 7: Weights for summed Scores.

	Energy-Kernel	Energy-Variogram	Kernel-Variogram
α_1	1/70	1	1
α_2	1	$6.94 \cdot 10^{-7}$	$1.3 \cdot 10^{-8}$

For the Patched Energy Score, we use the following two setups in our experiments:

- Patches of size 16 separated by 8 grid points: this leads to 32 patches. As the Energy Score scales as the data dimensionality, each of the $16 \times 16 = 256$ patches has relative magnitude with respect to Energy Score computed on the full WeatherBench grid $256/2048 = 0.125$, where $32 \times 64 = 2048$ is the size of the WeatherBench grid. However, we sum the Score for each of the 32 patches, which leads to a quantity with magnitude 4 times the one of the overall Energy Score.
- Patches of size 8 separated by 4 grid points: this leads to 128 patches. Following the argument above, each $8 \times 8 = 64$ patch gives a Score with relative magnitude $64/2048 = 0.03125$. As there are 128 patches, again the cumulative patched score has magnitude 4 times the overall one.

In both cases, we leave therefore $\alpha_1 = \alpha_2 = 1$, as the patched and overall components are already of similar magnitude (they just differ by a factor 4).

E.4.3 Neural Networks architecture

For the generative network, we use a U-NET architecture [39], which is an encoder-decoder structure, where each subsequent layer of the encoder outputs a downscaled latent representation of the input variables. The final output of the encoder is passed to a bottleneck layer, which performs no up/down scaling. The output of this bottleneck layer is then passed to the decoder. Conversely to the encoder, each subsequent layer of the decoder outputs an upscaled latent representation of the bottleneck layer output. Additionally, skip connections allow information to pass directly between layers of the encoder and decoder at the same scale; in this way, both large scale structures and high-frequency information contributes to the output. The latent variable \mathbf{Z} is summed to the latent representation in the bottleneck layer. Figure 5 gives a graphical representation of the UNet. For the deterministic setting trained with the regression loss, the architecture is analogous, the only difference being that no latent variable \mathbf{Z} is summed to the latent representation.

In the adversarial setups, we use the PatchGAN critic suggested in [27]. Specifically, this is a convolutional network which considers separate patches of the input image and outputs a numerical value for each patch, corresponding, in the original GAN setting of 21, to the confidence with which the critic believes that patch is real, in contrast to generated from the generative network. The GAN or WGAN loss is then computed for each of the output values and averaged.

The PatchGAN critic employs some Batch Normalization layers; however, these cannot be used when the gradient penalization strategy of WGAN-GP is used [24]. Therefore, as suggested in 24, we replace the Batch Normalization layers with Layer Normalization.

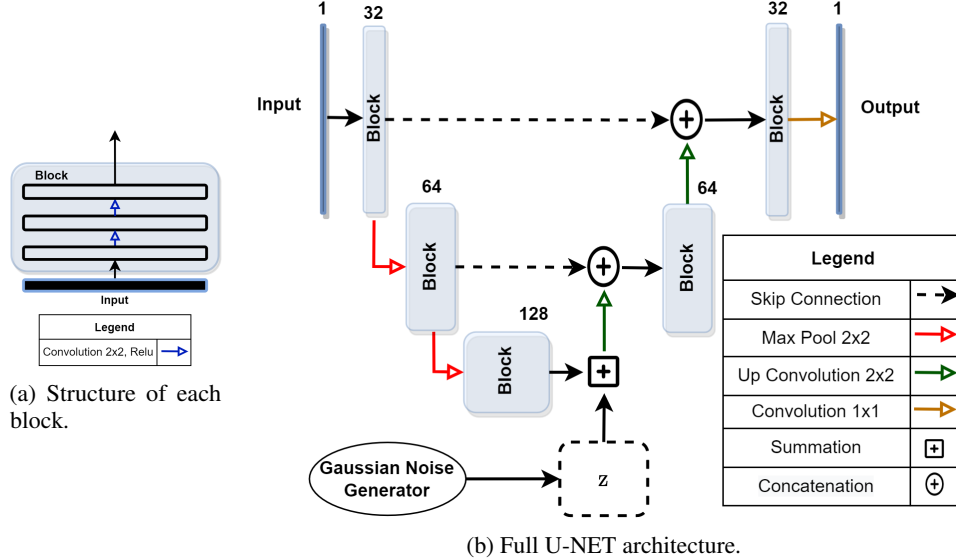


Figure 5: U-NET architecture.

As before, in the GAN case, the critic outputs a value between 0 and 1 indicating how confident the critic believes that is a fake sample. In the WGAN-GP case, the critic output is a real number.

E.4.4 Training hyperparameters

For the SR approaches for the WeatherBench dataset, we considered the batch size to be 128 for all experiments, except for those on the Energy-Variogram and Kernel-Variogram score, which resulted in GPU memory overflow with that batch size (in fact, computing the Variogram Score is an operation requiring quadratic memory with respect to data size); for these two, we fixed therefore the batch size to be 48. We used Adam optimizer and tested the following learning rate values 10^{-i} for $i = 1, \dots, 6$. We report then the performance achieved with the learning rate yielding lower loss on the validation set in Table 8.

For the deterministic network trained via regression, we test learning rule values 10^{-i-1} for $i = 1, \dots, 4$; additionally, we use an exponential learning rate scheduler which reduces the learning rate by multiplying it by a factor γ every 10 training epochs. We also use a ℓ_2 weight regularization with weight λ . We try different values of these parameters in conjunction with the learning rate values; the ones with which best validation loss is obtained are $\gamma = 0.8$ and $\lambda = 0.001$. The best learning rate value is reported in Table 8. Notice that the same learning rate value was optimal for the full (non-patched) regression loss and for the patched loss in both configurations.

Table 8: Optimal learning rate values for the SR and regression (deterministic) approaches for WeatherBench.

	Regression	Energy	kernel	Energy-Kernel	Energy-Variogram
Learning rate	0.01	0.0001	0.0001	0.0001	10^{-5}
	Kernel-Variogram	Patched Energy (8)	Patched Energy (16)		
Learning rate	10^{-5}	10^{-5}	10^{-5}		

For the GAN and WGAN-GP approach, we used Adam optimizer and we tested the following learning rate values for both critic and generative network: 10^{-i} , $i = 1, \dots, 7$. In total, those are 7 learning rate values, which result in $7^2 = 49$ experiments. Notice additionally that the adversarial approaches does not allow to select hyperparameters according to loss on a validation set, as the generator loss depends on the current state of the discriminator (i.e., there is no absolute loss scale). Additionally,

the adversarial approaches do not allow to select hyperparameters according to loss on a validation set, as the generator loss depends on the current state of the discriminator (i.e., there is no absolute loss scale). Therefore, we report results for 3 different configurations for GAN, maximizing either deterministic performance (1) or calibration (2), or striking the best balance between these two (3). For WGAN-GP, a single configuration maximized both calibration and deterministic performance, so that we report that one. The resulting learning rates are in Table 9 below.

Table 9: Optimal hyperparameter values for adversarial approaches for WeatherBench.

	GAN (1)	GAN (2)	GAN (3)	WGAN-GP
Generator learning rate	0.001	10^{-6}	10^{-5}	10^{-5}
Critic learning rate	0.0001	0.0001	10^{-5}	0.01

F Additional experimental results

F.1 Lorenz63 model

F.1.1 Additional results with RNN

We report here additional results with the RNN used in the main text of the paper. Figure 6 contains separate plots for all methods showing forecasts and realization for a portion of the test set (the same used in Section 5.1 in the main text).

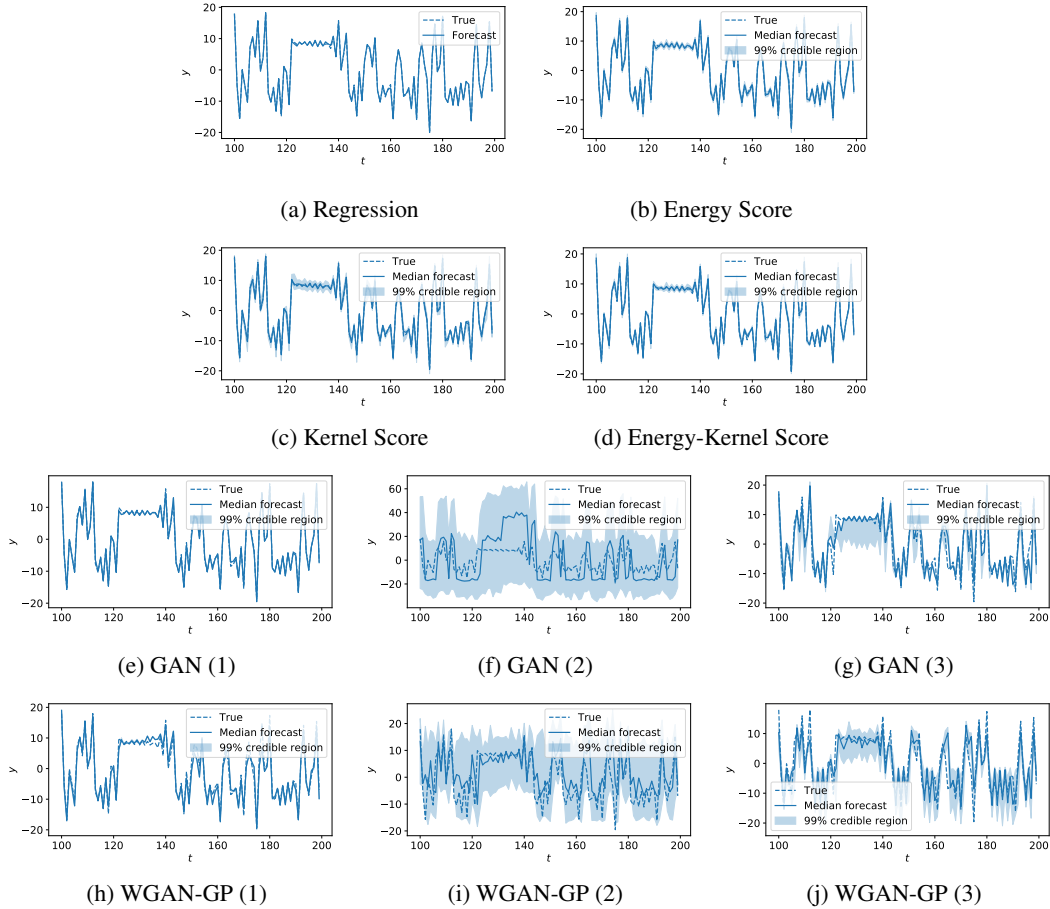


Figure 6: Results for the Lorenz63 model with all considered methods, for RNN. The figures show observations, median forecast and 99% credible interval for a portion of the test set. For each time-step, forecasts are obtained using the previous observation window.

F.1.2 Results with FCNN

We report here results with the Fully Connected NN (FCNN). Table 10 contains performance metrics for the different methods. Figure 7 contains separate plots for all methods showing forecasts and realization for a portion of the test set. Overall, performances are worse than with RNN.

Table 10: Performance measures for forecasts obtained with the different methods, on the test set for the Lorenz63 dataset, with FCNN.

	Cal. error ↓	NRMSE ↓	R ² ↑
Regression	-	0.0297	0.9682
Energy	0.0510	0.0293	0.9692
Kernel	0.1220	0.0155	0.9913
Energy-Kernel	0.0800	0.0188	0.9873
GAN (1)	0.4930	0.0651	0.8475
GAN (2)	0.3710	0.1890	-0.2857
GAN (3)	0.4580	0.1201	0.4805
WGAN-GP (1)	0.4410	0.1018	0.6269
WGAN-GP (2)	0.3260	0.1164	0.5120
WGAN-GP (3)	0.4330	0.1083	0.5776

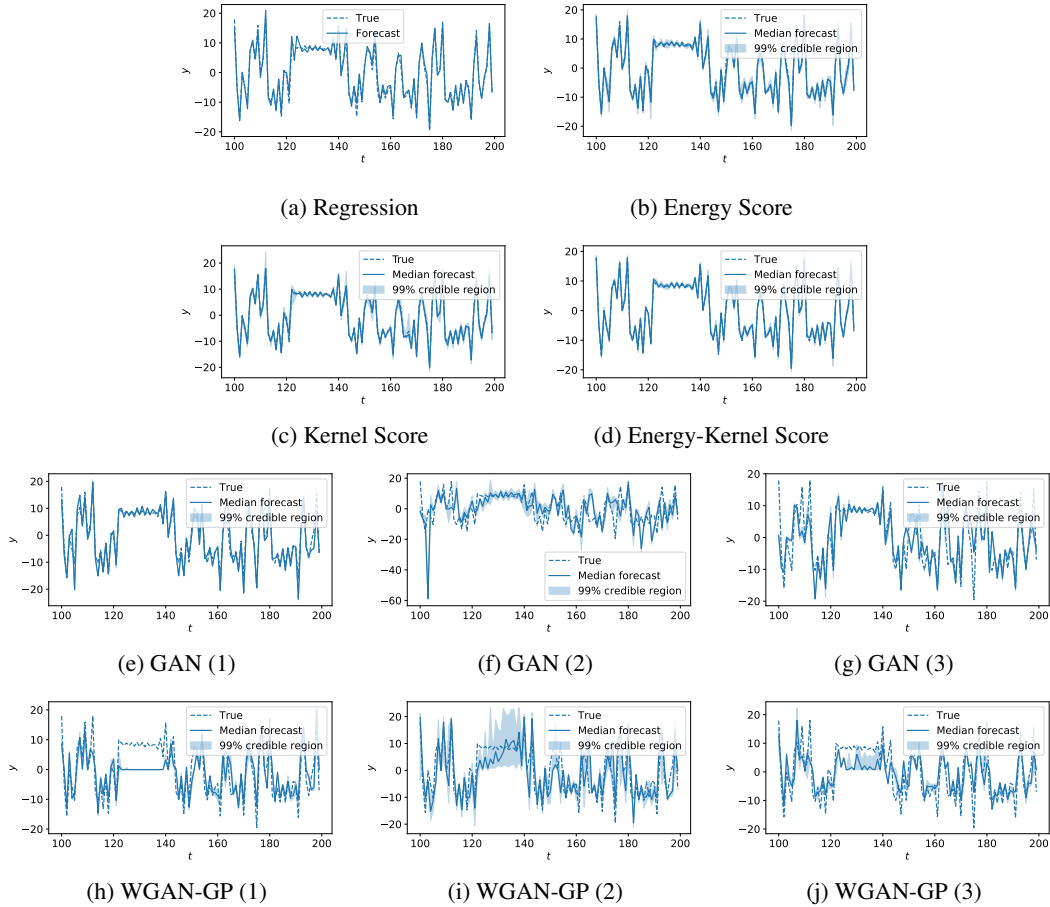


Figure 7: Results for the Lorenz63 model with all considered methods, for FCNN. The figures show observations, median forecast and 99% credible interval for a portion of the test set. For each time-step, forecasts are obtained using the previous observation window.

F.2 Lorenz96 model

F.2.1 Additional results with RNN

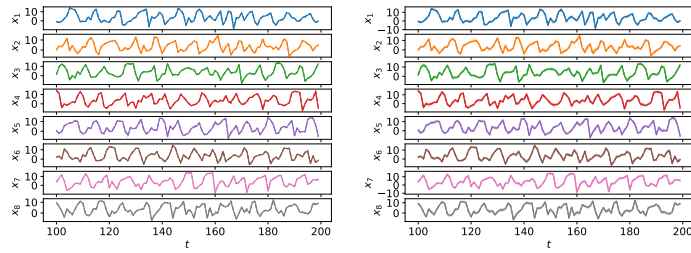
We report here additional results with the RNN used in the main text of the paper.

Table 11 reports the average and standard deviation of the different performance measures computed across the different data components. It contains the same results as Table 1 in the main text, where however the standard deviation was not reported.

Figure 8 contains separate plots for all methods showing forecasts and realization for a portion of the test set (the same used in Section 5.1 in the main text).

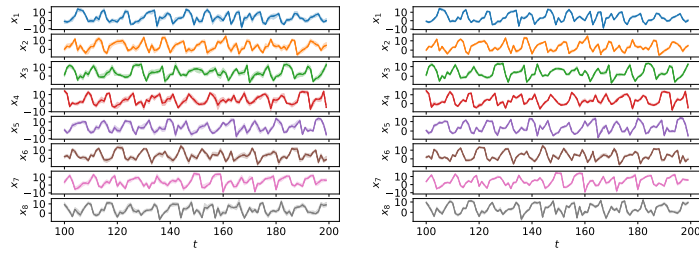
Table 11: Average and standard deviation of performance measures for forecasts obtained with the different methods, on the test set for the Lorenz96 dataset, with the RNN. Metrics are computed on each data component individually; then, the average and standard deviation is computed.

	Cal. error ↓	NRMSE ↓	R ² ↑
Regression	-	0.0198 ± 0.0006	0.9905 ± 0.0006
Energy	0.0205 ± 0.0176	0.0166 ± 0.0014	0.9933 ± 0.0012
Kernel	0.2196 ± 0.0123	0.0164 ± 0.0003	0.9935 ± 0.0003
Energy-Kernel	0.0104 ± 0.0060	0.0173 ± 0.0004	0.9928 ± 0.0004
GAN (1)	0.4644 ± 0.0062	0.0354 ± 0.0026	0.9696 ± 0.0044
GAN (2)	0.2671 ± 0.0559	0.1500 ± 0.0090	0.4537 ± 0.0619
GAN (3)	0.3700 ± 0.0369	0.0763 ± 0.0030	0.8590 ± 0.0099
WGAN-GP (1)	0.4134 ± 0.0051	0.0330 ± 0.0007	0.9736 ± 0.0009
WGAN-GP (2)	0.0565 ± 0.0339	0.1081 ± 0.0037	0.7165 ± 0.0200
WGAN-GP (3)	0.1648 ± 0.0444	0.0786 ± 0.0041	0.8502 ± 0.0149



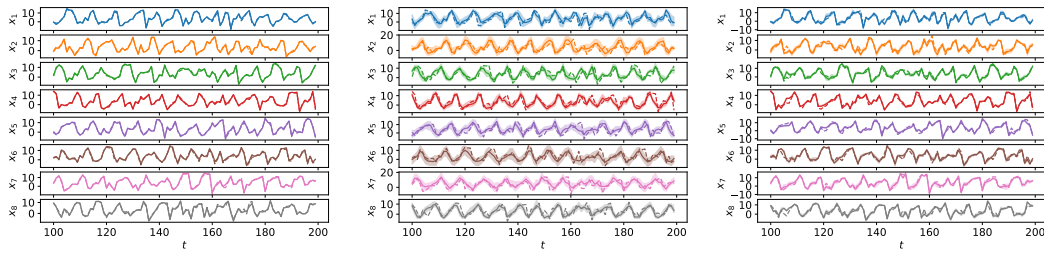
(a) Regression

(b) Energy Score.



(c) Kernel Score.

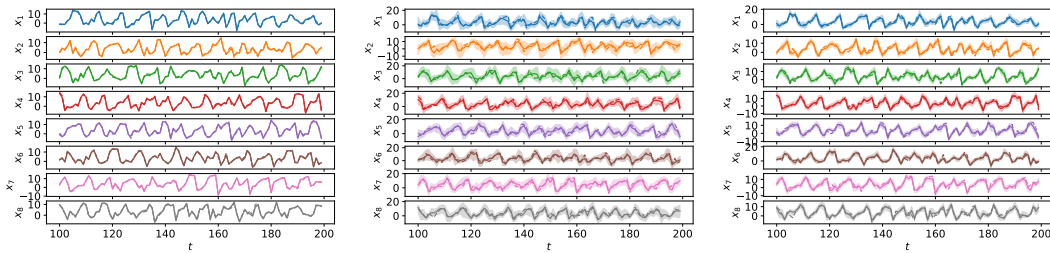
(d) Energy-Kernel Score



(e) GAN (1)

(f) GAN (2)

(g) GAN (3)



(h) WGAN-GP (1)

(i) WGAN-GP (2)

(j) WGAN-GP (3)

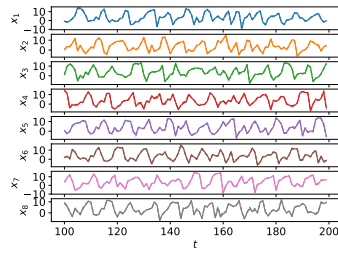
Figure 8: Results for the Lorenz96 model with all considered methods for RNN. Panels show observations (dashed line), median forecast (solid line) and 99% credible interval (shaded region) for a portion of the test set. That is done for all 8 components of x . For each time-step, forecasts are obtained using the previous observation window.

F.2.2 Results with FCNN

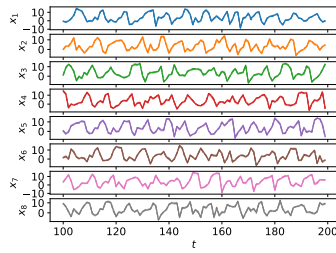
We report here results with the Fully Connected NN (FCNN). In Table 12 below, the average and standard deviation of the different performance measures are computed across the different data components, for the various methods. Figure 7 contains separate plots for all methods showing forecasts and realization for a portion of the test set, as done before for FCNN. Overall, performances are worse than with RNN.

Table 12: Average and standard deviation of performance measures for forecasts obtained with the different methods, on the test set for the Lorenz96 dataset, with FCNN. Metrics are computed on each data component individually; then, the average and standard deviation is computed.

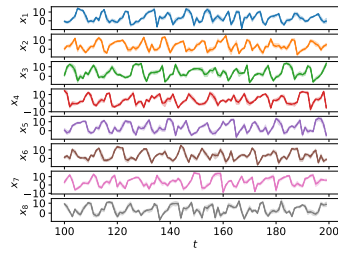
	Cal. error ↓	NRMSE ↓	R ² ↑
Regression	-	0.0243 ± 0.0007	0.9857 ± 0.0008
Energy	0.1230 ± 0.0366	0.0176 ± 0.0015	0.9925 ± 0.0012
Kernel	0.1179 ± 0.0244	0.0175 ± 0.0009	0.9926 ± 0.0008
Energy-Kernel	0.1560 ± 0.0172	0.0145 ± 0.0005	0.9949 ± 0.0003
GAN (1)	0.4875 ± 0.0025	0.0873 ± 0.0039	0.8151 ± 0.0167
GAN (2)	0.3775 ± 0.0125	0.1113 ± 0.0079	0.6994 ± 0.0372
WGAN-GP (1)	0.2054 ± 0.0218	0.0762 ± 0.0017	0.8593 ± 0.0040
WGAN-GP (2)	0.1678 ± 0.0181	0.0928 ± 0.0025	0.7913 ± 0.0091
WGAN-GP (3)	0.2016 ± 0.0208	0.0823 ± 0.0022	0.8361 ± 0.0075



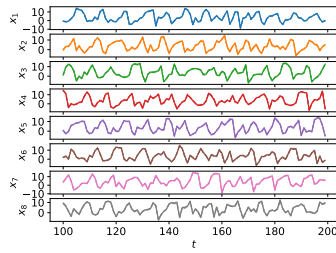
(a) Regression



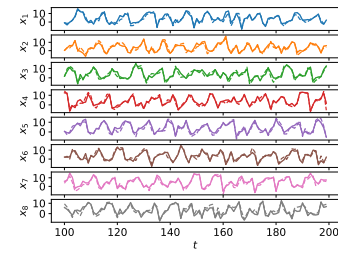
(b) Energy Score.



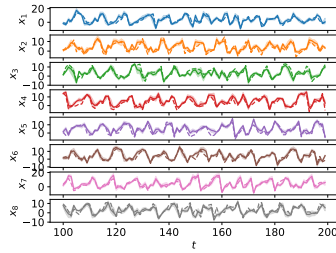
(c) Kernel Score.



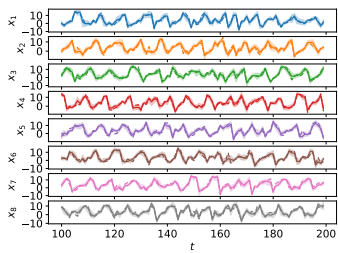
(d) Energy-Kernel Score



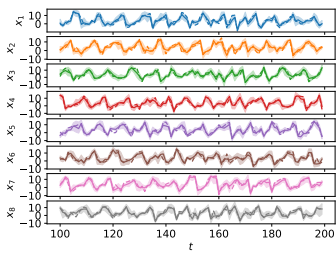
(e) GAN (1)



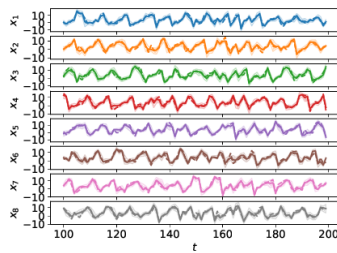
(f) GAN (2)



(g) WGAN-GP (1)



(h) WGAN-GP (2)



(i) WGAN-GP (3)

Figure 9: Results for the Lorenz96 model with all considered methods for FCNN. Panels show observations (dashed line), median forecast (solid line) and 99% credible interval (shaded region) for a portion of the test set. That is done for all 8 components of x . For each time-step, forecasts are obtained using the previous observation window.

F.3 WeatherBench dataset

F.3.1 Standard deviation of performance measures

In Table 13 below, the average and standard deviation of the different performance measures are computed across the different data components.

Table 13: Average and standard deviation of performance measures for forecasts obtained with the different methods, on the test section of the WeatherBench dataset. Metrics are computed on each data component individually; then, the average and standard deviation is computed.

	Cal. error ↓	NRMSE ↓	R ² ↑
Regression	-	0.1162 ± 0.0256	0.5300 ± 0.2559
Patched Regression, 8	-	0.1147 ± 0.0238	0.5459 ± 0.2297
Patched Regression, 16	-	0.1144 ± 0.0227	0.5509 ± 0.2188
Energy	0.0863 ± 0.0407	0.1208 ± 0.0256	0.4968 ± 0.2596
Kernel	0.0797 ± 0.0455	0.1200 ± 0.0226	0.5097 ± 0.2226
Energy-Kernel	0.0794 ± 0.0433	0.1194 ± 0.0226	0.5150 ± 0.2225
Energy-Variogram	0.0899 ± 0.0541	0.1192 ± 0.0220	0.5177 ± 0.2180
Kernel-Variogram	0.1704 ± 0.0607	0.1203 ± 0.0238	0.5050 ± 0.2399
Patched Energy, 8	0.0550 ± 0.0348	0.1189 ± 0.0209	0.5217 ± 0.2064
Patched Energy, 16	0.0690 ± 0.0478	0.1186 ± 0.0208	0.5248 ± 0.2034
GAN (1)	0.4845 ± 0.0089	0.1573 ± 0.0391	0.1418 ± 0.5267
GAN (2)	0.3130 ± 0.1143	0.2487 ± 0.2248	-2.7970 ± 17.1346
GAN (3)	0.3625 ± 0.0545	0.1693 ± 0.0494	-0.0117 ± 0.8348
WGAN-GP	0.1009 ± 0.0679	0.1302 ± 0.0214	0.4340 ± 0.2271

F.3.2 Number of generator simulations for the SR methods

We study here the effect of using different numbers of simulations from the generative network for each input (i.e., how many forecasts the generative network provides) during training. Recall in fact how the Energy and Kernel Score need multiple samples to be estimated (Appendix B.2).

Specifically, we consider the WeatherBench dataset and the Energy Score, with learning rate 0.0001, which was found to be the optimal value when using 10 generator simulations (Appendix E.4.4). We report the measures used in the main text in Table 14. Notice how good performance is achieved when using as little as 2 or 3 simulations.

Table 14: Performance on test set of probabilistic forecasts obtained by training with the Energy Score, with different numbers of generator simulations, for the WeatherBench dataset.

	Cal. error ↓	NRMSE ↓	R ² ↑
2	0.0625 ± 0.0340	0.1211 ± 0.0258	0.4935 ± 0.2656
3	0.0701 ± 0.0342	0.1176 ± 0.0208	0.5338 ± 0.1961
5	0.0727 ± 0.0348	0.1164 ± 0.0198	0.5446 ± 0.1842
10	0.0863 ± 0.0407	0.1208 ± 0.0256	0.4968 ± 0.2596
20	0.0738 ± 0.0336	0.1179 ± 0.0206	0.5329 ± 0.1925
30	0.0738 ± 0.0350	0.1169 ± 0.0202	0.5407 ± 0.1864
50	0.0749 ± 0.0356	0.1172 ± 0.0203	0.5379 ± 0.1889

F.3.3 Computational cost and early stopping

In Table 15, we report the computational cost and the early stopping achieved by the methods presented in the main text. All experiments are run on a Tesla v100 GPU, and methods are run for a maximum of 1000 epochs. We use early stopping for the SR methods, but not for GAN and WGAN-GP, for which early stopping is not possible. Recall that the methods with the Variogram Score used

training batch size 48, while all others used 128; this fact contributes to the larger computational time for both the Energy-Variogram and Kernel-Variogram Scores.

Table 15: Per-epoch and total computational cost, in seconds, for the different methods reported in the main text. We also report epoch at which early stopping occurred.

	Per-epoch Computational cost	Early stopping at epoch	Total computational cost
Regression	8.45	250	2112
Patched Regression, 8	8.65	200	1729
Patched Regression, 16	8.5	250	2122
Energy	54.2	100	5417
Kernel	53.3	100	5329
Energy-Kernel	55.4	100	5542
Energy-Variogram	97.38	250	24346
Kernel-Variogram	95.52	250	24393
Patched Energy, 8	56.71	400	22682
Patched Energy, 16	54.93	450	24717
GAN (1)	8.36	-	8357
GAN (2)	8.37	-	8373
GAN (3)	8.33	-	8326
WGAN-GP	7.00	-	7000

Additionally, recall that, in order to achieve the performance reported in the main text, we tried 49 learning rate values for GAN and WGAN-GP, but only 6 for the SR methods. Therefore, the total computing time for GAN and WGAN-GP is the one below multiplied by 49, with respect to 6 for the SR methods. Under that perspective, even the total computing time for Energy-Variogram and Kernel-Variogram Scores is smaller than the one for the adversarial methods. For instance, if we consider Energy-Variogram, do not use early stopping and run for 1000 epochs 6 times, we get a total of $97.38 \times 6000 = 584280$ seconds. For WGAN-GP, we obtain instead $7.00 \times 49 \times 1000 = 343000$ seconds, which is only slightly smaller than the grand total for Energy-Variogram. For the latter, this number does not take into account early stopping which, as can be seen from Table 15, reduces largely the total number of epochs required for training.

Additionally, we highlight how, in the results used for Table 15, the SR methods were trained using 10 simulations from the generator for each observation window (i.e., 10 forecasts). In Appendix F.3.2, we studied the effect of the number of simulations used on training, highlighted how the performance is good with as little as 2 or 3 simulations. This greatly reduces the computational cost; we report that in Table 16; for this study, the Energy Score was used.

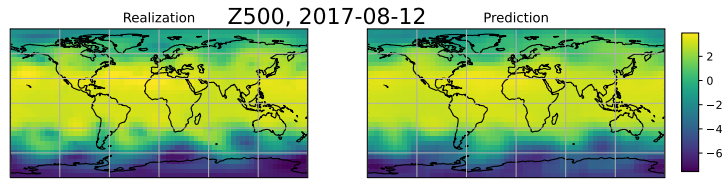
Table 16: Per-epoch and total computational cost, in seconds, for the Energy Score for different numbers of generator simulations. We also report epoch at which early stopping occurred.

	Per-epoch Computational cost	Early stopping at epoch	Total computational cost
2	13.7	100	1371
3	19.1	100	1913
5	29.6	100	2967
10	54.2	100	5417
20	107.0	100	10700
30	159.2	100	15916
50	258.7	100	25865

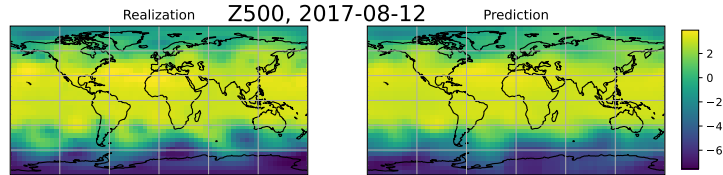
F.3.4 Maps for a chosen date

Figure 10 reports realization and prediction with the deterministic regression methods; instead, in Figures 11, 12, and 13 we report realization and 5 different forecasts obtained with all probabilistic methods discussed in the main text (Section 5.2). In Figures 14, 15, and 16, we show the deviation of the same realizations and forecasts from the forecast mean (obtained empirically from 100 forecasts). If the forecast distribution is calibrated, the realization should look similar to the forecasts themselves.

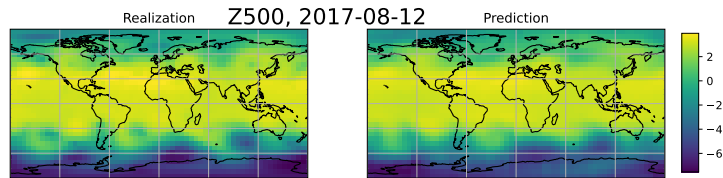
You can see how this is roughly the case for the best performing SRs (as for instance the Patched Energy Score in Figure 15) as well as for WGAN-GP, but it clearly not the case for GAN (Figure 16).



(a) Regression

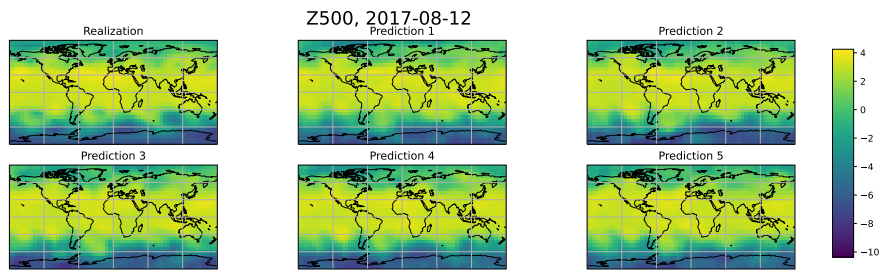


(b) Patched Regression, 8

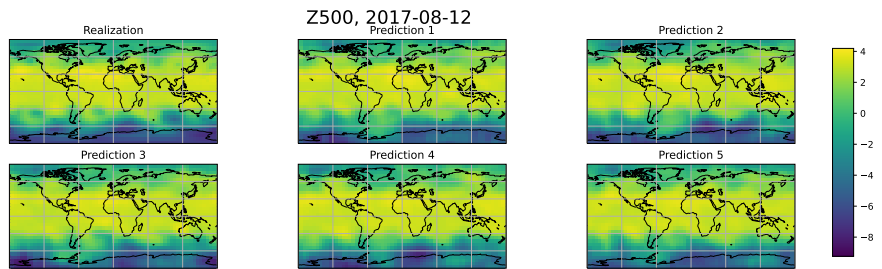


(c) Patched Regression, 16

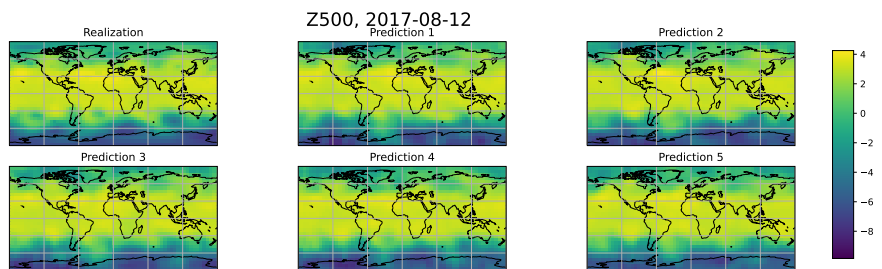
Figure 10: Realization and prediction obtained with the Regression and Patched Regressions for a specific date in the test set for the WeatherBench dataset.



(a) Energy Score

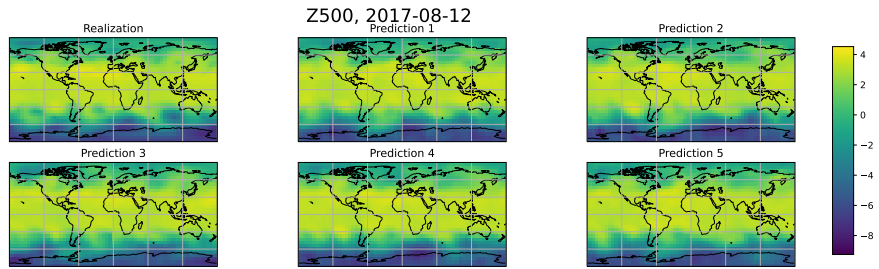


(b) Kernel Score

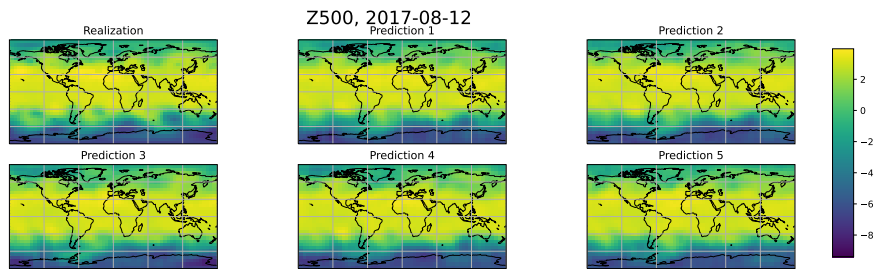


(c) Energy-Kernel Score

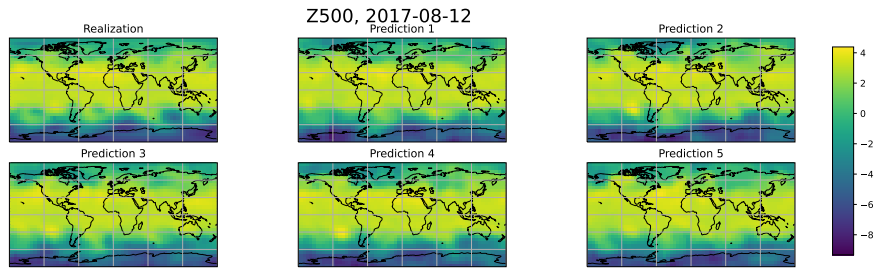
Figure 11: Realization and example of predictions obtained with the Energy, Kernel and Energy-Kernel Scores for a specific date in the test set for the WeatherBench dataset.



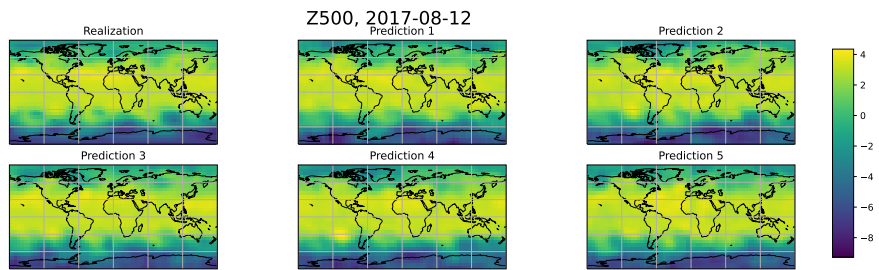
(a) Energy-Variogram Score



(b) Kernel-Variogram Score

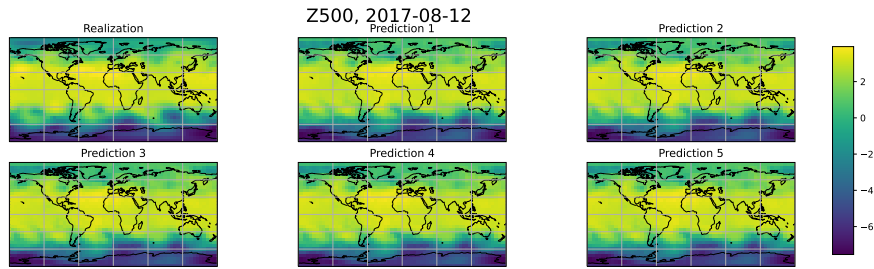


(c) Patched Energy Score (8)

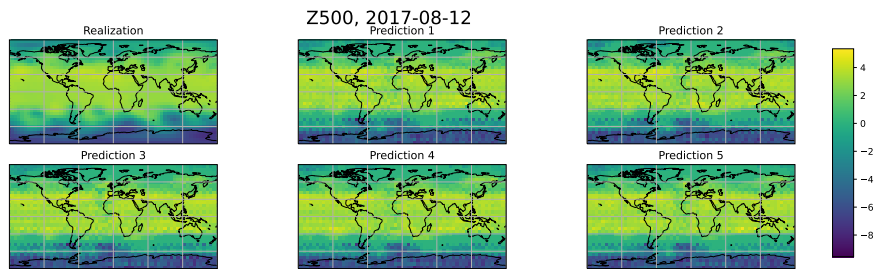


(d) Patched Energy Score (16)

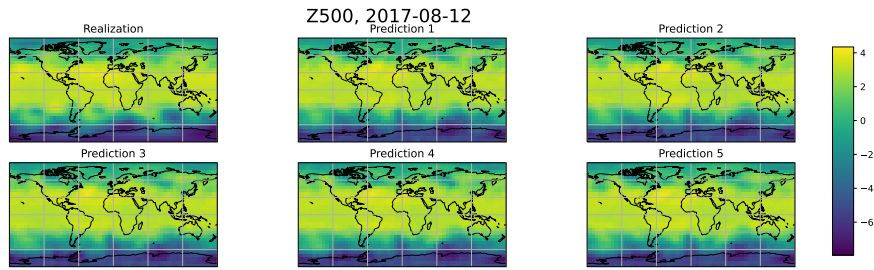
Figure 12: Realization and example of predictions obtained with the Energy-Variogram, Kernel-Variogram and Patched Energy Score (with patch size 8 and 16) for a specific date in the test set for the WeatherBench dataset.



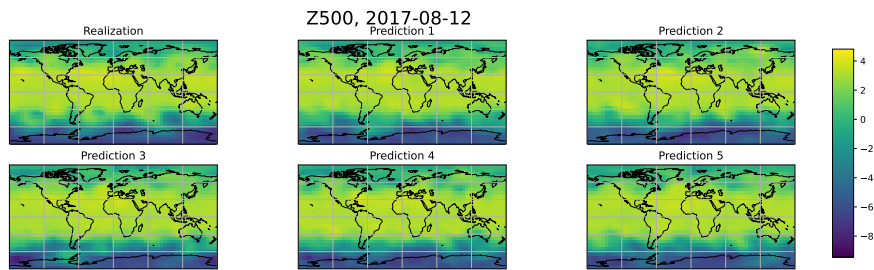
(a) GAN (1)



(b) GAN (2)



(c) GAN (3)



(d) WGAN-GP

Figure 13: Realization and example of predictions obtained with the three considered GAN setups and WGAN-GP for a specific date in the test set for the WeatherBench dataset. Notice how the second GAN setup leads to unphysical features.

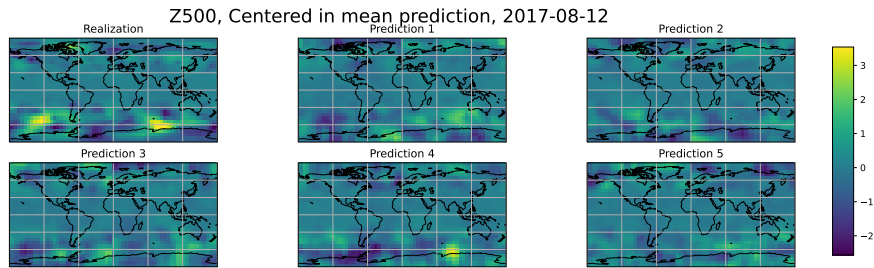
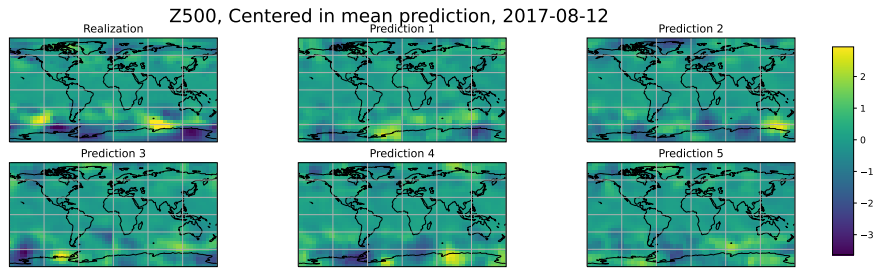
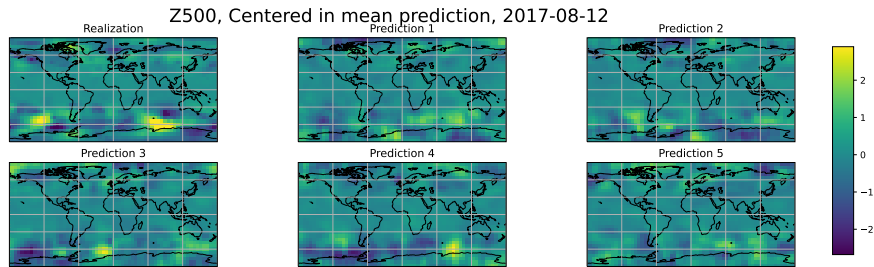
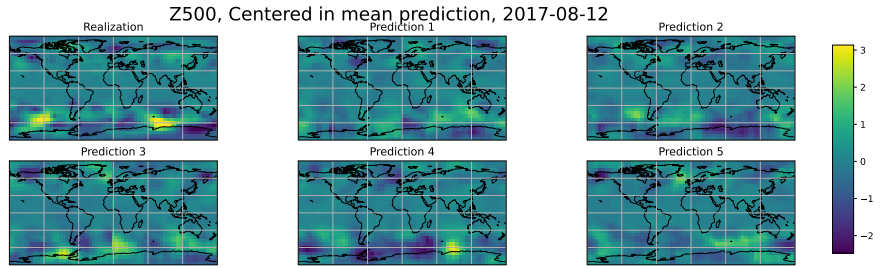
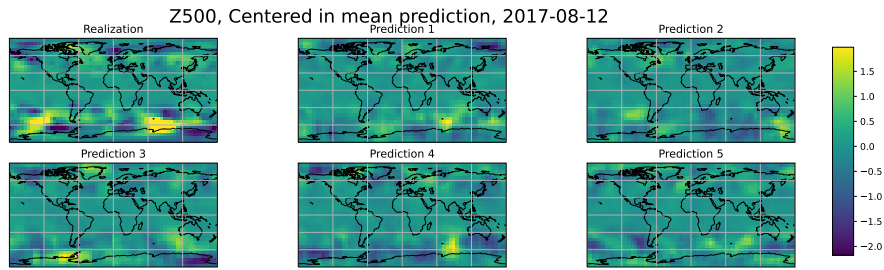


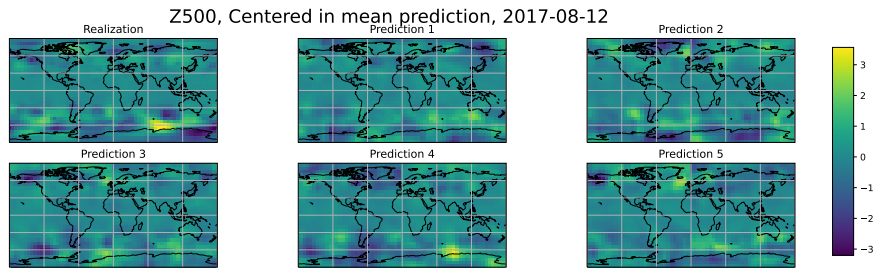
Figure 14: Deviations of the realization and forecasts from the forecast mean (obtained empirically from 100 forecasts) for the Energy, Kernel and Energy-Kernel Scores for a specific date in the test set for the WeatherBench dataset. The absolute values of the forecasts used here are shown in Figure 11.



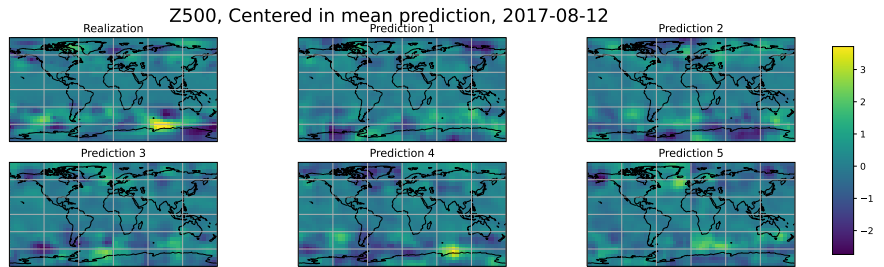
(a) Energy-Variogram Score



(b) Kernel-Variogram Score

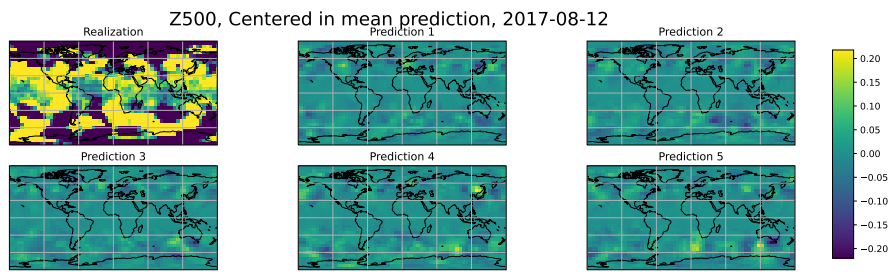


(c) Patched Energy Score (8)

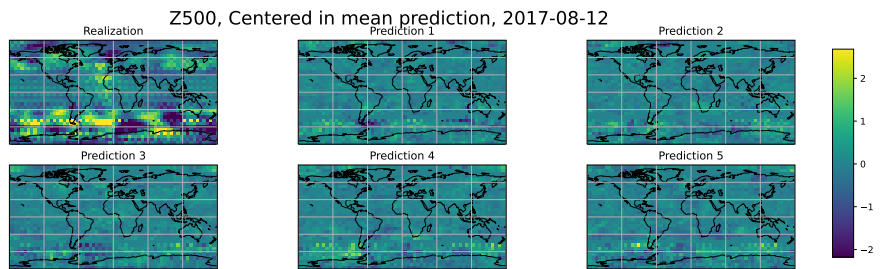


(d) Patched Energy Score (16)

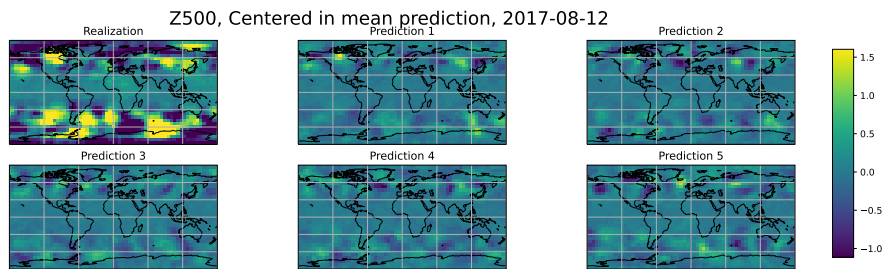
Figure 15: Deviations of the realization and forecasts from the forecast mean (obtained empirically from 100 forecasts) for the Energy-Variogram, Kernel-Variogram and Patched Energy Score (with patch size 8 and 16) for a specific date in the test set for the WeatherBench dataset. The absolute values of the forecasts used here are shown in Figure 12.



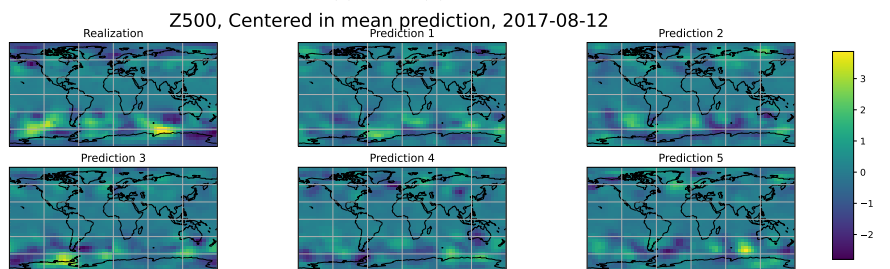
(a) GAN (1)



(b) GAN (2)



(c) GAN (3)



(d) WGAN-GP

Figure 16: Deviations of the realization and forecasts from the forecast mean (obtained empirically from 100 forecasts) for the three considered GAN setups and WGAN-GP for a specific date in the test set for the WeatherBench dataset. Notice how, for the first and third GAN setups, the scale of variations with respect to the predictive mean to the realization is much larger for the realization than for the predictions. Instead, the second GAN setup leads to unphysical features. The absolute values of the forecasts used here are shown in Figure 13.

E3.5 Time-series plots for selected variables on the grid

In Figures 17, 18, 19 and 20, and show the time series evolution, for a portion of the test period, for 8 randomly selected locations on the WeatherBench grid, for all considered methods (the same locations are shown for all methods). The dashed line represents the true evolution, the solid one the forecast mean, while the shaded region represents 99% credible intervals.

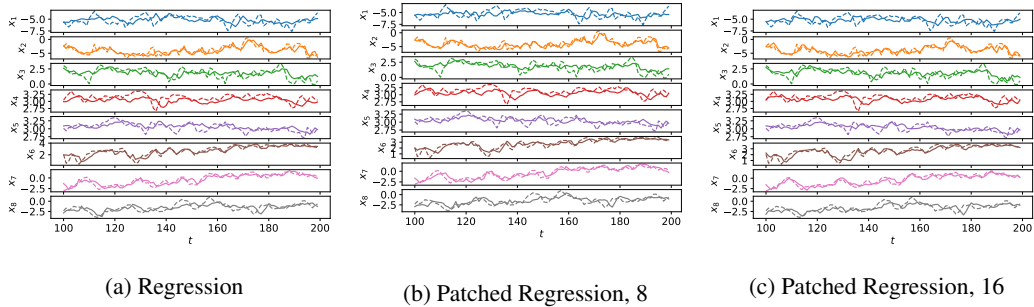


Figure 17: Results with the Regression and patched regression losses for 8 locations on the WeatherBench grid. The panels show observations (dashed line) and median forecast (solid line)

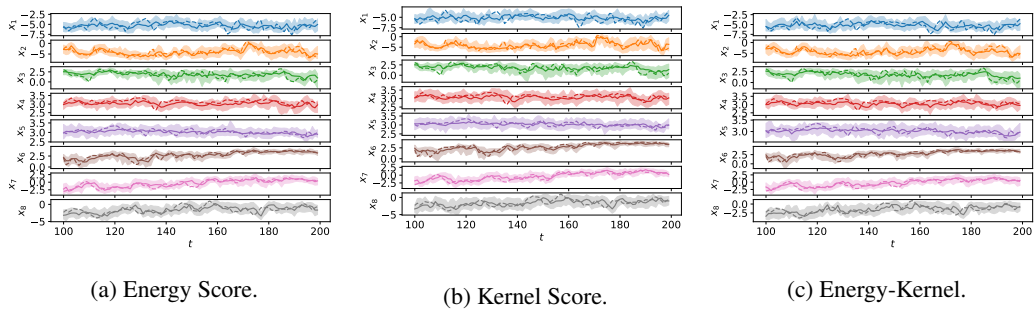


Figure 18: Results with the the Energy, Kernel and Energy-Kernel Scores for 8 locations on the WeatherBench grid. The panels show observations (dashed line), median forecast (solid line) and 99% credible interval (shaded region) for a portion of the test set.

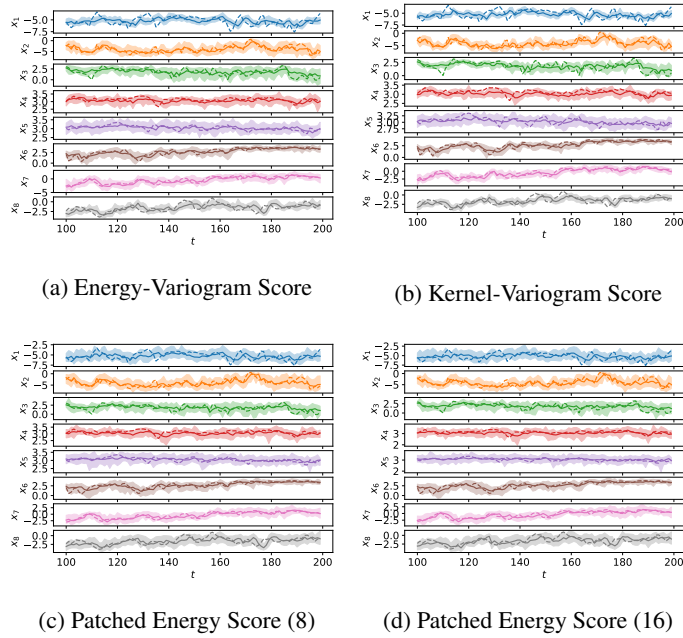


Figure 19: Results with the Energy-Variogram, Kernel-Variogram and Patched Energy Score (with patch size both 8 and 16) Scores for 8 locations on the WeatherBench grid. The panels show observations (dashed line), median forecast (solid line) and 99% credible interval (shaded region) for a portion of the test set.

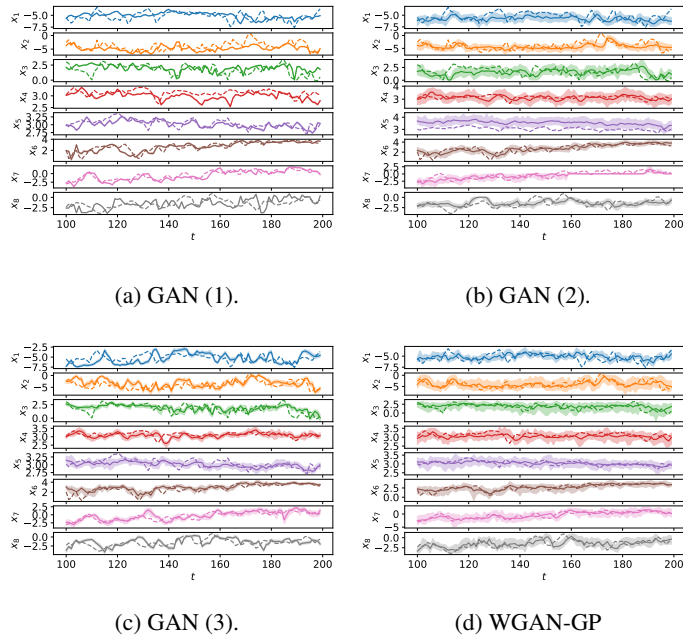


Figure 20: Results with the three considered GAN setups and WGAN-GP Scores for 8 locations on the WeatherBench grid. The panels show observations (dashed line), median forecast (solid line) and 99% credible interval (shaded region) for a portion of the test set. Notice how the first GAN setup severely underestimates the uncertainty region, while the second one forecasts unphysical evolution for some time intervals.